

THESIS ON CIVIL ENGINEERING F62

The Rapid Prediction of Grounding Behavior of Double Bottom Tankers

MARTIN HEINVEE

TUT
PRESS

Department of Mechanics
Faculty of Civil Engineering
TALLINN UNIVERSITY OF TECHNOLOGY

Thesis was accepted for the defense of the degree of Doctor of Philosophy on
June 21, 2016

Supervisor: PhD Kristjan Tabri, Department of Mechanics, Faculty of Civil
Engineering, Tallinn University of Technology

Opponents: Joško Parunov, Professor, Faculty of Mechanical Engineering and
Naval Architecture, University of Zagreb, Croatia

Manolis S. Samuelides, Professor, School of Naval Architecture
and Marine Engineering, National Technical University of Athens,
Greece

Defense of the thesis: August 30, 2016

Declaration:

Hereby I declare that this doctoral thesis, my original investigation and
achievement, submitted for the doctoral degree at Tallinn University of
Technology has not been submitted for any academic degree.

/Martin Heinvee/

Copyright: Martin Heinvee, 2016

ISSN 1406-4766

ISBN 978-9949-83-003-9 (publication)

ISBN 978-9949-83-004-6 (PDF)

EHITUS F62

Arvutusmeetod laeva karilesõidu vigastuste kiireks hindamiseks

MARTIN HEINVEE

ABSTRACT

The thesis studies the grounding behavior of double bottom tankers and proposes a simplified model for the rapid prediction of bottom damage. The model is intended for risk analyses studies where a large number of grounding scenarios are simulated.

Simplified equations were developed on the basis of a regression analysis of the results of a series of numerical grounding simulations conducted with tankers of different lengths for different ground topologies and penetration depths. First, the simplified equations were derived to calculate the grounding resistance. The longitudinal length of the damage was evaluated based on the resistance and the kinetic energy of the ship. The damage opening widths in the outer and inner bottom were given as a function of the penetration depth and the parameters describing the rock size and the ship size. To improve the prediction of the onset of the inner bottom failure, a critical relative penetration depth required for the breaching of the inner hull was derived.

The influence of the longitudinal and transverse bulkheads was analyzed via an additional set of numerical simulations conducted with the tanker models including the bulkheads. Our analysis showed that the presence of the longitudinal bulkhead increases the average grounding force substantially, while the effect of the transverse bulkheads is less significant. A term which depends on the penetration depth was added to the grounding resistance to take into account the contribution from the longitudinal bulkhead. The damage opening formulas were updated to account for the bulkheads.

The relevancy of the mathematical models in the bottom shape description was investigated. Grounding response in terms of dissipated energy was evaluated for a real rock and for four mathematical approximations. It was revealed that the mathematical representation of the bottom topology is of great importance in the grounding response. It was shown that the parabolic rock model used in this thesis yields to sufficiently accurate predictions for the grounding response and thus is applicable for the risk analysis studies.

To exemplify practical application of the damage assessment model, it was combined with the oil spill model, the spill propagation model and the environmental consequence assessment model. To demonstrate the performance of the integrated model, geographic site- and date-specific grounding accidents were simulated: evaluating the size of damage opening, oil spill amount and duration, spill propagation trajectory and resulting environmental consequences. In conclusion, this thesis presents a set of simplified equations for the calculation of the grounding resistance, the longitudinal damage extent and the opening widths in the double bottom structure of a tanker. Since only a limited number of parameters are required to define the grounding scenarios, the simplified equations are easily applicable in the risk analysis studies.

KOKKUVÕTE

Käesolevas doktoritöös on uuritud topeltpõhjaliste tankerite karilesõidul tekkivaid vigastusi ja on välja töötatud lihtsustatud mudel vigastuste kiireks hindamiseks. Mudel on mõeldud rakendamiseks riskianalüüsides, kus analüüsitakse suurt hulka karilesõidu stsenaariume.

Mudel põhineb erineva suurusega tankerite karilesõidu simulatsioonidel kasutades lõplike elementide meetodit. Algul vaadati ilma vaheseinteta tankereid ja eri suurusega karisid. Andes ette kari sissetungisügavuse laeva, arvatati kontaktjõud, vigastuse laiused ja dissipeerunud energiad plaadistutes. Füüsikaliste parameetrite vaheliste seoste saamiseks on kasutatud regressioonanalüüsi.

Algul on tuletatud lihtsustatud seosed horisontaalse kontaktjõu hindamiseks tankeri kokkupõrkel kariga. Vigastuse pikkuse saamiseks on võrdsustatud kontaktjõu töö ja laeva kineetiline energia. Laeva topeltpõhja välimise ja sisemise plaadistu vigastuse laius on avaldatud sissetungisügavuse ning laeva ja kivi iseloomustavate parameetrite funktsioonina. Tankeri sisepõhja purunemise täpsemaks hindamiseks on välja töötatud kriteerium, mis määrab siseplaadistiku purunemise kriitilise sissetungisügavuse.

Tankeri piki- ja põikivaheseinte mõju uurimiseks on arvatud karilesõidul tekkivad vigastused vaheseinu sisaldavate laevade korral. Analüüsides selgus, et pikivaheseinte olemasolu korral vigastuste tekkimiseks vajalik kontaktjõud suureneb märkimisväärselt, samas põikivaheseinte mõju vigastuste tekkimisele on vähene. Seetõttu kontaktjõu avaldis on korrutatud läbi korrektsioonteguriga, mis võtab arvesse pikivaheseina mõju. Vigastuse laiuse hindamisel on arvesse võetud vaheseinte mõju.

Töös on uuritud ka kari mudelite mõju tankeri vigastustele. Selleks arvatati karilesõidul tekkiv dissipeerunud deformatsioonienergia nelja reaalse (mõõdetud) kujuga kari (kivi) ja nende ligikaudsete approksimatsioonide korral. Selgus, et karilesõidul tekkiv dissipeerunud energia ja kontaktjõud oli tundlik aproksimatsioonide suhtes. Osutus, et väljatöötatud mudelis kasutatud paraboloidne kari mudel võimaldab piisavalt täpselt hinnata karilesõidul tekkivaid nähtusi.

Demonstreerimaks välja töötatud vigastuste hindamise mudeli praktilisust, seoti see mudelitega, mis hindavad õli väljavoolamist vigastatud laevast, sellele järgnevat õli levikut ja vastavaid keskkonna kahjustusi. Integreeritud mudelit on demonstreeritud juhtumi analüüsiga, milles simuleeriti õlitankeri karilesõitu reaalses kohas, reaalsetel ilmastikutingimustel kindlal kuupäeval.

Kokkuvõtteks, käesolevas doktoritöös on välja töötatud lihtsustatud seosed, mis võimaldavad hinnata kontaktjõudu, vigastuse pikkust ja selle laiust karile sõitnud õlitankeri topeltpõhjas. Kuna mudel vajab karilesõidu stsenaariumi kirjeldamiseks vähe sisendparameetreid ja on seostatav õli väljavoolu mudeliga (Sergejeva et. al., 2013), seetõttu on sobiv kasutamiseks riskianalüüsides.

ACKNOWLEDGEMENTS

This work has been carried out at the Department of Mechanics in the Tallinn University of Technology. During the process of this thesis the financial support has been provided by Central Baltic Interreg IV A program project MIMIC (“Minimizing risks of maritime oil transport by holistic safety strategies”), BONUS+ STORMWINDS project (“Strategic and Operational Risk Management for Wintertime Maritime Transportation System”), Estonian Science Foundation Research Grant project ETF8718 (“Numerical model to assess the structural damage in ship grounding considering motion dynamics”), Institutional Research Funding project IUT19-17 (“Dynamical processes in hydraulic networks, marine structures and sea environment”) and project B18 (“Tool for direct damage calculations for ship collision and grounding accidents”). This financial support is greatly appreciated.

I would like to express special thanks to my supervisor PhD Kristjan Tabri for his continuous guidance and advice throughout the PhD studies. Many thanks also to all my colleagues at the Department of Mechanics. Special thanks also to my family and friends for the support and encouragement throughout the years.

TABLE OF CONTENTS

ABSTRACT	5
KOKKUVÕTE	6
ACKNOWLEDGEMENTS	7
LIST OF PUBLICATIONS	9
AUTHOR'S CONTRIBUTION	10
ORIGINAL FEATURES	11
1 INTRODUCTION	12
1.1 Background	12
1.2 State of the art	13
1.3 Objective of the Thesis	15
1.4 Scope of work	16
1.5 Limitations	18
2 NUMERICAL GROUNDING SIMULATIONS	19
3 GROUNDING FORCE	21
3.1 Contact force and pressure	21
3.2 Structural resistance coefficient as a function of material volume ...	23
3.3 Effect of the longitudinal and transverse bulkheads	23
3.4 Grounding force as a function of the deformed material volume	25
4 DAMAGE OPENING SIZE	27
4.1 Damage opening length	27
4.2 Opening width in the outer and in the inner bottom	27
4.3 Influence of the bulkheads on the damage size	29
5 VALIDATION	32
5.1 Grounding force and energy	32
5.2 Damage opening width	34
5.3 Modelling of the rock: mathematical approximation versus real bottom topology	35
6 APPLICATION EXAMPLE	37
7 CONCLUSIONS	40
REFERENCES	42
CURRICULUM VITAE	45
ELULOOKIRJELDUS	47
PUBLICATIONS	49

LIST OF PUBLICATIONS

P1: Heinvee, M., Tabri, K., Kõrgesaar, M. (2013). **A simplified approach to predict the bottom damage in tanker grounding.** *Proceedings of International Conference on Collision and Grounding of Ships and Offshore Structures: International Conference on Collision and Grounding of Ships and Offshore Structures*, 17-19.06.2013, Trondheim, Norway. Taylor & Francis, 161–171.

P2: Heinvee, M., Tabri, K. (2015). **A simplified method to predict grounding damage of double bottom tankers.** *Marine Structures*, 43, 22–43.

P3: Heinvee, M., Tabri, K., Kõrgesaar, M., Urbel, A. **Influence of longitudinal and transverse bulkheads on ship grounding resistance.** *Proceedings of International Conference on Collision and Grounding of Ships and Offshore Structures: International Conference on Collision and Grounding of Ships and Offshore Structures*, 15-18.06.2016, South Korea.

P4: Tabri, K., Aps, R., Mazaheri, A., Heinvee, M., Jönsson, A., Fetissov, M. (2015). **Modelling of structural damage and environmental consequences of tanker grounding.** *In: Analysis and Design of Marine Structures V: 5th International Conference on Marine Structures*, 25–27.03.2015, Southampton UK. Ed. C. Guedes Soares and R. Ajit Sheno. Taylor & Francis, 703–710.

P5: Sormunen, O-V., Kõrgesaar, M., Tabri, K., Heinvee, M., Urbel, A., Kujala, P. **Comparing rock shape models in grounding damage modelling.** *Marine Structures*. Accepted for publication on 08.07.2016.

AUTHOR'S CONTRIBUTION

Publication 1: “A simplified approach to predict the bottom damage in tanker grounding“

The author proposed the approach, prepared and analyzed the numerical grounding simulations, developed the simplified formulas and prepared the manuscript. Kristjan Tabri contributed to the development of the approach, provided valuable comments and contributed to the manuscript. Mihkel Kõrgesaar provided the tanker FE models for the grounding simulations.

Publication 2: “A simplified method to predict grounding damage of double bottom tankers”

The author proposed the approach, analyzed the numerical grounding simulations and developed simplified formulas. Kristjan Tabri contributed to development of the approach, provided valuable comments and contributed to the manuscript.

Publication 3: “Influence of longitudinal and transverse bulkheads on ship grounding resistance and damage size”

The author proposed the approach, analyzed the numerical grounding simulations and developed simplified formulas. Annika Urbel prepared the tankers FE models and conducted numerical simulations. Mihkel Kõrgesaar provided the material model with fracture criteria for the tanker FE models. Kristjan Tabri contributed to development of the approach, provided valuable comments and contributed to the manuscript.

Publication 4: “Modelling of structural damage and environmental consequences of tanker grounding”

Martin Heinvee prepared the MATLAB scripts to be used in the study within the integrated model. Martin Heinvee also contributed to the manuscript with the part limited to the model developed by the author.

Publication 5: “Comparing rock shape models in grounding damage modelling”

Martin Heinvee prepared the ground/seabed topologies which were the basis for creating the corresponding FE models. Martin Heinvee also extracted grounding energies from numerical simulations for further analysis and added his contribution to the manuscript.

ORIGINAL FEATURES

In the risk analyses, large numbers of accidental grounding scenarios are studied. To be able to evaluate consequences within reasonable time and with limited input data, a fast damage assessment tool is needed. The existing models require either too detailed information or are too time consuming. This thesis presents a set of practical simplified equations for the calculation of the grounding resistance and the damage extent in a double bottom structure of a tanker. Since only a limited number of parameters are required to define the grounding scenarios, the simplified equations are easily applicable in the risk analyses studies.

The following features of this thesis are believed to be original:

1. In P1, an approach for the evaluation of the grounding resistance and the extent of structural damage based on a limited number of parameters is proposed. In the resistance formula, the influence of the rock size and the ship size on the grounding force is given in separate functions so their contribution is separated. Ship's characteristic resistance to the grounding is defined via single constant – a structural resistance coefficient.
2. In P2, the ship structural resistance coefficient is presented as a function of ship length. In P3, a procedure based on deformed steel volume is presented to account for the ship's structural configuration in the resistance coefficient.
3. In P3, a term that depends on the rock penetration depth was added to the grounding resistance formula to take into account the contribution from the bulkheads.
4. In P2, the damage opening widths in the outer and inner bottom were expressed as a function of the penetration depth, rock size and ship size. A critical relative penetration depth required for the breaching of the inner hull was derived as a criterion. The bulkheads effect on the damage opening formulas is taken into account in P3.
5. P4 presents the practical application of the developed formulas. For that, the developed formulas are combined with the oil spill model, spill propagation model and the environmental consequence assessment model. Such integrated simulation environment allows for a rapid analysis of a grounding accident and resulting consequences in means of the description of the oil spill and the environmental consequences. In P5, the relevancy of the mathematical models used to describe the bottom shapes is studied. It was revealed that the mathematical representation of the bottom topology has a great importance on the grounding response. It is shown that the parabolic rock model used in this thesis yields to sufficiently accurate predictions for the grounding response.

1 INTRODUCTION

1.1 Background

Increasing cargo flows all over the world have affected the density of marine traffic and thus risks for accidents. For example, it was shown by Brunila and Storgård (2012) that in the past ten years, the oil transportation in the Gulf of Finland has quadrupled, which makes it a region of the highest risk in the world. However, the number of collisions and groundings with oil and chemical tankers in the mentioned region has stabilized (Kujala et. al., 2009), indicating the efficiency of existing measures towards increased safety at seas.

As the traffic continues to increase, it is necessary to further improve various measures to increase safety at seas. The most severe environmental consequences are caused by accidents with oil and chemical tankers, which in the worst case can lead to extensive oil spill. Accidents can be prevented and their consequences reduced by implementing safety measures that can be developed through risk analyses conducted for certain transportation areas. In a risk analysis, possible impact on the environment and on human lives, i.e. the consequences, can be evaluated for typical accidental scenarios. The consequences in terms of oil spill can be determined directly if there is information on the damage opening size in the ship bottom. In the risk analyses, the severity of a grounding scenario is typically assessed by using a combination of reported accidental statistics and expert opinions (Valdez et. al., 2016). Such risk analyses are sea area specific and large numbers of scenarios are considered. Typically, the ships participating in accidents are described only by their type and main dimensions, i.e. the information about the ship's structural configuration is not available. With limited available information, there are no effective tools or methods to provide damage assessment. Thus, this thesis aims to develop a practical model where the damage extent can be evaluated for scenarios in which only the ship size and the bottom characterization are used as input.

Any model development is related to simplifications and thus uncertainties with respect to the reality. The grounding process is a complex nonlinear process where highly coupled effects, such as large contact forces, large structural deformations and hydrodynamic loads, are coupled. To simplify the problem, grounding analyses are generally divided into two sub tasks- external dynamics and internal mechanics. The external dynamics evaluates the ship motions, resulting in the energy to be absorbed by structural deformations, while the inner mechanics evaluates the deformations that the structures undergo while absorbing that energy.

Furthermore, the complexity of a grounding problem depends on whether the ship moves horizontally, vertically or is a combination of them with respect to the seabed obstruction. If a ship grounds over a sharp rock, then the grounding is termed as “bottom raking” and if over blunt “shoal”-type seabed, then the term of “bottom sliding” is used (Alsos and Amdahl, 2007). Furthermore,

“hard” grounding refers to a grounding with undeformable seabed such as rocks, while the “soft” grounding takes place on deformable seabed. These different classifications correspond to different structural behaviors of a ship bottom, which yield to different failure models. Most of the studies in the field of grounding analyses address the inner mechanics in accidental grounding scenarios where detailed information for ship structural arrangement is commonly required.

1.2 State of the art

Assessment of ship grounding consequences has been a subject for a large number of research studies. The methods used for the assessment of grounding consequences can be divided into four categories:

- 1) empirical and statistical models
- 2) numerical simulation models
- 3) simplified expressions for ship structural elements
- 4) analytical and semi-analytical analysis tools for ship grounding analysis.

One of the first empirical models in the field was created by Minorsky (1959) who studied actual collision accidents and found that the energy absorbed by ship structures is in linear correlation with the deformed steel volume. It was shown by Vaughan (1977) that similar linear dependence is also valid for ship groundings. To determine the damage extent, both models require rather detailed information for ship scantlings. However, these models can be used as remote experimental validation for other simplified models. A convenient application in terms of risk analysis was adopted in 1995 by the International Maritime Organization (IMO, 1995) which was revised in 2003 (IMO, 2003). These guidelines present a probabilistic procedure for assessing the damage extent and oil outflow performance of an oil tanker design in collision and grounding. The guidelines are based on the damage density distributions which were derived from the actual damage data of 63 groundings and 52 collision accidents of oil tankers, chemical tankers and Ore/Bulk/Oil carriers. It has been argued (e.g. by Sirkar et. al., 1997, Rawson et al., 1998, Pedersen and Zhang, 2000) that a major shortcoming in the IMO guidelines is that grounding and collision damages normalized by the main dimensions of the ship have the same probability density distributions regardless of a particular structural design and ship size. Furthermore, Pedersen (2010) claims that the grounding damage does not scale linearly with respect to the ship dimensions, thus questioning the approach based on the statistical curves. The probability density functions also overlook the size and shape of the bottom topology, i.e. there is no relationship between the damage size and the bottom topology.

Experiments are the most straightforward method to understand structural failure mechanisms. In the mid 1990s several large-scale grounding experiments at a scale of 1/4 were conducted, as reported by Rodd and Sikora (1995) and Vredeveldt and Wevers (1995). In both tests, double bottom structures for

tanker models and cone shaped models for intruding rocks were used to provoke the tearing failure modes. Due to the high, costs such tests are rare and clearly are not an option for analyzing large numbers of grounding scenarios. However, these results still provide valuable validation for the analysis models and are here considered when developing the criteria for critical penetration depth in P2. Due to the rapid evolution of computer capability, the numerical grounding and collision simulation models are regarded as the “new experiments”, which allow more elaborated studies of the grounding phenomenon. The main challenges in such simulations are the proper representation of structural configuration, definition of material properties, simulation of the material failure and the selection of the element size. Numerous publications presenting the nonlinear finite element (NLFE) technique for grounding simulations exist, see among others Kitamura (2002), Naar et. al. (2002), Alsos and Amdahl (2007), Samuelides et. al (2007), AbuBakar and Dow (2013). The material and failure modeling in the NLFE analyses is discussed, for example, in Woelke et. al. (2013), Walters (2014) Körgesaar and Romanoff (2014), and Körgesaar (2015). Concerning the complexity of the problem, NLFEA is still expensive because it is time- consuming in terms of modeling and computation, and requires detailed description of the structural configurations.

One alternative to the NLFEA grounding simulations is the simplified analytical models where the total response of bottom structure is obtained through the summation of the responses of separate structural members. Simplified models focusing on the raking-type grounding are contributed by Wang et. al. (1997), Wang et. al. (2000), Zhu et. al. (2002), Friis-Hansen and Simonsen (2002). One of the primary energy absorbing mechanisms in a “raking” is the plate tearing process for which theoretical models have been developed among others by Ohtsubo and Wang (1995), Simonsen and Wierzbicki (1997), Simonsen (1998), Zhang (2002). Significantly fewer models are dedicated to “sliding”-type grounding (with blunt seabed) (Hong and Amdahl, 2012, Gao and Hu, 2015). The primary deformation modes for individual structural members are sliding deformation of longitudinal girders, denting and crushing of transverse members and indentation of bottom plating. Simplified models for web girder crushing are proposed by Hong and Amdahl (2008), Liu and Soares (2015), Yu et. al. (2015). Based on simplified methods for external and internal mechanics, several tools or software packages have been made available for collision and grounding analysis, for example, DAMAGE (Damage Assessment of Grounding Events) developed by Little et. al. (1996) and Simonsen (1999). This tool predicts grounding damages assuming a penetrating rock to have a conical shape. It solves the external problem uncoupled from internal problem and applies calculated absorbed energy to the plastic deformation for response calculations. External problem applies the principle of conservation of linear and angular momentum. The model for internal mechanics is based on the direct contact deformation of super-elements.

Friis-Hansen and Simonsen (2002) developed GRACAT software for ship grounding and collision analysis. The software consists of three basic modules: accident frequency, damage and consequence. The damage can be evaluated in a deterministic or probabilistic mode. Internal mechanics and external dynamics are uncoupled in the grounding simulation problem. To evaluate the structural deformations, theoretical models for structural elements are considered.

These simplified models and software tools that include different theoretical models provide very deterministic assessment for the grounding response. The theoretical models are highly dependent on the topology of the seabed obstacle assumed in the development of the methods. These theoretical models require detailed data about ship scantlings, e.g. plate thicknesses, girder and stiffener spacing, etc. As such detailed information is not often available, their application for risk analysis purposes is difficult.

Methods that combine numerical simulations or accidental data or experiments with the regression analysis allow developing formulas that consider main dependencies between the grounding response and the relevant parameters. Simonsen et. al. (2009) developed an empirical damage prediction formula, which is based on a combination of full-scale testing and extensive non-linear finite element analyses. Curves expressing horizontal force as a function of the damage extent were obtained from 12 grounding finite element simulations and then tuned to give a best possible fit with the formula. The shortage is that the formula is limited only to groundings over sharp rocks (raking) where plate tearing is a dominant failure mode. Furthermore, this model calculates the damage size, which is not the same as the damage opening, thus the output cannot be directly used for the basis of the oil spill calculations. A major shortcoming of the existing simplified models and tools is that while focusing mainly on determining the resistance force and the dissipated energy, they require rather detailed information on the ship structural scantlings. Moreover, the existing models do not enable assessment for the size of the damage opening, which is essential for the calculation of oil spill.

1.3 Objective of the Thesis

The objective of this thesis is to develop a simplified model suitable to assess the damage of double bottom tankers for hard grounding accidents where only limited information regarding the ship is available. Therefore, the thesis has the following objectives:

- To develop simplified formulas for the grounding resistance as a function of main input parameters: – rock penetration depth, rock size and the ship size;
- To develop simplified formulas for the damage opening width in the outer and inner plating of a double bottom tanker;
- To develop a criterion for the onset of failure in the inner bottom;

- To develop simple relationships to characterize ship's structural resistance based in its length or, if available, based on its structural configuration;
- To study the influence of the mathematical approximation of the bottom shapes;
- To integrate the damage assessment model into a combined simulation tool, allowing us to evaluate the description of the damage opening, the amount and the duration of the oil spill, spill trajectory in the sea and the environmental consequences.

1.4 Scope of work

The thesis comprises the method development and the application example (see Figure 1). Focus in P1 to P3 is on the development of the simplified formulas for the grounding resistance and the damage size. The resistance formula consists of functions that express the contribution from the ship size, rock size and a contact area in between. Such architecture allows changing each component individually. The equations are based on a series of numerical grounding simulations conducted with tankers of different lengths. The simulations were performed for different bottom topologies and penetration depths.

In P1, a simplified approach was developed for the evaluation of the grounding force and the longitudinal extent of the structural damage. P1 excludes the contribution of the longitudinal and transverse bulkheads and focuses on the relationships between the main parameters such as the rock shape and ship's main dimensions. Here, grounding force is assumed proportional to the product of contact pressure and the contact area. A ship's structural resistance was characterized by a single parameter denoted as structural resistance coefficient that depends on the ship length. The longitudinal length of the damage was evaluated based on the kinetic energy of the ship.

P2 addresses the evaluation of the vertical and transverse damage extent. The damage opening widths in the outer and inner bottom were given as a function of the penetration depth, the rock size and the ship size. To improve the prediction of the onset of the inner bottom failure, a critical relative penetration depth required for the breaching of the inner hull was derived.

P3 studied the influence of the longitudinal and transverse bulkheads on the grounding behavior. In total, additional 90 grounding scenarios were numerically simulated with the tanker models, including the bulkheads. Analysis showed that the presence of the longitudinal bulkhead increases the average grounding force substantially, while the effect of transverse bulkheads is less significant. An additional term was introduced to the grounding resistance formula to take into account the contribution from the longitudinal bulkhead. Also, the damage opening formulas were updated to account the bulkhead's effect. P3 also proposes a routine where the ships structural resistance coefficient can be approximated based on the steel volume deformed

in grounding. Moreover, simulations revealed that a linear relationship exists between the steel volume of the deformed material and the energy absorbed in ship grounding. This relationship can be used to predict the grounding force if detailed data for the ship scantlings are available.

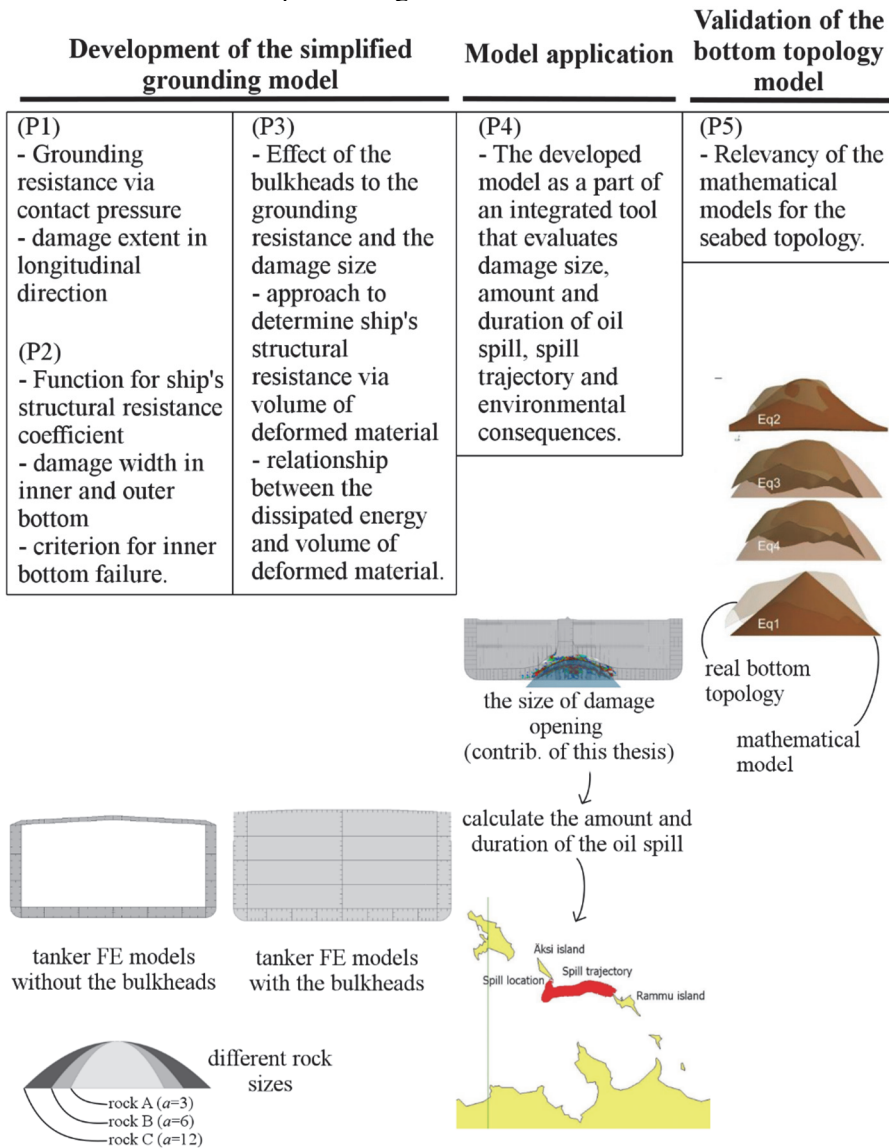


Figure 1. Outline of the investigation.

P4 presents the practical application of the developed damage assessment model for an accidental scenario. For the analysis, the damage assessment model is combined with the oil spill model (Sergejeva et. al., 2013), spill propagation model (SMHI, 2012) and the environmental consequence assessment model (Aps et. al., 2009), (Aps et. al., 2014). The performance of the integrated model was exemplified by simulating a number of grounding

accidents and resulting environmental consequences. The study showed the possible environmental consequences in terms of spilled shore line lengths and the affected Natura and Natura Bird area if a 180 m long tanker grounds close to the Port of Muuga, Estonia, in October 2013.

P5 investigated the relevancy of the mathematical models used to describe the bottom shapes. Four different bottom topologies were studied, each described with four mathematical models and with one model following the real shape of the rock. Grounding response in terms of dissipated energy was evaluated for all the models. It was revealed that the mathematical representation of the bottom topology is of great importance in the grounding response. It was also shown that the parabolic rock model used in this thesis yields to sufficiently accurate predictions for grounding response and thus is applicable for the risk analysis studies.

In conclusion, this thesis presents a set of simplified equations for the calculation of the grounding resistance, the damage extent and the opening widths in a double bottom structure of a tanker. Since only a limited number of parameters are required to define the grounding scenarios, the simplified equations are easily applicable in the risk analysis studies.

1.5 Limitations

This thesis proposes a simplified model that allows quantifying the grounding response and the damage size. The simplicity of the model is achieved by considering only main dependencies. Thus, the following simplifications were made:

- a) The thesis focuses on the hard grounding while deformable seabed is not considered.
- b) The developed simplified formulas are applicable only for tankers with double bottom structures.
- c) The aim of the numerical simulations was to analyze how the ship particulars and the rock size influence the grounding resistance and the extent of the damage at a given penetration depth. Therefore, as a simplification, actual grounding dynamics was neglected, penetration was assumed constant and the numerical simulations were conducted in a displacement-controlled manner.
- d) The seabed topology is described with a parabolic function.
- e) The developed simplified formulas depend on the material and structural configuration used in the numerical grounding simulations. Ships used in the analysis satisfy the requirements of Harmonized Common Structural Rules for Oil Tankers (HCSR-OT) by IACS (2014).

2 NUMERICAL GROUNDING SIMULATIONS

In total, 150 numerical grounding simulations were conducted to study the grounding response of the double-bottom tankers. The aim of the numerical simulations was to analyze how the ship particulars and the rock size influence the grounding resistance and the extent of the damage at a given penetration depth. Four double bottom tankers of different lengths were studied to cover the range from 120 m to 260 m in length. Each tanker was analyzed for different penetration depths and for different rock sizes.

In P1 and P2, the grounding resistance and the damage size was studied without including the bulkheads since the focus was on the double-bottom structures as the main contributor to the grounding resistance. Such simplification was considered to reveal a relationship that is more apparent between the main input parameters, grounding resistance and the damage extent. For each tanker, only part of the midship region was modelled. The length of the model was selected to provide sufficiently long data series for the evaluation of the grounding force and the damage size. Moreover, the length of the models was chosen such that the influence from the boundary conditions is minimal. Numerical simulations were conducted with four different rock sizes covering the range from sharp rock to blunt “shoal”-type rock. The shapes of all the rocks were given with the parabolic equations where a single parameter a defines the rock size:

$$z = \frac{y^2}{a}, \quad (1)$$

where z and y denote the vertical and horizontal coordinate. The following rocks sizes and notations were used in the analysis and the development of simplified formulas: $a=3$ (rock A), $a=6$ (rock B), $a=12$ (rock C) and $a=24$ (rock D).

As the focus was on the determination of the structural resistance and the damage size at a given penetration depth, the rigid body ship motions were restricted. The numerical simulations were conducted in a displacement-controlled manner, where the rigid rock first moved to a required penetration depth and continued to move at the constant penetration depth along the ship at a constant velocity of 10 m/s.

In P3, additional 90 grounding simulations were conducted to study the influence of the longitudinal and transverse bulkheads. FE models of double-bottom tankers with bulkhead structures were generated using GL Poseidon software. Tankers with the lengths of 150, 190 and 260 m were included in the analysis. In order to investigate the effect of the bulkheads on the grounding resistance and the damage size, the grounding simulations were done for two transverse rock locations: (i) between the longitudinal bulkhead and the ship side, i.e. at B/4 and (ii) directly under the central longitudinal bulkhead, i.e. at B/2, see Figure 6a.

Each numerical simulation provided (i) horizontal grounding force-time history, (ii) average damage widths in the outer and inner bottom, (iii) volume

of the deformed elements, (iv) deformation energy (see Figure 2) and critical penetration depth required for the inner bottom failure. These outputs formed the basis for the derivation of simplified formulas for the grounding resistance, damage size and the criterion for estimating inner bottom failure. In order to present the force outcome of each numerical simulation via single value, an average grounding force was evaluated over each force time-history.

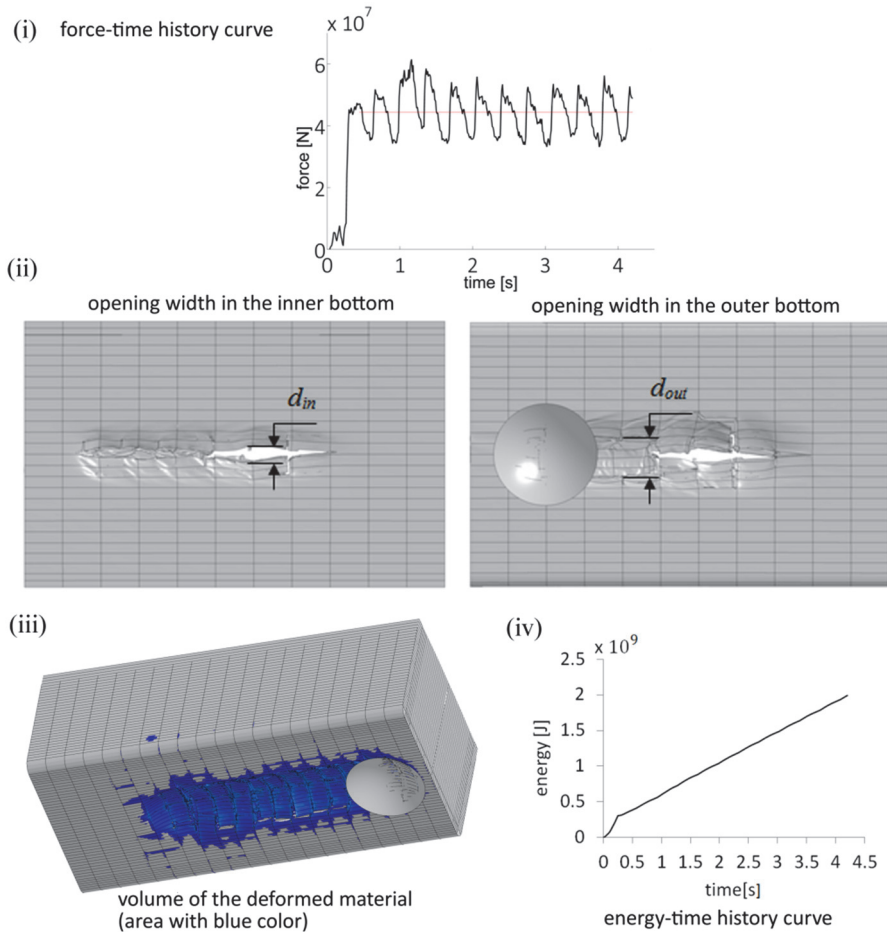


Figure 2. Output from numerical simulations.

3 GROUNDING FORCE

In P1, the simplified formula was developed for the average grounding force as a function of penetration depth and the parameters describing the rock size and the ship size. In P3, an additional term taking into account of the bulkheads was introduced to the equations. To derive the universal equations for different rock and ships sizes, the grounding resistance was evaluated as a function of contact pressure and the contact area.

3.1 Contact force and pressure

As a result of numerical simulations, the average grounding force was obtained for each combination of ship length, penetration depth and rock size. The aim in P1 was to derive a single universal equation describing these dependencies. This was achieved by presenting the horizontal contact force F as a product of the contact pressure and the contact area:

$$F(L, a, \delta, h_{db}) = P \cdot A = \underbrace{f_{cT}(L) \cdot \bar{P}(a)}_{\text{contact pressure } P} \cdot \underbrace{A(a, \delta, h_{db})}_{\text{contact area } A} \quad (2)$$

where the function $f_{cT}(L)$ characterizes the structural resistance level of the ship as a function of its length L , $\bar{P}(a)$ is the normalized ship size-independent contact pressure as a function of the rock size a and $A(a, \delta, h_{db})$ is the contact area between the rock and the double-bottom structure. For the sake of simplicity, the contact area A is defined as a projection of the contact surface to YZ plane, see the hatched area in Figure 3. The contact area is a function of the penetration depth δ , the rock size a and the double bottom height h_{db} , see Eqs. (4)-(5) in P1.

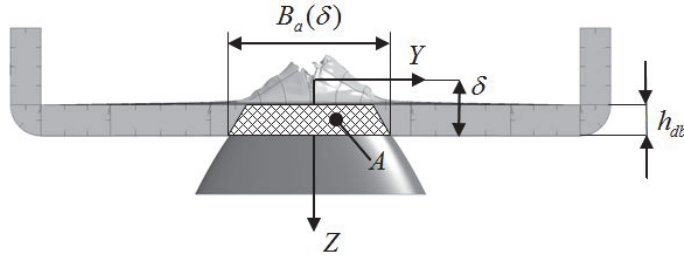


Figure 3. Contact area between the rock and the ship.

The concept of normalized contact pressure $\bar{P}(a)$ was found useful in P1 to separate the dependency of the ship parameters and the penetration depth from that of the rock size a . The normalized contact pressure polynomial $\bar{P}(a)$ was derived with the help of the regression analysis as follows. From the numerical analysis, the contact pressure was obtained for each simulation by dividing the numerically obtained average grounding force F_H with the contact area A :

$$p(a, \delta, h_{db}) = \frac{F_H}{A} \quad (3)$$

This operation removes the double bottom height h_{ab} from the pressure equations. The pressure values obtained with Eq. (3) are presented in Figure 4a with markers. Fitting a polynomial trendline through the pressure values results in three polynomials $P^i(a)$ (superscript i denotes the ship and $i=T120, T190$ or $T260$), each presenting the contact pressure for a certain tanker i as a function of the rock size a . Since the shape of polynomials is similar but the magnitude differs, the polynomials were normalized with respect to the area S^i under the corresponding polynomial i . The normalized polynomials are gathered to Figure 4b. Due to practically identical shape of the normalized polynomials, they can be presented via the single uniform pressure polynomial $\bar{P}(a)$, see Figure 4b and P1:

$$\bar{P}(a) = (1.8 \cdot 10^{-3} a^2 - 7.4 \cdot 10^{-2} a + 1.2) \quad (4)$$

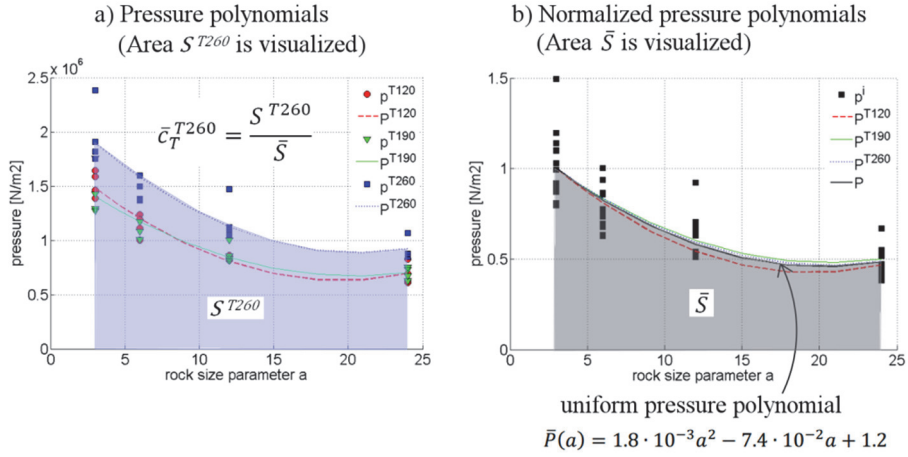


Figure 4. Contact pressure polynomials and structural resistance coefficients.

The ratio of the areas under the curves $P^i(a)$ and $\bar{P}(a)$ characterizes ship's structural resistance. Throughout the thesis it is termed as the ship structural resistance coefficient $\bar{c}_T = S^i / \bar{S}$, where \bar{S} is the area under $\bar{P}(a)$. In P2, it was concluded that the coefficient \bar{c}_T^i can be approximated with a bilinear function $f_{c_T}(L)$, which depends only on the ship length L , see Figure 5 and Eq. (7) in P2. In P3, the tankers with the longitudinal and transverse bulkheads were analyzed. The tankers were designed according to the HCSR-OT rules using GL Poseidon software. Using the above approach, the functions $\bar{P}(a)$ and $f_{c_T}(L)$ were updated to account the bulkhead effects, see Section 3.3.

Given the formulations for the structural resistance coefficient \bar{c}_T^i , for the pressure polynomials and for the contact area, the average horizontal grounding force for a scenario where a ship i runs over a rock a at the penetration depth δ can be calculated using Eq. (2).

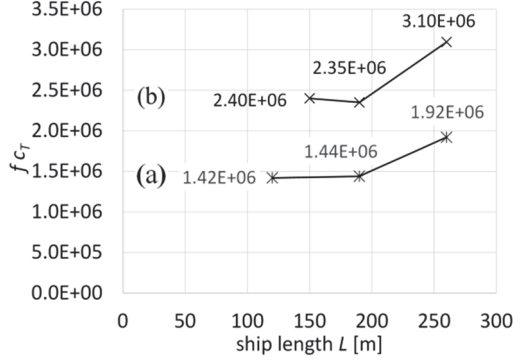


Figure 5. Functions $f_{c_T}(L)$ for the structural resistance coefficient \bar{c}_T^i : (a) based on tankers used in P1 and P2 and (b) based on tankers (with the bulkheads) used in P3.

3.2 Structural resistance coefficient as a function of material volume

Previous section presented the structural resistance coefficient c_T as a function of the ship length. However, if information about the ship structural configuration is given, it might be desirable to evaluate the c_T value corresponding to this configuration. In P3, an analytical procedure was used a more ship-specific estimate of the coefficient through the approximation of the volume of the deformed material. It was shown in P3 that the ratio between the resistance coefficients is roughly equal to the ratio between the deformed steel volume (superscripts i and j denote different ships):

$$\frac{\bar{c}_T^i}{c_T^j} = \frac{\bar{V}_{mat}^i(a, \delta)}{\bar{V}_{mat}^j(a, \delta)} \rightarrow \bar{c}_T^j = \frac{\bar{V}_{mat}^j(a, \delta)}{\bar{V}_{mat}^i(a, \delta)} \bar{c}_T^i, \quad (5)$$

where $\bar{V}_{mat}^i(a, \delta)$ and $\bar{V}_{mat}^j(a, \delta)$ are approximations for the steel volume to be deformed per unit length in a certain grounding scenario defined via the rock size a and the penetration depth δ . A routine to evaluate \bar{V}_{mat} values is presented in the appendix of P3. Only the parts of the structural members which are in direct contact with the rock contribute to the steel volume. The \bar{c}_T^i and V_{mat}^i values presented in P3 for three different tanker lengths can be used as a basis to evaluate a \bar{c}_T^j value for any ship j once the steel volume V_{mat}^j is determined.

3.3 Effect of the longitudinal and transverse bulkheads

In P3, the effect of the bulkheads on the grounding resistance was studied. Two transverse locations of the penetrating rock were analyzed: one directly under the longitudinal bulkhead (position $B/2$) and the other in between the

longitudinal bulkhead and the ship side (position $B/4$), see Figure 6a. Four average grounding force values were calculated:

$\bar{F}^{B/2}$ (or $\bar{F}^{B/4}$) – average force over the whole horizontal travel distance including the effect of the transverse bulkhead, see blue solid line in the figure;

$\bar{F}_{wf}^{B/2}$ (or $\bar{F}_{wf}^{B/4}$) – average force over the reduced horizontal travel distance excluding the effect of the transverse bulkhead, see blue dashed line in the figure.

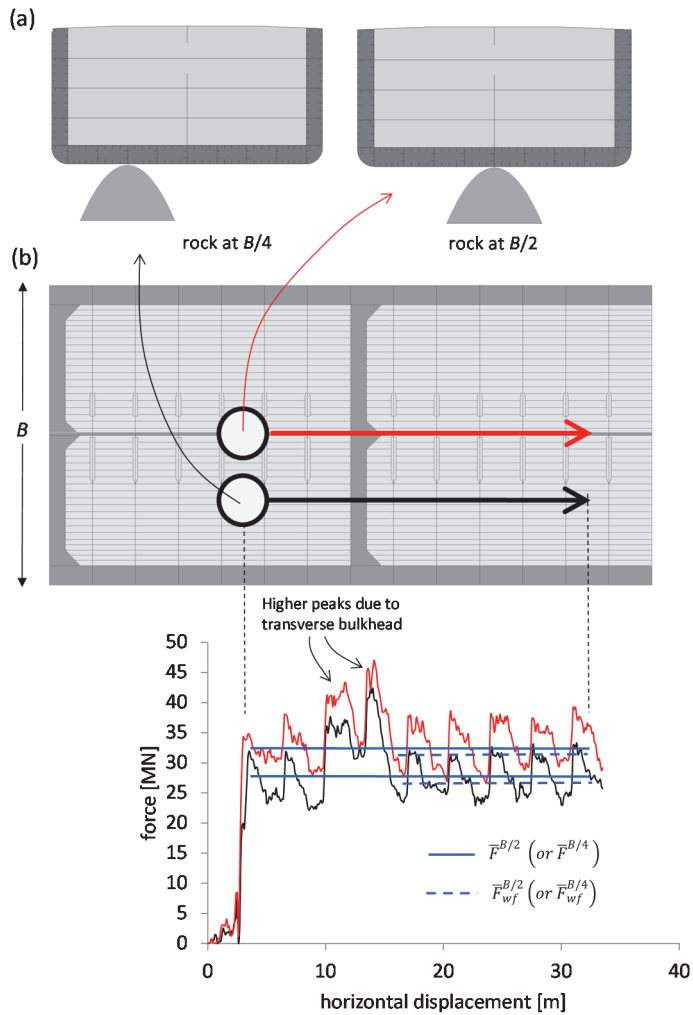


Figure 6. The effect of longitudinal bulkhead on the average grounding force: the ratio between average forces calculated at $B/2$ and $B/4$.

The influence of the longitudinal bulkhead on the grounding force was determined by comparison of the average forces $\bar{F}_{wf}^{B/2}$ (longitudinal bulkhead contributes to the grounding resistance) and $\bar{F}_{wf}^{B/4}$ (no resistance contribution

from the longitudinal bulkhead), see Figure 6. For the calculated scenarios, the ratios are presented in the left graph of Figure 7 as a function of the penetration depth. Observed linear relationship is presented as:

$$\frac{\bar{F}_{wf}^{B/2}}{\bar{F}_{wf}^{B/4}} = 0.105\delta + 1.04. \quad (6)$$

Thus, when the grounding resistance is given without the longitudinal bulkhead, i.e. $\bar{F}_{wf}^{B/4}$ calculated by Eq. (2) or obtained from numerical simulations, the average grounding force under the bulkhead can be approximated as

$$\bar{F}_{wf}^{B/2} = \bar{F}_{wf}^{B/4} \cdot (0.105\delta + 1.04) = \bar{c}_T^i \cdot \bar{P} \cdot A \cdot (0.105\delta + 1.04). \quad (7)$$

To study the influence of the transverse bulkheads, the ratio $\bar{F}_{wf}^{B/4} / \bar{F}_{wf}^{B/4}$ was evaluated, presented in the right graph of Figure 7 for tanker T150. The behavior is similar to other tankers. The ratios remain almost constant as a function of the penetration depth and is approximately equal to 1. Similar behavior of the ratio was observed also for $\bar{F}_{wf}^{B/2} / \bar{F}_{wf}^{B/4}$. This means that the transverse bulkhead has only small influence on the average grounding force. Thus, its contribution is not explicitly included in the simplified formulation, but is explicitly included in the updated \bar{c}_T and \bar{P} values in P3.

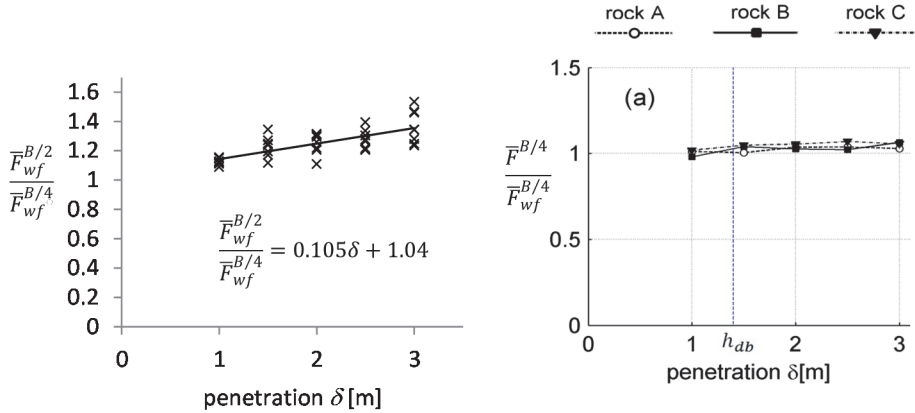


Figure 7. Influence of longitudinal (left) and transverse (right) bulkhead on the average force.

3.4 Grounding force as a function of the deformed material volume

In P3, it was shown that the average grounding force can be alternatively calculated based on the linear relationship between the dissipated energy and the volume of the deformed material. Deformation energies and damaged material volumes during the horizontal travel of the rock were obtained from the numerical simulations. Linear relationship similar to the formula proposed for collisions by Minorsky (1959) was obtained, see Figure 8. The formula for the energy \bar{E} per unit length of horizontal rock movement is provided in P3 as

$$\bar{E} = \begin{cases} 38.11(1.07\bar{V}_{mat} + 0.021) + 3.85 \text{ [MJ/m]} & \text{for rock at } B/4 \\ 38.11(1.26\bar{V}_{mat} - 0.016) + 3.85 \text{ [MJ/m]} & \text{for rock at } B/2' \end{cases} \quad (8)$$

where the volume \bar{V}_{mat} of the deformed material was approximated with the analytical procedure briefly introduced in Section 3.2. The energy per unit length \bar{E} has the unit of force [N] and thus Eq. (8) predicts the average grounding force.

Depending on the available information for the grounding scenario, either Eq. (2), Eq. (7) or Eq. (8) can be used for the calculation of the average grounding force. If the ship scantlings are available, then Eq. (8) can be used to take into account the resistance of the specific ship. However, if such detailed data for the ship is not available, then Eq. (2) or Eq. (7) can be employed.

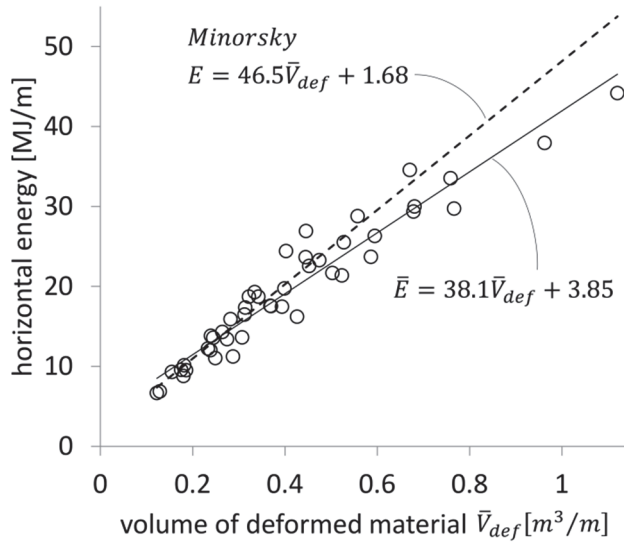


Figure 8. Averaged energy vs volume of deformed material per unit damage length.

4 DAMAGE OPENING SIZE

The damage opening size is defined with the length and the widths of the damage openings in the outer and inner bottom of the ship's double-bottom. The formulas for the opening size were developed in P2 and P3. This chapter gives an overview of the formulas and their derivation.

4.1 Damage opening length

Damage opening length is measured along the longitudinal direction of the ship. For simplicity, it is assumed that the opening lengths in the outer and in the inner bottom are equal. The damage length l_{dam} , see Figure 9, can be calculated by equalizing the work done by the grounding force with the kinetic energy of the ship:

$$F \cdot l_{dam} = \frac{\Delta \cdot v^2}{2} \rightarrow l_{dam} = \frac{\Delta \cdot (1 + a_x) \cdot v^2}{2F}, \quad (9)$$

where Δ is ship's displacement, a_x is non-dimensional surge added mass and v is ship's velocity. Here, F is to be calculated with Eq. (2), Eq. (7) or Eq. (8).

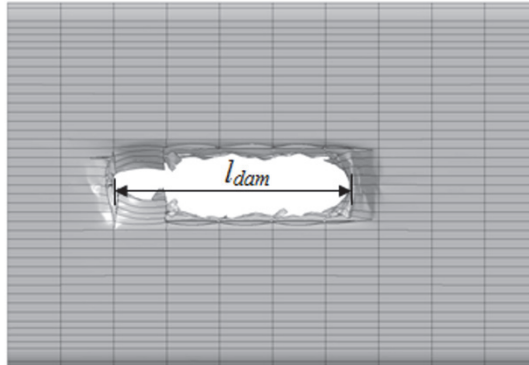


Figure 9. Length of the damage opening.

4.2 Opening width in the outer and in the inner bottom

In P2, the formulas for the calculation of the damage opening widths in the double bottom and a criterion for the inner bottom failure were developed based on the numerical simulations described in Chapter 2. The formulas were developed based on the following observations:

- i. Numerical simulations showed that the relative rock size a/S_{gir}^i (S_{gir}^i is the girder spacing) determines the deformation mode, which leads either to wide (rocks A and B) or narrow damage openings (rock C). Rock D did not result in the damage opening, but in the very wide global deformation of the whole bottom structure. Thus, the damage opening in the outer plating is given separately for these two ranges:

$$D_{out}^I(a, \delta) = 2\sqrt{a \cdot \delta} - \left[DIF_A(\delta) + \left(\frac{DIF_B(\delta) - DIF_A(\delta)}{a_B - a_A} \right) (a - a_A) \right] \quad (10)$$

for $0.9 \leq a/S_{gir}^i \leq 2.3$, ship length $120 \text{ m} \leq L \leq 260 \text{ m}$, $a_A = 3$, $a_B = 6$

$$D_{out}^{II}(a, \delta) = 2\sqrt{a \cdot \delta} - \left[DIF_B(\delta) + \left(\frac{DIF_C(\delta) - DIF_B(\delta)}{a_C - a_B} \right) (a - a_B) \right] \quad (11)$$

for $2.3 \leq a/S_{gir}^i \leq 4.6$, ship length $120 \text{ m} \leq L \leq 260 \text{ m}$, $a_B = 6$, $a_C = 12$

with $DIF(\delta)$ describing the difference between the rock width and the width of the damage opening:

$$\begin{aligned} DIF_A(\delta) &= -0.0614\delta^2 - 0.76\delta + 2.68, \text{ for rock size } a = 3 \text{ (rock A)} \\ DIF_B(\delta) &= -1.55\delta^2 + 4.33\delta + 1.69, \text{ for rock size } a = 6 \text{ (rock B)} \\ DIF_C(\delta) &= -5.85 \cdot 10^{-1}\delta^2 + 4.28\delta + 2.96, \text{ for rock size } a = 12 \text{ (rock C)}. \end{aligned} \quad (12)$$

- ii. The opening width in the inner bottom behaves similar to the opening width in the outer bottom, i.e. the curves are of similar shape. In terms of the penetration depth, the onset of failure in the inner bottom is delayed with respect to the onset in the outer plating by $\delta = 0.75h_{db}$. Thus, the width of the damage opening in the inner bottom can be evaluated as

$$\begin{aligned} D_{in}^I(a, \delta, h_{db}) &= B_a(a, \delta - 0.75h_{db}) - \\ &\left[DIF_A(\delta - 0.75h_{db}) + \left(\frac{DIF_B(\delta - 0.75h_{db}) - DIF_A(\delta - 0.75h_{db})}{a_B - a_A} \right) (a - a_A) \right] \end{aligned} \quad (13)$$

for $0.9 \leq a/S_{gir}^i \leq 2.3$, ship length $120 \text{ m} \leq L \leq 260 \text{ m}$, $a_A = 3$, $a_B = 6$

$$\begin{aligned} D_{in}^{II}(a, \delta, h_{db}) &= B_a(a, \delta - 0.75h_{db}) - \\ &\left[DIF_B(\delta - 0.75h_{db}) + \left(\frac{DIF_C(\delta - 0.75h_{db}) - DIF_B(\delta - 0.75h_{db})}{a_C - a_B} \right) (a - a_B) \right] \end{aligned} \quad (14)$$

for $2.3 \leq a/S_{gir}^i \leq 4.6$, ship length $120 \text{ m} \leq L \leq 260 \text{ m}$, $a_B = 6$, $a_C = 12$

where $B_a(a, \delta)$ is the rock width at the outer plating presented as

$$B_a(a, \delta) = 2\sqrt{a \cdot \delta}. \quad (15)$$

Our analysis revealed that Eqs. (13) and (14) predict a premature onset of inner bottom failure, i.e. the failure occurs at too low penetration depths. Thus, in P2, an additional criterion was developed based on numerical simulations, giving a critical penetration depth δ_f that corresponds to the onset of inner bottom failure. Only vertical penetration was considered, i.e. there was no longitudinal movement of the rock. It was revealed in P2 that the critical penetration depth depends on whether the rock is between the floors or under the intersection of the floor and the girder, see Figure 10. It was shown that if the rock is between the floors, the critical penetration depth depends on the ship

double bottom height h_{db} , relative rock size a/B , where a is the rock parameter and B is the ship breath. This gave the upper bound for the criterion (less conservative assessment), see sloped curve in Figure 10. However, if the rock is positioned under the intersection of the floor and the girder, the criterion depends only on the double bottom height

$$\delta_f \geq 1.05h_{db}. \quad (16)$$

This lower bound is obviously a more conservative assessment as it predicts the onset of the inner bottom failure at the penetration depth approximately equal to ship's double-bottom height. The criterion is to be used in conjunction with Eqs. (13) and (14) for the determination of the onset inner bottom failure.

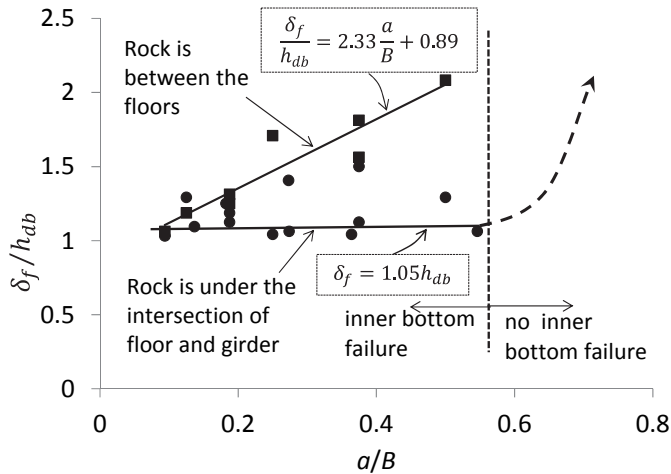


Figure 10. Fracture criterion for the inner bottom.

4.3 Influence of the bulkheads on the damage size

In P3, the effect of the bulkheads on the opening size was studied and damage opening formulas were updated. The numerical simulations showed that the grounding damages with respect to the ship size were relatively local and concentrated to the vicinity of the intruding rock, see Figure 11b. Thus, the presence of the transverse and longitudinal bulkheads contributes to the localization of the damage. In the simulations without the bulkheads (P2), the stiffness of the double bottom was lower and, especially in the case of larger rocks, the resulting damage was global deformation of the whole double bottom, see Figure 11a. When the bulkheads are included, the dominating deformation mode is a combination of local tearing and global crushing in the case of all three rocks, see Figure 11b.

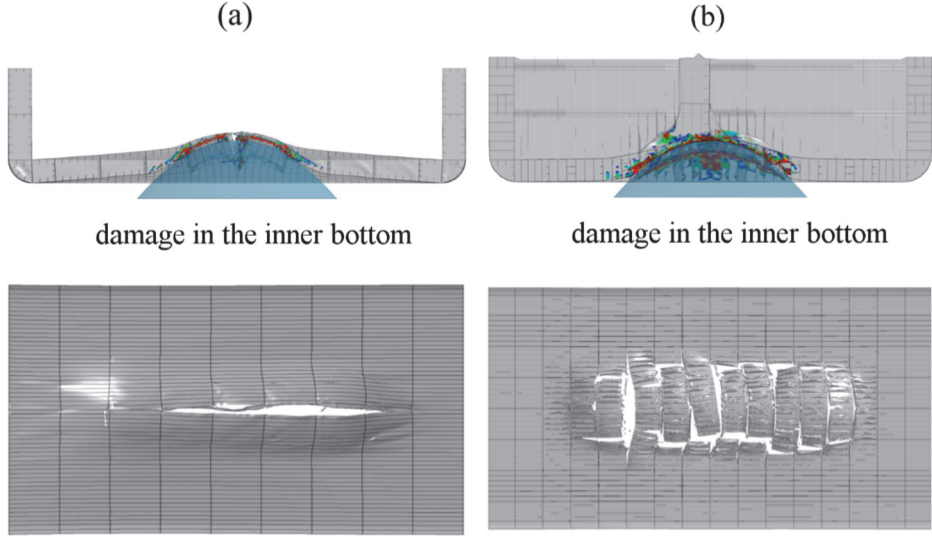


Figure 11. Comparison of bottom damages: (a) tanker without the bulkheads in P2 (b) tanker with bulkheads in P3.

Due to the changed deformation mode and the damage localization, the opening formulas are simplified as the second term in the opening formulas in P2 diminishes. Analysis in P3 revealed that within the range of penetration depths the behavior of the opening width in the outer bottom generally follows the rock width. Furthermore, the opening width in the inner bottom grows similar to the opening width in the outer bottom. The onset of the inner bottom failure is delayed by $\delta = \bar{b} \cdot h_{db} = 0.75 \cdot h_{db}$ with respect to that of the outer bottom. Thus, the opening widths in the outer and inner bottom are as follows:

$$D_{out}(a, \delta) = \begin{cases} 2\sqrt{a \cdot \delta} \cdot [1.6\delta - 0.8] & \text{for } \delta \leq 1[\text{m}] \\ 0.8 \cdot 2\sqrt{a \cdot \delta} & \text{for } \delta > 1[\text{m}] \end{cases} \quad (17)$$

$$\text{for } 150 [\text{m}] \leq L \leq 260 [\text{m}], 3 \leq a \leq 12$$

$$D_{in}(a, \delta, h_{db}) = \begin{cases} 2\sqrt{a(\delta - 0.75h_{db})} [1.6(\delta - 0.75h_{db}) - 0.8] & \text{for } \delta \leq 1 [\text{m}] \\ 0.8 \cdot 2\sqrt{a(\delta - 0.75h_{db})}, & \text{for } \delta > 1[\text{m}] \end{cases} \quad (18)$$

$$\text{for } 150 [\text{m}] \leq L \leq 260 [\text{m}], 3 \leq a \leq 12.$$

In P3, the failure criterion to predict the onset of inner bottom failure was derived similar to that in P2 and is given as follows (see also Figure 12):

$$\frac{\delta_f}{h_{db}} = 0.75 \frac{a}{B} + 1.17 \rightarrow \delta_f = \left(0.75 \frac{a}{B} + 1.17\right) h_{db}. \quad (19)$$

This criterion corresponds to a situation where the rock is under the floors, i.e. it presents the upper bound of the critical penetration. For the lower bound, i.e. when the rock is under the intersection between the floor and the girder, Eq. (15) hold. Smaller slope of the upper bound as compared to Figure 10 indicates

the higher stiffness of double bottom structures and thus, more local deformations.

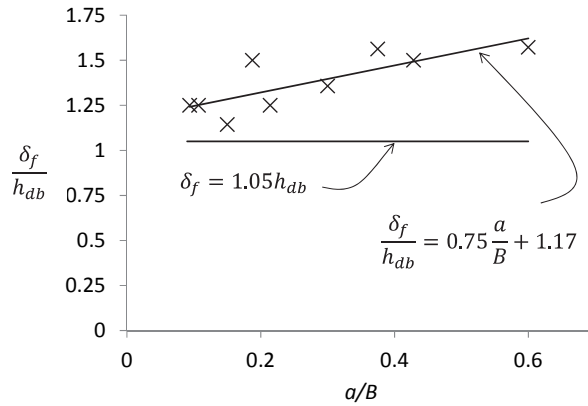


Figure 12. Fracture criterion for the inner bottom.

Figure 13 shows the performance of the developed formulas for damage openings. The filled markers are the outer widths and the empty markers are the inner widths from the numerical simulations. The lines represent the corresponding formulas. The figure shows that without the criterion, the inner width is significantly overestimated at lower penetration depths. Using the criteria by Eq. (19) improves the prediction significantly.

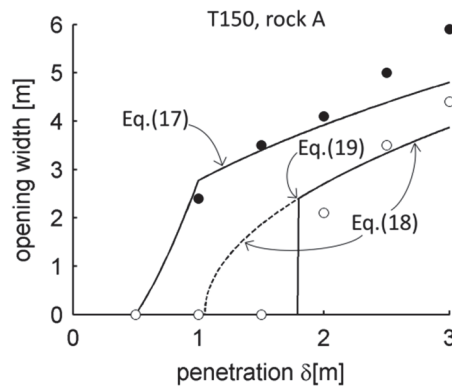


Figure 13. Opening width in the inner and the outer bottom: FE simulations vs. equations.

5 VALIDATION

5.1 Grounding force and energy

In P3, the average grounding forces were calculated with Eq. (2) and Eq. (8) and then compared to the numerical simulations, see Figure 14. In the figure, empty circles present the average grounding force from numerical simulations, filled circles show the energy per unit length from the numerical simulations, solid lines present Eq. (2) and dashed lines Eq. (8). Good correlation exists between the equations and the numerical simulations, except for Eq. (8) and tanker T260, where the deviation is about 15-20%.

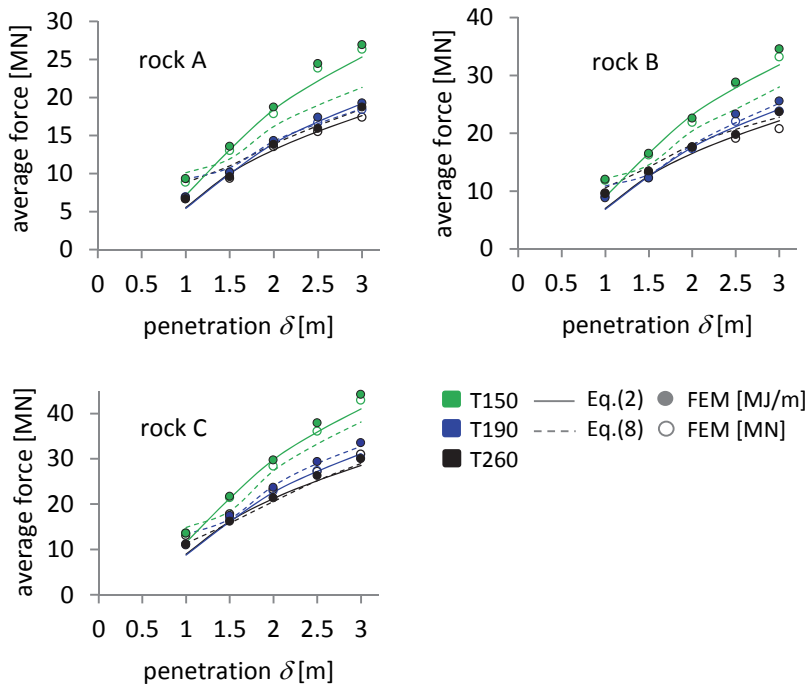


Figure 14. Comparison of average forces.

In order to obtain the comparison to real accidents, the results provided by the derived equations were compared to real accidental data in P2, which were presented in Luukkonen (1999). Based on the ship velocities registered for 18 grounding accidents, Luukkonen (1999) calculated the loss of the kinetic energy E_{kin} and compared it with the deformation energy evaluated with the simplified models given by Minorsky (1959), Vaughan (1977) and Luukkonen (1999). To compare Eq. (2) to these results, the deformation energy was evaluated as a product of the damage length l and the grounding force F , given by Eq. (2). As the report did not include the description for the bottom topology, the rock size

parameter for Eq. (2) was derived using the reported data for the damaged area, see Figure 15. Furthermore, the report gave the vertical extent of the damaged material (Figure 15), which was not necessarily equal to the rock penetration depth used in Eq. (2). Furthermore, as seen in Figure 15, the penetration depth varies along the damaged length. Thus, for precise evaluation of damage pattern, the ship motion dynamics should be included.

The results of the comparison are provided in Table 1 (Table 3 in P2). The results showed that the energy was often over predicted with Eq. (2), indicating that the actual penetration depth δ and the rock size are smaller than approximated, based on the registered maximum vertical extent of damage. Approximately similar level of accuracy was obtained compared to other simplified formulas analyzed in the paper. It can be concluded that the level of reporting the accidental damage and the interpretation of accidental damage data have a substantial influence on the accuracy of the energy predictions.

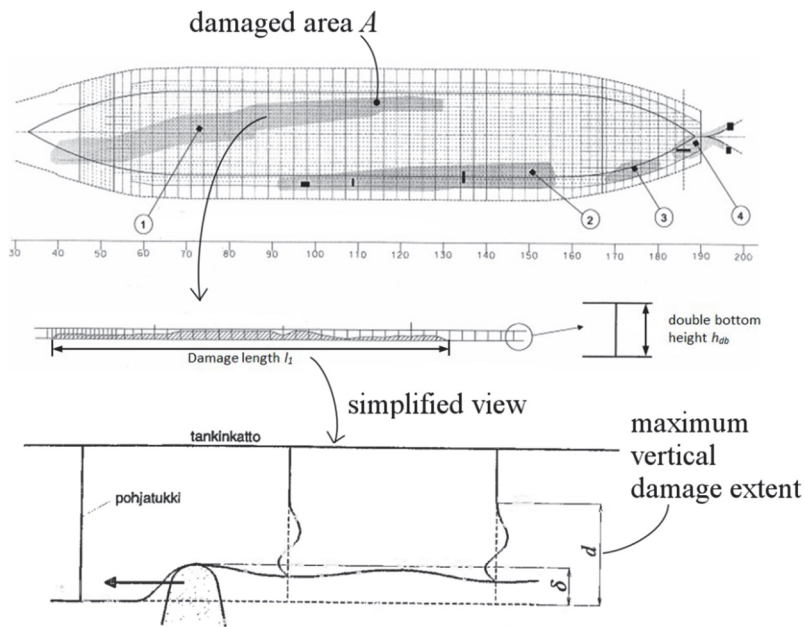


Figure 15. Detailed bottom damage layout of a tanker #1 (Luukkonen, 1999).

Table 1. Comparison between the grounding energies (Table 3 in P2 based on the data adapted from Luukkonen (1999)).

Ship type	Ship length [m]	Minorsky			Vaughan		Luukkonen		Eq. (2)*/l	
		E_{kin} [MJ]	E_{calc} [MJ]	Dif. from E_{kin} [%]						
bulker #1	159,2	691	423	39	387	44	324	53	572	-18
tanker#1	150	208	312	-50	278	-34	233	-12	667 (75,2)	-237 (-64)
RoRo#2	130	86,9	59	32	27	69	23	74	60,8	38
RoRo#3	130	3,2	49	-1424	17	-425	15	-353	10,8	-237
RoRo#4	146	342	837	-144	798	-133	662	-93	897	-400
bulker #2	180,5	43,6	94	-115	61	-41	52	-20	131	-183
ferry#1	142,4	57,8	150	-159	116	-102	99	-71	61,8	-7
ferry#2	139,8	487	825	-69	786	-61	653	-34	512	-19
RoRo#5	118,5	116	96	17	63	45	54	54	72,6	37
RoRo#6	171,6	144	171	-18	137	5	116	19	104	28
RoRo#7	146	174	246	-41	212	-22	178	-2	514	-244
tanker#3	126,5	53,9	53	2	20	62	18	67	43,2	24
bulker #3	134,3	300	351	-17	317	-5	265	12	475	-58
RoRo#8	128,8	245	333	-36	298	-22	250	-2	394	-61
bulker #4	130	24,5	86	-250	53	-117	45	-85	39,2	-42

5.2 Damage opening width

The performance of the derived formulas for the outer and the inner opening widths were analyzed in P2 and in P3. The calculated opening widths were compared to the numerical simulations.

In P2, it was shown that the derived equations estimate the opening widths in the outer and inner bottom with relatively good accuracy and the maximum deviation from the numerical simulations was up to 25%. As the inner bottom failure is dependent on the deformation of the outer bottom, clearly, the opening width is estimated better for the outer bottom than for the inner bottom.

Similar correspondence to the FE simulations was also obtained with the updated formulas in P3 for the tankers with bulkheads, see Figure 16. The figure shows that the outer width is slightly underestimated, especially in the case of larger penetration depths. The deviation is about 20%. For the inner plating opening, the width for lower penetration depths is often over-estimated while at higher penetrations, the estimations are reasonable.

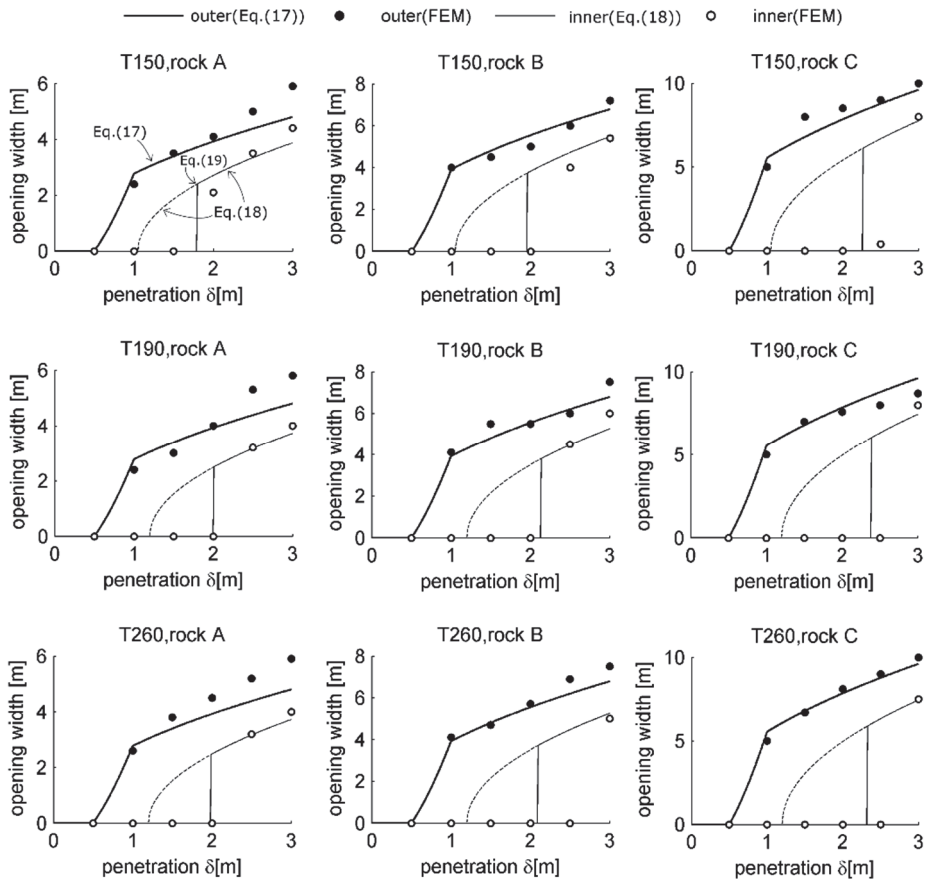


Figure 16. Opening widths compared with numerical simulations in P3.

5.3 Modelling of the rock: mathematical approximation versus real bottom topology

P5 studied the relevancy of the mathematical models used to describe the bottom shapes. Four different bottom topologies were analyzed, each described with four mathematical models and with one model following the real shape of the rock, see Figure 17 (only one of four bottom topologies is shown here). Grounding response in terms of dissipated energy was evaluated for each mathematical and real model. It was revealed that the mathematical representation of the bottom topology is of great importance in grounding force and energy, see Figure 18. The projection area of the contact surface was found to have the strongest correlation with the grounding response and thus, it is the main characteristic to assess the quality of the mathematical bottom model. It was also revealed that the actual surface roughness of real ground shape may trigger deformation mechanisms, which cannot be captured with simple mathematical models. However, a detailed bottom topology is hardly available

for grounding studies. It can be concluded that the parabolic rock model used in this thesis yields to reasonable predictions for the grounding response.

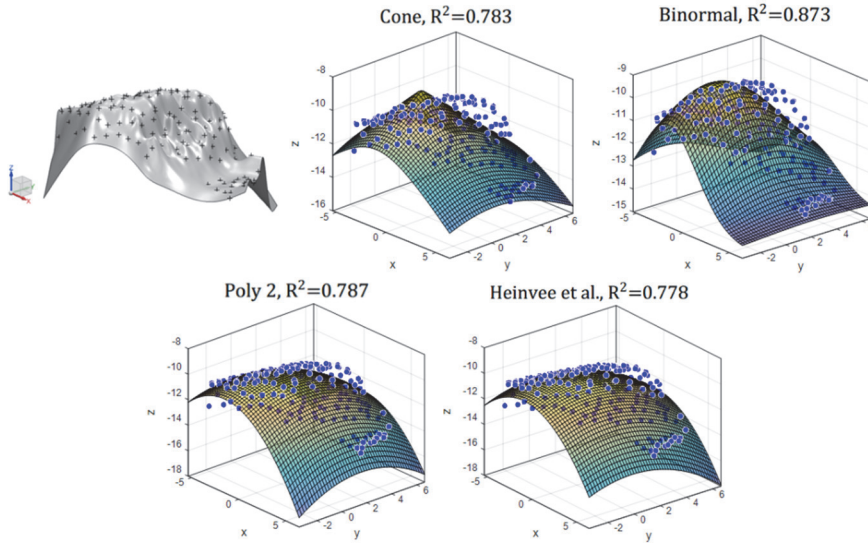


Figure 17. Approximated real rock surface and four fitted models (P4).

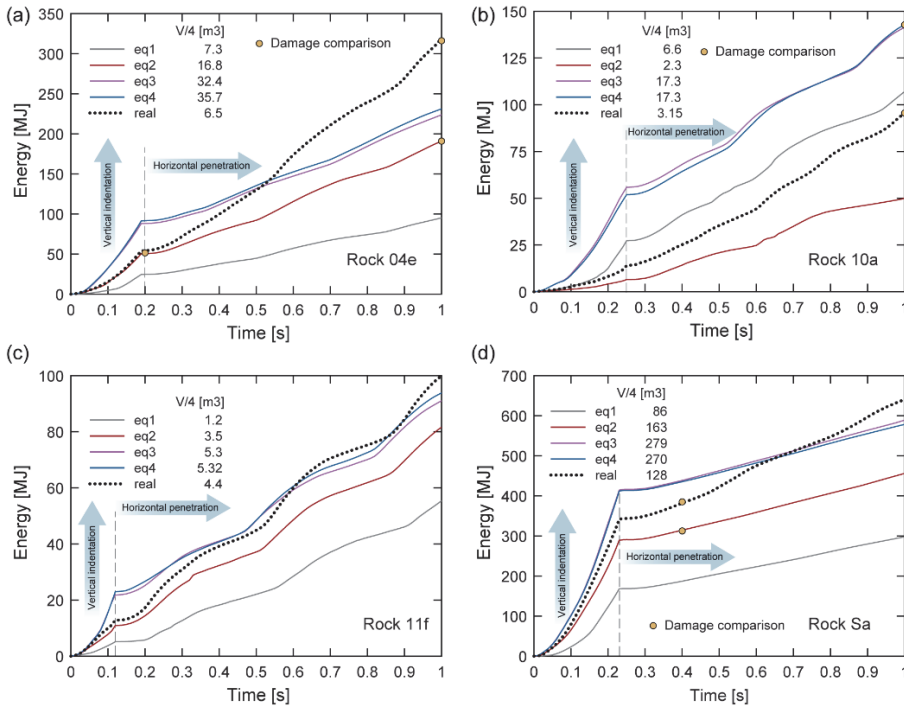


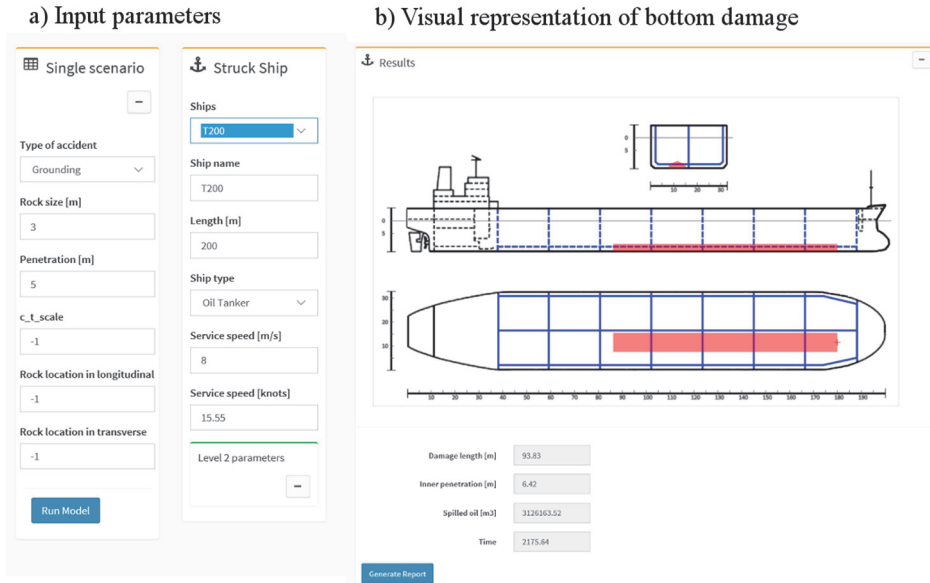
Figure 18. Deformation energy (excluding friction) absorbed during grounding using different rock models (eq4 represent the mathematical model used in this thesis, figure from P4).

6 APPLICATION EXAMPLE

P4 presents the practical application of the derived simplified equations. The damage assessment model developed in this thesis was combined with the oil spill model by Sergejeva et. al. (2013) to form the Accidental Damage and Spill Assessment Model (ADSAM). For a practical application, the ADSAM is developed into a web-based tool in Figure 19. The web-based tool allows for convenient definition of the accidental scenario and provides the report including the damage description and the amount and the duration of the oil spill, see Figure 19c.

To provide even more tangible and crucial information regarding the consequences, ADSAM is linked with the oil spill propagation model by SMHI (2012) and the environmental consequence assessment model by Aps et. al. (2009), Aps et al. (2014). Such integrated simulation environment allows for a rapid analysis of a grounding accident and resulting consequences in terms of the description of the oil spill amount and the environmental consequences. This combined tool can be used in the oil spill recovery exercises or as a tool for risk analysis studies to develop the measures and regulations to improve safety at seas.

The performance of the integrated tool is exemplified in P4 with the case study where a number of grounding accidents with 180 m long tanker were simulated close to the Port of Muuga, Estonia. As the spill propagation model requires actual weather data, it was assumed that the accident takes place on 2nd October 2013. The principle scheme of the analysis of the grounding accident is shown in Figure 20. First, the grounding scenarios were defined via statistical analysis. According to the given scenarios, the ship structural damage, i.e. the size of the damage opening (Figure 20a) and the amount and the duration of the oil spill were calculated (Figure 20b). Given the accident location, spill amount, oil properties and actual weather conditions, the Seatrack Web (SMHI, 2012) simulated the oil spill propagation and the sizes of polluted areas (Figure 20c). Once the spill movement analysis was complete, the SmartResponse Web evaluated of the environmental impact by analyzing the character (e.g. Natura area, Natura Bird area) and environmental sensitivity indices of the polluted area (see Figure 20d).



c) Grounding scenario report

Ship parameters			
Name	T200	Block coefficient	0,77
Type	Oil Tanker	Mass [kg]	61615,32
Length [m]	200,00	Tanks (longitudinal)	7
Service speed [m/s]	8,00	Tanks (transverse)	2
Service speed [knots]	15,60	Tanks total	14
Breadth [m]	32,93	Double bottom height [m]	2,00
Draft (fully loaded) [m]	12,15	Breadth of double hull [m]	2,00
Depth [m]	17,40	Cargo type	Crude oil
Deadweight [t]	51807,96	Cargo density	865,00

Scenario			
Rock size [m]	4,00	Rock location (longitudinal)	-1,00
Penetration [m]	3,00	Rock location (transverse)	-1,00
c_t_scale	-1,00		

Damage		Oil spill	
Length [m]	93,83	Volume (m ³)	3126163,52
Inner width [m]	6,42	Duration	2175,64
Outer width [m]	8,02		

Figure 19. ADSAM web application for the grounding analysis. a) definition of the input parameters, b) the visual representation of the location and the size of the resulting damage opening, c) Report including the results of a simulated grounding scenario.

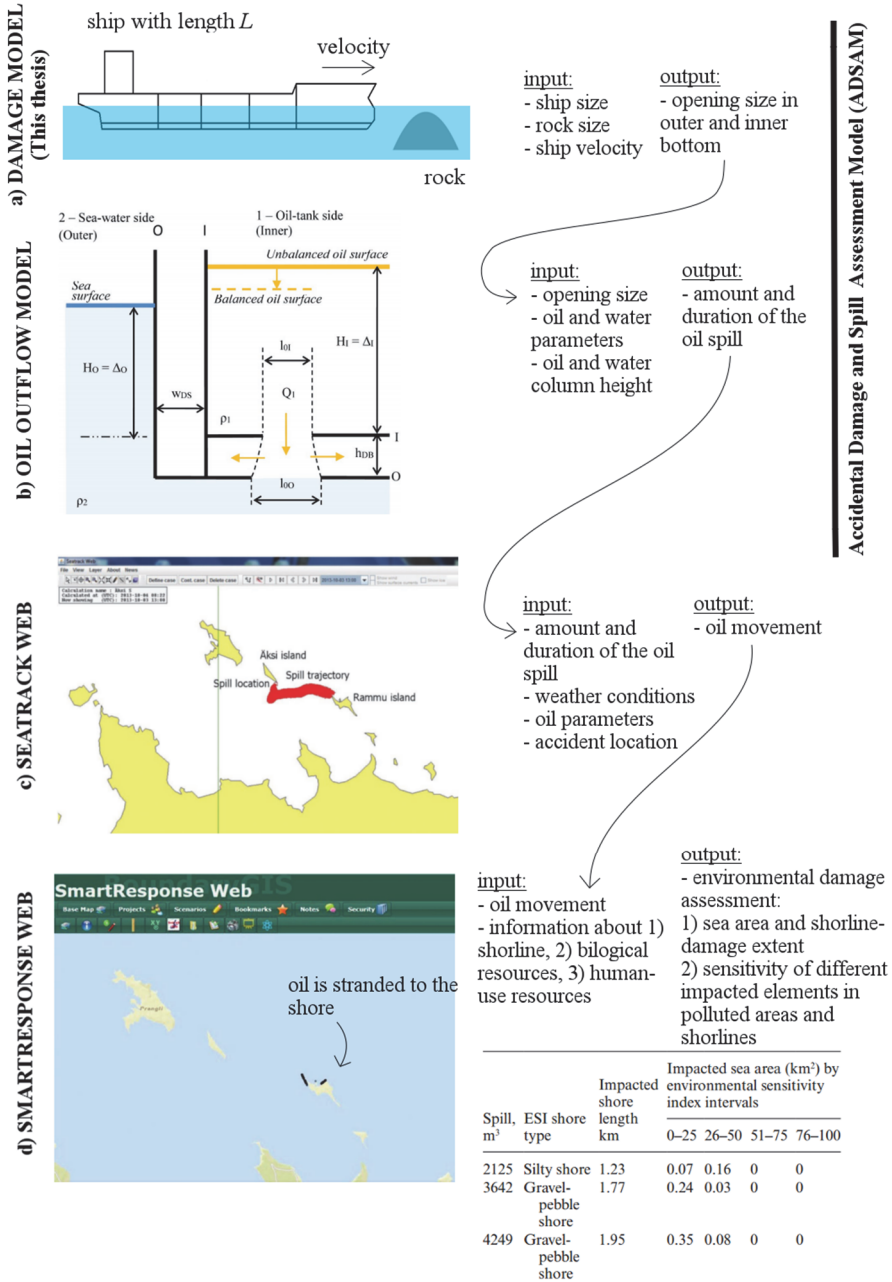


Figure 20. Principle scheme of the integrated model.

7 CONCLUSIONS

Simplified formulas were derived for the grounding force, longitudinal structural damage and the opening width in the inner and outer plating of a tanker's double bottom. The formulas derived are based on the numerical simulations conducted with tankers of different dimensions and different rock sizes at various penetration depths and at two rock transverse positions.

In the derivations, the effects of ship size and structural resistance were separated from those of the rock size and the penetration depth. This allows, for example, modifications of the level of ship's structural resistance while leaving the effect of rock size unchanged. Formulas for the grounding force and the longitudinal extent of structural damage are based on a uniform pressure that depends on the rock size alone. This pressure is scaled to the ship level by using the structural resistance coefficient c_T of the ship and the contact area that depends on the rock size and ship's double-bottom height. It was shown that the resistance coefficient can be predicted by bilinear a function that depends only on the ship length. This behavior was confirmed by a more ship-specific approach where the resistance coefficient was evaluated by using approximated volume of the deformed material.

The analysis of the numerical simulations showed that the longitudinal bulkhead increases the average grounding force substantially. If the intruding rock is directly under the longitudinal bulkhead, the grounding force can be up to 50 % higher compared to the situation when the rock is between the bulkhead and the ship side. This influence is included in the simplified formulas via an additional term depending on the penetration depth. Analysis also revealed that, in general, the transverse bulkhead has small influence on the average grounding force and thus its contribution is not explicitly included in the equations, while its influence is implicitly included in the structural resistance coefficient. The comparison showed good agreement between the average force formula and the numerical results.

In addition, real accidental damage data and the deformation energy obtained with several simplified formulas were compared. The deformation energy calculated as a product of the horizontal grounding force and damage length was predicted at an accuracy similar to that of other simplified methods. However, discrepancies between the simplified formulas and the reported energies occur due to the variations in the quality of the reported data. Furthermore, real accidental data revealed that the penetration depth varies along the damaged length. Thus, for precise evaluation of damage pattern, the ship motion dynamics should be included. This can be done by combining the grounding force and the damage size opening formulas with the external dynamics model such as, for example by Tabri (2010).

Moreover, simulations revealed that a linear relationship exists between the volume of the deformed material and the energy absorbed in the ship grounding. The volume was approximated with a routine. This relationship can be used to

predict the grounding resistance if detailed data for the ship scantlings are available.

The damage opening widths in the outer and inner bottom were given as a function of the penetration depth and the parameters describing the rock size and the ship size. Our analysis showed that the opening width in the outer bottom generally follows the rock width and the opening width in the inner bottom grows similar to the opening width in the outer bottom. Furthermore, the onset of failure in the inner bottom was delayed by approximately $0.75 \cdot h_{db}$ compared to that in the outer bottom. A criterion was included to the inner width formula in order to predict the onset of the inner bottom failure more accurately. It was shown that the outer width is slightly underestimated by the formula especially in the case of larger penetration depths. The deviation is about 20%.

The relevancy of the mathematical models that were used to describe the bottom shapes was studied. Four different bottom topologies were analyzed, each described with four mathematical models and with one model following the real shape of the rock. Grounding response in terms of dissipated energy was evaluated for all the models. It was revealed that the mathematical representation of the bottom topology is of great importance in the grounding response. It was shown that the parabolic rock model used in this thesis yields to sufficiently accurate predictions for the grounding response and thus is applicable for the risk analysis studies.

To provide practical application for the derived simplified equations (damage assessment model), the damage assessment model was combined with the oil spill model (Sergejeva et. al., 2013), spill propagation model (SMHI, 2012) and the environmental consequence assessment model (Aps et. al., 2009), (Aps et. al., 2014) to analyze grounding accidents. This integrated model is of substantial practical value as grounding accidental scenarios can be analyzed within the risk analyses, oil spill recovery operations or exercises. To exemplify the performance of the integrated model, a case study was conducted. It showed possible environmental consequences in terms of spilled shore line lengths and the affected Natura and Natura Bird area if a 180 m long tanker grounds close to the Port of Muuga, Estonia, in October 2013.

This thesis presents a set of simplified practical equations for the calculation of the grounding resistance, the damage extent and the opening widths in a double-bottom structure of a tanker. Since only a limited number of parameters are required to define the grounding scenarios, the simplified equations are easily applicable in risk analysis studies.

REFERENCES

- AbuBakar, A., & Dow, R. S. (2013). Simulation of ship grounding damage using the finite element method. *International Journal of Solids and Structures*, 50(5), 623–636.
- Alsos, H. S., & Amdahl, J. (2007). On the resistance of tanker bottom structures during stranding. *Marine Structures*, 20(4), 218–237.
- Aps, R., Fetissov, M., Herkül, K., Kotta, J., Leiger, R., Mander, U., & Suursaar, U. (2009). Bayesian inference for predicting potential oil spill related ecological risk. *WIT Transactions on the Built Environment*, 108, 149–159.
- Aps, R., Tõnisson, H., Anfuso, G., Perales, J. A., Orviku, K., & Suursaar, Ü. (2014). Incorporating dynamics factor to the Environmental Sensitivity Index (ESI) shoreline classification – Estonian and Spanish example. *Journal of Coastal Research*, (70), 235–240.
- Brunila, O.-P., & Storgård, J. (2012). *Oil Transportation in the Gulf of Finland in 2020 and 2030. Publications from the Centre for Maritime Studies*. Turku.
- Friis-Hansen, P., & Simonsen, B. C. (2002). GRACAT: Software for grounding and collision risk analysis. *Marine Structures*, 15(4-5), 383–401.
- Gao, Z., & Hu, Z. (2015). Structural response of ship bottom floor plating during shoal grounding, 685–692.
- Hong, L., & Amdahl, J. (2008). Crushing resistance of web girders in ship collision and grounding. *Marine Structures*, 21(4), 374–401.
- Hong, L., & Amdahl, J. (2012). Rapid assessment of ship grounding over large contact surfaces. *Ships and Offshore Structures*, 7(1), 5–19.
- IACS. (2014). *Common Structural Rules for Bulk Carriers and Oil Tankers*. London: International Association of Classification Societies Ltd.
- IMO. (1995). *Interim guidelines for approval of alternative methods of design and construction of oil tankers under regulation 13F(5) of Annex I of MARPOL 73/78, Resolution MEPC 66(37)*.
- IMO. (2003). *Revised Interim Guidelines for the Approval of Alternative Methods of Design and Construction of Oil Tankers under Regulation 13F(5) of Annex I of MARPOL 73/78, Resolution MEPC 110(49)*.
- Kitamura, O. (2002). FEM approach to the simulation of collision and grounding damage. *Marine Structures*, 15, 403–428.
- Kujala, P., Hänninen, M., Arola, T., & Ylitalo, J. (2009). Analysis of the marine traffic safety in the Gulf of Finland. *Reliability Engineering & System Safety*, 94(8), 1349–1357.
- Kõrgesaar, M. (2015). *Modeling ductile fracture in ship structures with shell elements. Doctoral thesis*. Aalto University.
- Kõrgesaar, M., & Romanoff, J. (2014). Influence of mesh size, stress triaxiality and damage induced softening on ductile fracture of large-scale shell structures. *Marine Structures*, 38, 1–17.
- Little, P., Pippenger, D., & Simonsen, B. . (1996). Development of a

- computational model for predicting damage to tankers. In *Proceedings of the International Conference on Designs and Methodologies for Collision and Grounding Protection of Ships*. San Francisco.
- Liu, B., & Guedes Soares, C. (2015). Simplified analytical method for evaluating web girder crushing during ship collision and grounding. *Marine Structures*, *42*, 71–94.
- Luukkonen, J. (1999). *Vauriotilastot suomen aluevesien karilleajoista ja pohjakosketuksista. M-240*. Espoo.
- Minorsky, V. U. (1959). An Analysis of Ship Collisions with Reference to Protection of Nuclear Power Plants. *Journal of Ship Research*, 1–4.
- Naar, H., Kujala, P., Simonsen, B. C., & Ludolph, H. (2002). Comparison of the crashworthiness of various bottom and side structures. *Marine Structures*, *15*, 443–460.
- Ohtsubo, H., & Wang, G. (1995). An upper-bound solution to the problem of plate tearing. *Journal of Marine Science and Technology*, *1*(1), 46–51.
- Pedersen, P. T. (2010). Review and application of ship collision and grounding analysis procedures. *Marine Structures*, *23*(3), 241–262.
- Pedersen, P. T., & Zhang, S. (2000). Effect of ship structure and size on grounding and collision damage distributions. *Ocean Engineering*, *27*, 1161–1179.
- Rawson, C., Crake, K., & Brown, A. (1998). *Assessing the Environmental Performance of Tankers in Accidental Grounding and Collision*. SNAME Transactions (Vol. 106).
- Rodd, J. L., & Sikora, J. P. (1995). Double Hull Grounding Experiments. In *Proceedings of the Fifth (1995) International Offshore and Polar Engineering Conference* (Vol. IV, pp. 446–456). The Hague.
- Samuelides, M., Voudouris, G., Toullos, M., Amdahl, J., & Dow, R. (2007). Simulation of the behaviour of double bottoms subjected to grounding actions. In *4th International Conference on Collision and Grounding of Ships* (pp. 93–102). Hamburg.
- Sergejeva, M., Laanearu, J., & Tabri, K. (2013). Hydraulic modelling of submerged oil spill including tanker hydrostatic overpressure. In *4th International Conference on Marine Structures* (pp. 209–217). Espoo: Taylor & Francis.
- Simonsen, B. . (1999). *Theory and validation for the collision module*. Joint MIT-Industry Program on Tanker Safety, Report 66.
- Simonsen, B. ., & Wierzbicki, T. (1997). Plasticity, fracture and friction in steady-state plate cutting. *International Journal of Impact Engineering*, *19*(8), 667–691.
- Simonsen, B. C. (1997). Ship grounding on rock - I. Theory. *Marine Structures*, *10*, 519–562.
- Simonsen, B. C., Törnqvist, R., & Lützen, M. (2009). A simplified grounding damage prediction method and its application in modern damage stability requirements. *Marine Structures*, *22*, 62–83.
- Sirkar, J., Ameer, P., Brown, A., Goss, P., Michel, K., & Willis, W. (1997). *A*

- Framework for Assessing the Environmental Performance of Tankers in Accidental Groundings and Collisions. SNAME Transactions* (Vol. 105).
- SMHI. (2012). Manual Seatrack Web—a user-friendly system for forecasts and backtracking of drift and spreading of oil, chemicals and substances in water. Retrieved from <https://stw-helcom.smhi.se/>
- Zhang, S. (2002). Plate tearing and bottom damage in ship grounding. *Marine Structures, 15*, 101–117.
- Zhu, L., James, P., & Zhang, S. (2002). Statistics and damage assessment of ship grounding. *Marine Structures, 15*, 515–530.
- Tabri, K. (2010). *Dynamics of ship collisions. Doctoral thesis*. Aalto University, Espoo.
- Valdez Banda, O. A., Goerlandt, F., Kuzmin, V., Kujala, P., & Montewka, J. (2016). Risk Management Model of Winter Navigation Operations. *Marine Pollution Bulletin, 108*, 242–262.
- Walters, C. . (2014). Framework for adjusting for both stress triaxiality and mesh size effect for failure of metals in shell structures. *Int. J. Crashworthines, 19*(1), 1–12.
- Wang, G., Arita, K., & Liu, D. (2000). Behavior of a double hull in a variety of stranding or collision scenarios. *Marine Structures, 13*, 147–187.
- Wang, G., Ohtsubo, H., & Liu, D. (1997). A Simple Method for Predicting the Grounding Strength of Ships, *41*(3), 241–247.
- Vaughan, H. (1977). *Vaughan H. Damage to ships due to collision and grounding. DnV Technical Report No. 77-345*. Oslo.
- Woelke, P. B., Shields, M. D., Abboud, N. N., & Hutchinson, J. W. (2013). Simulations of ductile fracture in an idealized ship grounding scenario using phenomenological damage and cohesive zone models. *Computational Materials Science, 80*, 79–95.
- Vredeveltdt, A.W; Wevers, L, T. (1995). Full scale grounding experiments. In *Conference on Prediction Methodology of Tanker Structural Failure & Consequential Oil Spill*. Tokyo.
- Yu, Z., Hu, Z., & Wang, G. (2015). Plastic mechanism analysis of structural performances for stiffeners on bottom longitudinal web girders during a shoal grounding accident. *Marine Structures, 40*, 134–158.

CURRICULUM VITAE

1. Personal data

Name: Martin Heinvee
Date and place of birth: 06.12.1984, Võru, Estonia
Nationality: Estonian
E-mail: martin.heinvee@ttu.ee
Phone: (+372) 555 77 130

2. Education

University	Graduation year	Education (field of study/degree)
Tallinn University of Technology	2011	Mechatronics/MSc
Tallinn University of Technology	2007	Mechatronics/BSc

3. Languages

Language	Level
Estonian	Native language
English	High
Russian	Low

4. Professional employment

Date	Organisation	Position
2011-...	TUT Department of Mechanics	engineer
2007-2009	TUT Department of Mechatronics	engineer

5. Defended theses

“Double-hull breaching energy in ship-tanker collision”, Bachelor’s degree.

6. Main areas of scientific work

Non-linear response assessment of marine structures including accidental loads such as collision, grounding.

7. Scientific Work

Sormunen, O-V., Kõrgesaar, M., Tabri, K., Heinvee, M., Urbel, A., Kujala, P. (2016). **Comparing rock shape models in grounding damage modelling**. *Marine Structures*. (Accepted at 08.07.2016).

Heinvee, M., Tabri, K., Kõrgesaar, M., Urbel, A. (2016). **Influence of longitudinal and transverse bulkheads on ship grounding resistance.** *Proceedings of 7th International Conference on Collision and Grounding of Ships and Offshore Structures: 7th International Conference on Collision and Grounding of Ships and Offshore Structures, 15-18.06.2016, Ulsan, South-Korea.* SNAK, pp. 99–109.

Tabri, K., Aps, R., Mazaheri, A., Heinvee, M., Jönsson, A., Fetissof, M. (2015). **Modelling of structural damage and environmental consequences of tanker grounding.** *In: Analysis and Design of Marine Structures V: 5th International Conference on Marine Structures, 25–27.03.2015, Southampton UK.* Taylor & Francis, pp. 703–710.

Heinvee, M., Tabri, K. (2015). **A simplified method to predict grounding damage of double bottom tankers.** *Marine Structures*, pp. 43, 22–43. [DOI: 10.1016/j.marstruc.2015.04.002.]

Heinvee, M., Urbel, A., Tabri, K. (2013). **Dynamic grounding analysis.** *In: Proceedings of the 2nd International Conference on Optimization and Analysis of Structures: International Conference on Optimization and Analysis of Structures, 25-27.08.2013, Tartu, Estonia.* University of Tartu Press, pp. 39–44.

Heinvee, M., Tabri, K., Kõrgesaar, M. (2013). **A simplified approach to predict the bottom damage in tanker grounding.** *Proceedings of 6th International Conference on Collision and Grounding of Ships and Offshore Structures: 6th International Conference on Collision and Grounding of Ships and Offshore Structures, 17-19.06.2013, Trondheim, Norway.* Taylor & Francis, pp. 161–171.

Signature:

Date

ELULOOKIRJELDUS

1. Isikuandmed

Nimi: Martin Heinvee
Sünniaeg ja -koht: 06.12.1984, Võru, Eesti
Kodakondsus: Eestlane
E-post: martin.heinvee@ttu.ee
Telefon: (+372) 555 77 130

2. Hariduskäik

Ülikool	Lõpetamise aeg	Haridus
Tallinn University of Technology	2011	Magistrikraad mehhatroonikas
Tallinn University of Technology	2007	Bakalaureusekraad mehhatroonikas

3. Keelteoskus

Keel	Tase
Eesti keel	Emakeel
Inglise keel	Kõrg
Vene keel	Alg

4. Teenistuskäik

Töötamise aeg	Asutus	Amet
2011-...	TTÜ Mehaanikainstituut	insener
2007-2009	TTÜ Mehhatroonikainstituut	insener

5. Kaitstud lõputööd

“Tankeri küljekonstruktsiooni purunemisenergia kokkupõkel laevaga”, bakalaureusetöö.

6. Teadustöö põhisuunad

Mittelineaarselt käituvate konstruktsioonide analüüs sh. laevakonstruktsioonid karilesõidu või laevade kokkupõrke korral.

7. Teadustöö

Sormunen, O-V., Kõrgesaar, M., Tabri, K., Heinvee, M., Urbel, A., Kujala, P. (2016). **Comparing rock shape models in grounding damage modelling.** *Marine Structures*. (Avaldamiseks vastu võetud 08.07.2016).

Heinvee, M., Tabri, K., Kõrgesaar, M., Urbel, A. (2016). **Influence of longitudinal and transverse bulkheads on ship grounding resistance.** *Proceedings of 7th International Conference on Collision and Grounding of Ships and Offshore Structures: 7th International Conference on Collision and Grounding of Ships and Offshore Structures, 15-18.06.2016, Ulsan, Lõuna-Korea.* SNAK, lk. 99–109.

Tabri, K., Aps, R., Mazaheri, A., Heinvee, M., Jönsson, A., Fetissof, M. (2015). **Modelling of structural damage and environmental consequences of tanker grounding.** *In: Analysis and Design of Marine Structures V: 5th International Conference on Marine Structures, 25–27.03.2015, Southampton UK.* Taylor & Francis, lk. 703–710.

Heinvee, M., Tabri, K. (2015). **A simplified method to predict grounding damage of double bottom tankers.** *Marine Structures*, lk. 43, 22–43. [DOI: 10.1016/j.marstruc.2015.04.002.]

Heinvee, M., Urbel, A., Tabri, K. (2013). **Dynamic grounding analysis.** *In: Proceedings of the 2nd International Conference on Optimization and Analysis of Structures: International Conference on Optimization and Analysis of Structures, 25-27.08.2013, Tartu, Estonia.* University of Tartu Press, lk. 39–44.

Heinvee, M., Tabri, K., Kõrgesaar, M. (2013). **A simplified approach to predict the bottom damage in tanker grounding.** *Proceedings of 6th International Conference on Collision and Grounding of Ships and Offshore Structures: 6th International Conference on Collision and Grounding of Ships and Offshore Structures, 17-19.06.2013, Trondheim, Norra.* Taylor & Francis, lk. 161–171.

Allkiri:

Kuupäev:

PUBLICATIONS

PUBLICATION I

Heinvee, M., Tabri, K., Kõrgesaar, M. (2013). **A simplified approach to predict the bottom damage in tanker grounding.** *Proceedings of International Conference on Collision and Grounding of Ships and Offshore Structures: International Conference on Collision and Grounding of Ships and Offshore Structures*, 17-19.06.2013, Trondheim, Norway. Taylor & Francis, 161–171.

A simplified approach to predict the bottom damage in tanker grounding

Martin Heinvee, Kristijan Tabri

Dept. of Civil Engineering, Faculty of Mechanical Engineering, Tallinn University of Technology, Estonia

Mihkel Kõrgesaar²

Dept. of Applied Mechanics / Marine Technology, Aalto University, Espoo, Finland

ABSTRACT: A simplified formula to evaluate the grounding force and the longitudinal extent of structural damage in tanker groundings is derived in the paper. The formula is derived based on numerical simulations. First, a set of grounding accidents are simulated numerically for tankers of different dimensions- 120, 190 and 260 m in length. The simulations are conducted for five different penetration depths and for several rock/ground topology. Thus, the numerical simulations provide a response of different structural configurations to different combinations of penetration depth and bottom topology. Average horizontal grounding force is analysed and presented through the pressure acting on the contact surface between the rock and the ship's double-bottom. It is shown in the paper, that this pressure can be described as a function of rock size and a constant depending on the ship size. Simplified equations are derived for the average contact force and the longitudinal length of the penetration. Comparison to numerical simulations reveals that such a simplified equation is capable of describing the grounding force for penetration depths larger than 0.5 m i.e. for the scenarios, where significant structural damage occurs.

1 INTRODUCTION

The paper seeks for a simple formula for a rapid prediction of grounding damage of double hull tankers. Such simplified formulation could be used in risk analysis studies where there are no specific information regarding the structural arrangement of ships and the main available parameters are the main dimensions of the ships.

Several simplified models have been developed to describe a ship grounding accidents. The models either base on a simplified closed form expressions (Simonsen et al, 2009; Hong & Amdahl, 2012) or on numerical simulations (Alsos & Amdahl, 2007). Precise numerical simulations hardly suit to risk analysis studies as the simulation of a single scenario will take several hours. On the other hand, simplified models are often limited to a certain sea bottom topology or to ship's structural configuration. Moreover, often the methods require that to some extent the damage mechanics are prescribed: for example, the description of contact energy is based on the fracture propagation in the bottom plating.

Paper aims to derive a simple formulation based on small number of parameters that describe the structural resistance of a tanker in a grounding acci-

dent. The principle of the simplified approach is presented in Figure 1. The approach is similar to Ehlers & Tabri (2012), where such combined approach was presented for the analysis of ship collisions. The simplified formula is derived based on a number of numerical grounding simulations. Three double-bottom tankers of different length are included in the analysis- 120, 190 and 260 m in length. Each tanker is analyzed for five different penetration depths and for four different rock sizes. First, numerical simulations are conducted in displacement controlled manner as the aim of the numerical analysis is to study structural resistance alone. Analyses provide the contact force time-history for each grounding scenario. As here our aim is to evaluate the extent of damage, we concentrate on the horizontal grounding force as a main energy absorbing mechanism. Based on these time histories the average horizontal contact force is evaluated. Evaluating the average horizontal grounding forces for all the scenarios for a certain ship gives as a result a set of curves that describe the dependency of the average grounding force as a function of penetration depths and the rock size.

Other grounding simulation models such as GRACAT for example, are not included in the analysis as they require rather detailed presentation of the ship structure.

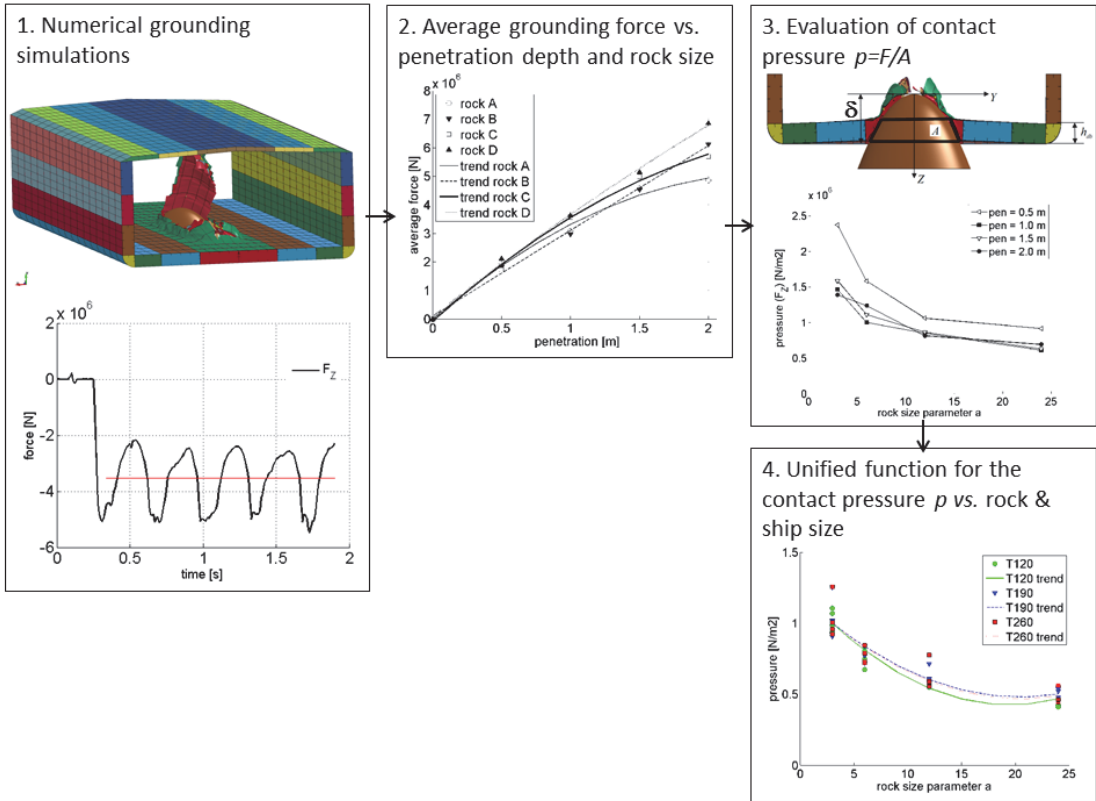


Figure 1. Principle of the simplified approach.

These curves are normalized with respect to the contact area between the rock and ship double-bottom providing a contact pressure that acts on the rock. Pressure dependence on the rock size, penetration depth and ship size is analyzed in the paper. It is shown in the paper that the pressure as a function of penetration depth and the rock size is similar for all the ships, only its magnitude depends on the actual ship size. Once the pressure acting between the ship and the rock is known from a simple relation, the horizontal grounding force can be evaluated as a product of this pressure and the rock dimensions. Furthermore, knowing the ship mass and the velocity, a simple equation can be derived for the longitudinal extent of the damage. It is shown in the paper, that such a simplified approach can provide a rapid estimation of horizontal structural resistance when compared to the numerical simulations.

2 NUMERICAL GROUNDING SIMULATIONS

This chapter presents an overview of numerical grounding simulations. The principle of numerical modeling and the post-processing of the analysis results is given.

2.1 FE models of tankers

Three double hull tankers with different dimensions are modeled. The cross-sections with the main structural dimensions are given in Figure 2 and in Table 1. Hereinafter we use superscripts T120, T190 and T260 to denote the tankers. If the superscript is replaced by i , it means that the description is common to all three ships.

Table 1. Main dimensions and parameters of tankers used in numerical simulations

Parameter/Tanker	T120	T190	T260
Length [m]	120	190	260
Breadth [m]	16	24	32
Depth [m]	8	16	18
Double-bottom height [m]	0.8	1.2	1.6
Outer plating thick. [mm]	10	13	15
Tank-top thick. [mm]	11	13	15
Girder spacing [m]	2.6	3.0	3.2
Floor spacing	2.2	3.5	4.0

Typical ship-building steel with yield stress of 235 MPa is used in the analysis. True stress-strain curve is presented in Figure 4. Only the double bottom structures are modeled in detail. The longitudinal and transverse bulkheads are left out from the analysis to maintain the conservative nature of the ap-

proach. The transverse bulkheads would result in rapid increase of the grounding resistance as could be seen from the numerical analysis presented by AbuBakar & Dow (2012), for example.

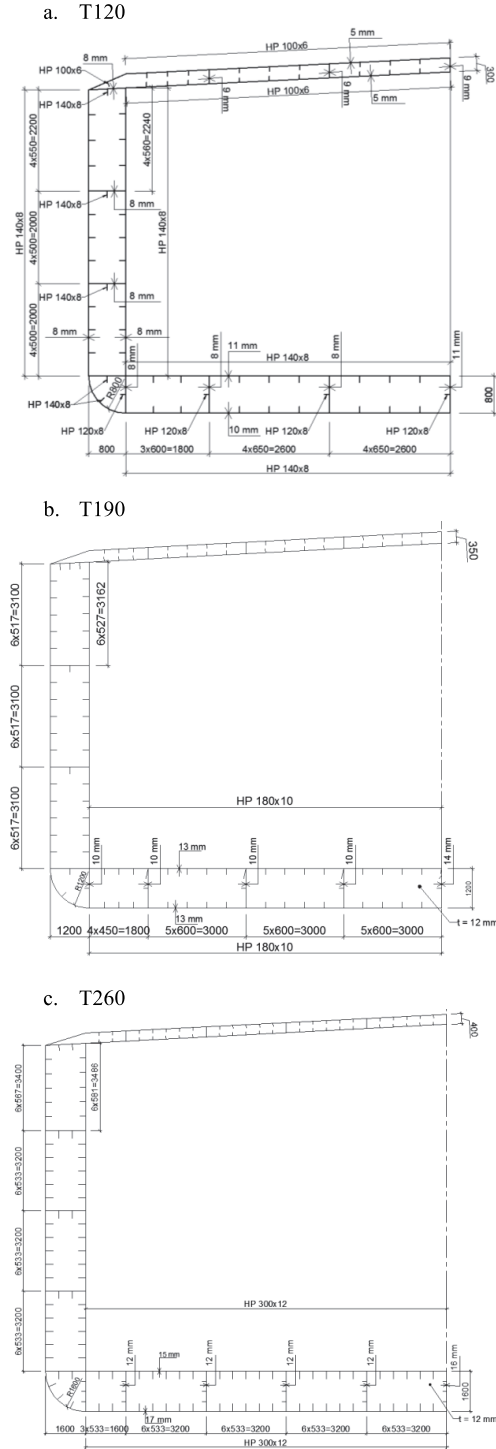


Figure 2. Tanker cross-sections

The corresponding finite element models are presented in Figure 3. The structure is modeled using quadrilateral Belytschko-Lin-Tsay shell elements with 5 integration points through their thickness. The prevailing element-length in the double-bottom structure was around 50-75 mm to properly account for the non-linear structural deformations.

Standard LS-DYNA hourglass control and automatic single surface contact (friction coefficient of 0.3) is used for the displacement controlled grounding simulations. The rigid rock first moves to a required penetration depth and continues to move at constant penetration depth along the ship at a constant velocity of 10 m/s. The nodes at the forward and aft end of the models are fixed.

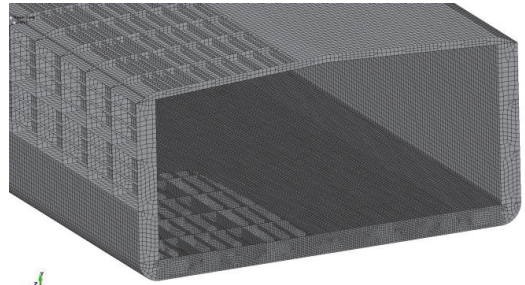


Figure 3. Finite element model of a tanker.

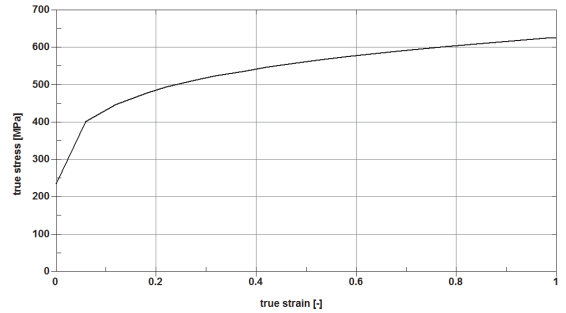


Figure 4. True stress-strain curve for S235 steel

The possible material failure is modeled using the thru thickness criteria, often referred to as Germanischer Lloyd criteria (Lehmann et al, 2001). This criterion establishes an element thickness and dimension dependent critical thickness strain after which an element is removed from the simulation. To evaluate the critical thru thickness strain at the moment of fracture, an empirical criterion is presented by (Lehmann et al, 2001):

$$\varepsilon_f(l_e) = \varepsilon_g + \varepsilon_e \cdot \frac{t}{l_e} \quad (1)$$

where ε_g is the uniform strain and ε_e is the necking strain, t is the plate thickness and l_e is the individual element length. It is commonly recommended that the ratio l_e/t is not less than 5 for shell element. The

values of uniform and necking strain achieved from thickness measurements related to the calculated stress states given in [3] are 0.056 for the uniform strain and 0.54 for the necking strain in the case of shell elements.

2.2 Grounding scenarios

The numerical simulations are conducted for five different penetration depths δ and for several rock/ground topologies. The penetration depth d is defined as the relative distance between the tip of the rock and the ship bottom, see Figure 8. Different rock sizes are selected with the purpose to determine rock size effect to structural resistance. Numerical simulations were conducted with four different rock sizes covering the range from sharp rock to blunt "shoal"-type rock.

The shapes of all the rocks are given through a polynomial equation as

$$z = \frac{y^2}{a} \quad (2)$$

where the parameter a defines the actual size of the rock, which values for different rocks sized are given in Table 2. The rocks are depicted in Figure 5.

Table 2. Rock size parameters

	rock A	rock B	rock C	rock D
a [m]	3	6	12	24

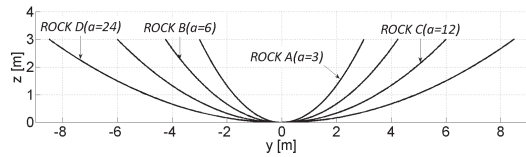


Figure 5. Different rocks used in the simulations.

With each rock, five penetration depths were simulated – 0.5, 1.0, 1.5, 2.0 and 2.5 m. Thus, the total number of numerical simulations became to $3 \times 4 \times 5 = 60$.

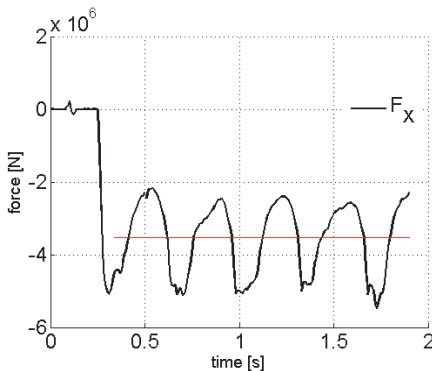


Figure 6. Numerical simulations: horizontal contact force as a function of time

2.3 Grounding force in numerical simulations

The numerical simulations provide a response of different structural configurations for different combinations of ship draft and bottom topology. Typical outcome of a simulation is information regarding the contact force and the description of damage.

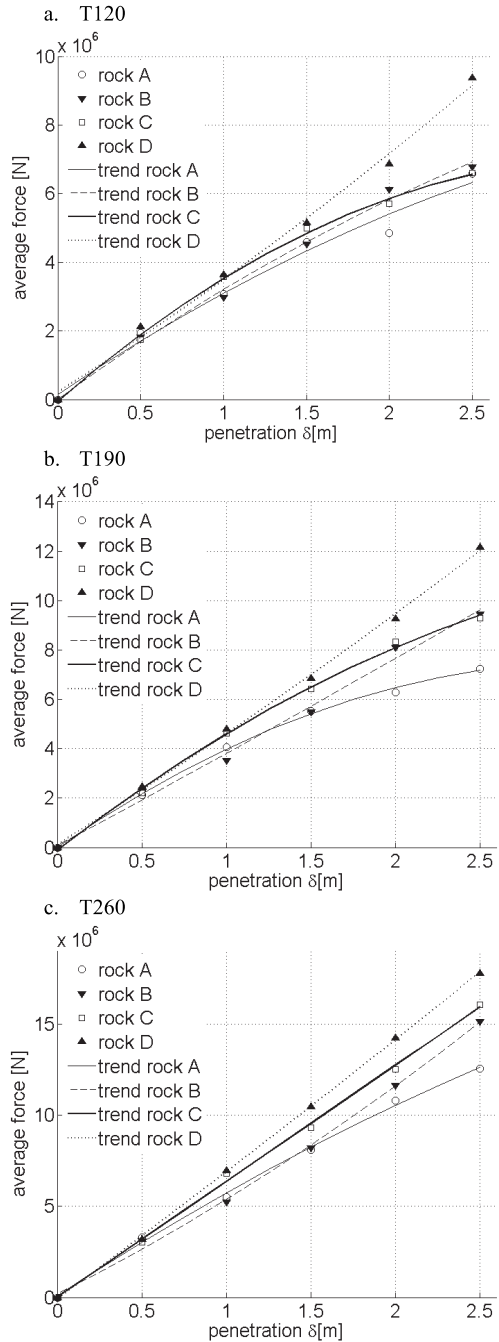


Figure 7. Average contact force as a function of penetration depth

We concentrate on the horizontal grounding force, which typical time-history is presented in Figure 6. We use the average horizontal grounding force to present the outcome of a numerical simulation with a single output value. This value is obtained as an average of the grounding force evaluated over the time where constant penetration depth has been reached; see the constant horizontal line in Figure 6. For brevity, hereinafter when referring to contact force and contact pressure the average contact force and average contact pressure are considered if not stated otherwise.

These average force values are presented as a function on penetration depths in Figure 7 with the ship and the rock size as variables. As expected, larger ships result in higher contact force. The rocks A and B cause parabolic force increase for tankers T120 and T190, while forces induced by rocks C and D increase linearly. For largest tanker T260, horizontal force increases linearly with all the rocks as the inner hull is penetrated later. The grounding force decreases as the bottom plating is thorn open. As the height of the double-bottom increases with ship length, the inner hull fractures later for larger ships resulting in more linear behavior for the average force. Since the double-bottom is highest in the case of tanker T260, then the inner is thorn later and the force-penetration curve remains linear for high penetration depths. However, it can be concluded that the contact force can be considered proportional to the penetration depth in all the simulated scenarios.

3 CONTACT PRESSURE AS A FUNCTION OF ROCK AND SHIP SIZE

To be able to express the grounding resistance conveniently it should be expressed with minimum number of variables. Average horizontal grounding force presented in Figure 7 includes the contribution from ship structural configuration, rock size and penetration depth. To reduce the number of unknowns, it is more convenient to express the resistance through pressure rather than force.

Therefore, here the aim is to derive an equation that gives pressure acting on a contact surface by including rock and ship sizes as independent variables. Such equation would make it possible to find pressure and thereby also the corresponding horizontal contact force with minimal effort. Furthermore, if the contact force is known, the longitudinal extent of the bottom damage can be evaluated. Figure 7 revealed that the relation between the contact force and the penetration depth is nearly linear. Moreover, for most of the scenarios the contact force increases together with the rock size. To study these depend-

encies and to be able to separate the effects of the structural configuration from those of the increasing contact area, we divide the contact force with the contact area i.e. evaluate the contact pressure. Direct contact between the rock and the bottom structure is within the height h_{db} of the double bottom. For the sake of simplicity, we define the contact area A as a projection of the contact surface to YZ plane, see Figure 8. With the shape of the rock defined with eq.(2) the contact area A within the double-bottom can be evaluated as

$$A(\delta, h_{db}, a) = \int_{\delta-h_{db}}^{\delta} 2 \cdot \sqrt{a \cdot z} \cdot dz \quad (3)$$

For $\delta \leq h_{db}$, eq. (3) can be rewritten to

$$A = \frac{4}{3} \sqrt{a} \cdot \delta^{\left(\frac{3}{2}\right)} \quad \text{when } \delta_z \leq h_{db} \quad (4)$$

and for $\delta > h_{db}$

$$A = \frac{4}{3} \sqrt{a} \cdot \left[\delta^{\left(\frac{3}{2}\right)} - (\delta - h_{db})^{\left(\frac{3}{2}\right)} \right] \quad \text{when} \quad (5)$$

$\delta > h_{db}$

The contact pressure can now be evaluated from

$$p(a, \delta, h_{db}) = \frac{F_H}{A} \quad (6)$$

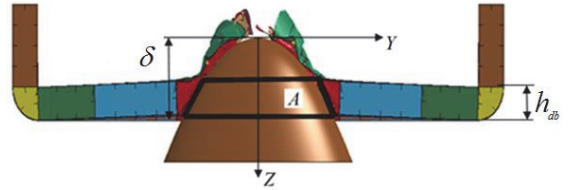


Figure 8. Cross-section of a ship during grounding

Applying eq. (6) on the force values presented on Figure 7 gives the discrete pressure values p as a function of the penetration depth and the rock size. These pressures are presented on Figure 9. On each graph, four pressure-penetration curves are drawn, each corresponding to a certain rock. Two patterns can clearly be recognized from pressure distributions. With lower penetration depths the pressure value is significantly higher compared to larger depths. With the penetration depths larger than 1.0 m the pressures remain almost constant.

This pattern becomes even more obvious when presenting the pressure as a function of rock size parameter a , see Figure 10. The figure reveals that when disregarding penetration depth 0.5 m the pressure value is almost constant with respect to the penetration depth and depends only on the rock size parameter a . For these higher penetration depths the pressure as a function of rock size can be approximated with a polynomial. Moreover, the shape of the

polynomial appears to be similar for all three ships while its magnitude differs. The function describing this uniform shape and the parameter describing the magnitude can now be evaluated.

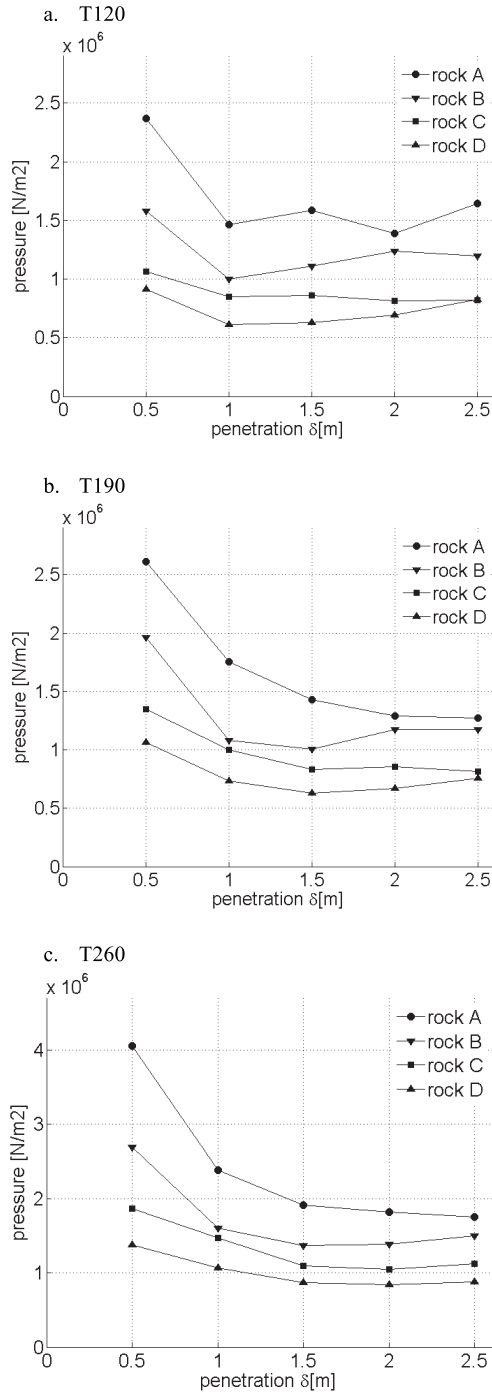


Figure 9. Pressure as a function of penetration depth

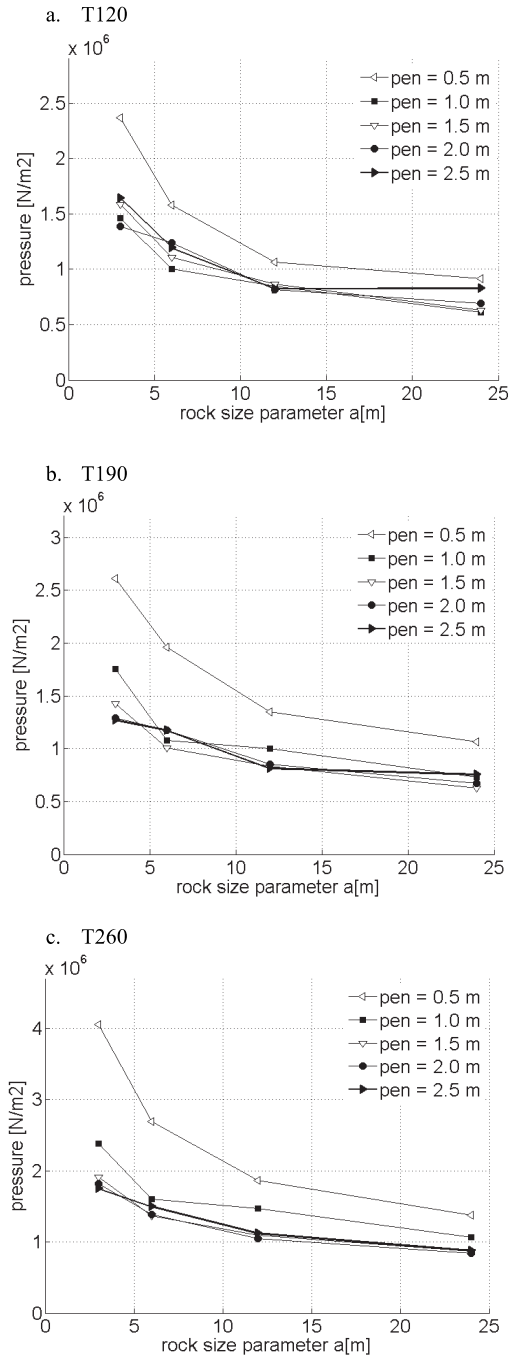


Figure 10. Pressure as a function of rock size parameter a [m]

For that we collect all the pressure points p^i from Figure 10, excluding those for $\delta=0.5$ [m] and present them in Figure 11a. The polynomial regression lines P^i are drawn for each ship i using these pressure points. To derive the uniform shape we normalize the pressures p_i and present them in Figure 11b together with the corresponding regression lines. For each ship i the normalization pressure p_{norm}^i is eval-

uated as an average pressure corresponding to the smallest rock size ($a=3$) as follows:

$$p_{norm}^i = \frac{\sum_{j=1}^4 p^i(a=3, \delta_j, h_{db}^i)}{4} \quad (7)$$

where

$$\begin{aligned} \sum_{j=1}^4 p^i &= p^i(a=3, \delta_1=1.0, h_{db}^i) + \\ &+ p^i(a=3, \delta_2=1.5, h_{db}^i) + \\ &+ p^i(a=3, \delta_3=2.0, h_{db}^i) + p^i(a=3, \delta_4=2.5, h_{db}^i) \end{aligned}$$

and denominator refers to the number of pressure values and h_{db}^i is the double-bottom height of the ship i .

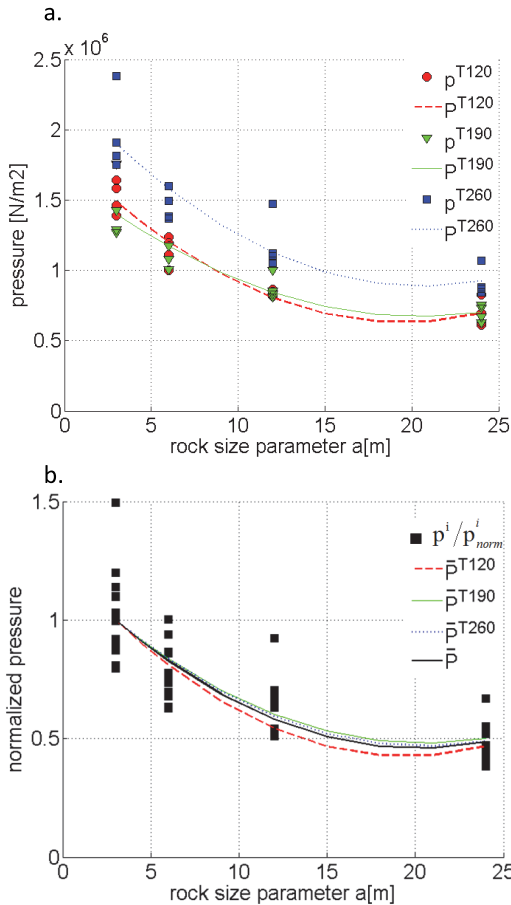


Figure 11. Pressure (a) and normalized pressure (b)

Since these normalized regression lines in Figure 11b match relatively well, they can be presented via uniform regression line \bar{P} that is fitted through all the normalized pressure values and takes the following shape:

$$\bar{P}(a) = \quad (8)$$

$$1.8 \cdot 10^{-3} a^2 - 7.4 \cdot 10^{-2} a + 1.2$$

To scale the \bar{P} to proper magnitude corresponding to the actual ship (Figure 11a), it has to be multiplied by a coefficient \bar{c}_T^i describing the ship's structural resistance, thus it becomes:

$$\begin{aligned} P^i(a, c_T) &= \bar{c}_T^i \cdot \bar{P} = \\ \bar{c}_T^i \cdot (1.8 \cdot 10^{-3} a^2 - 7.4 \cdot 10^{-2} a + 1.2) \end{aligned} \quad (9)$$

For each ship, the coefficient \bar{c}_T^i is evaluated as a ratio between the areas under the curves $P^i(a)$ and $\bar{P}(a)$, i.e.

$$\bar{c}_T^i = \frac{\int_3^{24} P^i(a) da}{\int_3^{24} \bar{P}(a) da} \quad (10)$$

For different ships the \bar{c}_T^i values are presented in Table 3.

Table 3. \bar{c}_T^i values

Tanker	\bar{c}_T^i
T120	$1.42 \cdot 10^6$
T190	$1.44 \cdot 10^6$
T260	$1.92 \cdot 10^6$

4 SIMPLIFIED GROUNDING DAMAGE PREDICTION FORMULA FOR DOUBLE-HULL TANKERS

Given the contact pressure, eq. (9), the response surface describing the grounding force can now be presented as a function of penetration depth, ship and rock size. This formulae can be derived as a combination of independent mathematical functions, each presenting the influence of a certain variable. These variables are ship main dimensions, ship mass, velocity, penetration depth and the structural configuration of the ship. Such simplified formula can be used to conduct, for example, a risk analysis, when the ship types, main dimensions and the grounding scenarios are known.

First, the expression is derived for horizontal grounding force F_H^i which depends on the pressure P^i acting on contact area A as follows

$$F_H^i = P^i(\delta, h_{db}, a) A(\delta, h_{db}, a) \quad (11)$$

where functions A and P^i are given with eqs.(4), (5) and (9). Substituting these into the eq. (11), takes horizontal force F_H to the following form

$$F_H^i = P^i A = \bar{c}_T^i (1.8 \cdot 10^{-3} a^2 - 7.4 \cdot 10^{-2} a + 1.2) \cdot A \quad (12)$$

In grounding analysis one of the main aims is to evaluate the length of bottom damage. For simplicity the ship motions except the surge are ignored and the kinetic energy of the ship is transformed to the work done by the grounding force. Comparing this work to the kinetic energy of the tanker, the length of damage l_{dam} can be evaluated as:

$$F_H^i l_{dam} = \frac{\Delta v^2}{2} = \frac{(1 + a_x) \Delta v^2}{2} \Rightarrow l_{dam} = \frac{(1 + a_x) \Delta v^2}{2 F_H^i} \quad (13)$$

where Δ is ship's displacement, a_x is non-dimensional surge added mass and v is ship's speed. Replacing eq.(12) into eq. (13), we can derive a formula for the damage length as a function of rock size parameter a , ship's double-bottom height h_{db} , parameter \bar{c}_T^i , rock penetration depth δ , surge added mass a_x and ship's speed v as

$$l_{dam} = \frac{(1 + a_x) \Delta v^2}{2 \bar{c}_T^i (1.8 \cdot 10^{-3} a^2 - 7.4 \cdot 10^{-2} a + 1.2) A} \quad (14)$$

5 VALIDATION OF SIMPLE FORMULA

In order to assess the applicability of eq. (9) and (12), horizontal force F_H is here calculated with eq. (12) and compared to the numerical simulations. The comparison is shown in Figure 12 where in each graph F_H is presented for a certain rock size. It reveals that F_H is under-predicted for penetration depths smaller than 1.0 m and slightly over-predicted for penetrations higher or equal to 1.0 m. Obviously this is caused by previous exclusion of pressure values at penetration depths of 0.5 m. However, as it can be seen from the figures that for penetrations $\delta \geq 1.0$ m eq.(12) predicts F_H with good accuracy and thus can be applied to eq.(13) for evaluation of grounding damage length.

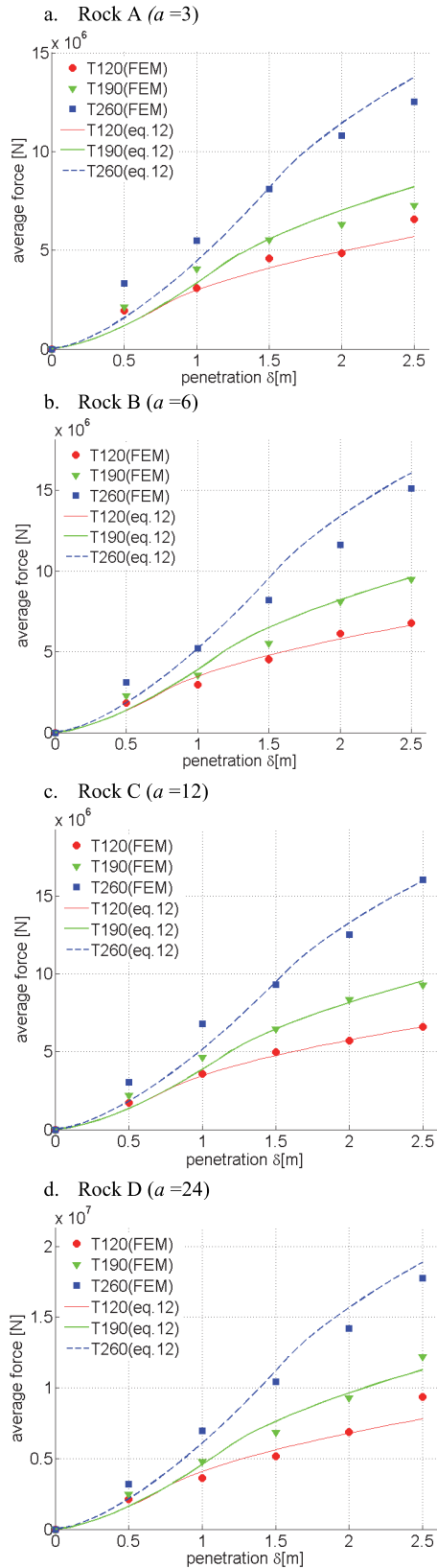


Figure 12. Comparison of horizontal forces

6 CONCLUSIONS

Simplified formulas to evaluate the grounding force and the longitudinal extent of structural damage in tanker groundings were derived in the paper. The formulas were derived based on the contact pressure acting on a grounding ship. The contact pressure as a function of penetration depth, rock and ship size were derived based on numerical simulations.

Comparison to the numerical simulations showed that derived simplified approach describes horizontal grounding force well for penetration depths above 0.5 m. For smaller penetration depths the force is under predicted. Therefore, the approach should be further developed to account for the mechanisms associated with smaller penetration depths, such as tearing of the bottom plating. Furthermore, a simplified criterion has to be derived to predict the size of the damage opening. For example, this would allow to provide the input for the assessment of oil outflow.

To increase usability of derived simplified formulas for practical use the following improvements are still to be made. The parameter c_T that characterizes ship structure and thus its structural resistance is evaluated only for three ships analysed in the paper, which limits the application of the derived formulas. Therefore, in order to evaluate c_T for any similar type of ship, a function is to be developed that would allow to evaluate c_T based on few main parameters defining the ship structure. Furthermore, the formulas are derived without any transverse or longitudinal bulkheads, thus presenting a lowest possible contact force level. This would assure conservative approach, but for more precise evaluation of contact force, the effect of the bulkheads is to be included.

Acknowledgements

This research work has been financially supported by Estonian Science Foundation (grant agreement ETF8718), European Social Fund (grant agreement no. MJD110) and by Central Baltic Interreg IV A program through MIMIC project (“Minimizing risks of maritime oil transport by holistic safety strategies”). This help is here kindly appreciated.

References

- AbuBakar A.,Dow, R.S. 2012. Simulation of Ship Grounding Damage using the Finite Element Method. *Int. J. Solids and Structures*, accepted manuscript.
- Alsos H, Amdahl J. 2007. On the resistance of tanker bottom structures during stranding. *Marine Structures*, 20: 218 – 237.
- Ehlers, S.,Tabri, K. 2012. A combined numerical and semi-analytical collision damage assessment procedure. *Marine Structures*, 28(1): 101 - 119.

- Hong, L.,Amdahl, J. 2012. Rapid assessment of ship grounding over large contact surfaces. *Ships and Offshore Structures*, 7(1):5 – 19.
- Lehmann E.,Egge, E.D.,Scharrer M.,Zhang L. 2001. Calculation of collisions with the aid of linear FE models, PRADS 2001, 2001.
- Simonsen, B.C.,Törnqvist, R.,Lützen, M. 2009. A simplified grounding damage prediction method and its application in modern damage stability requirements. *Marine Structures*, 22: 62 – 83.

PUBLICATION II

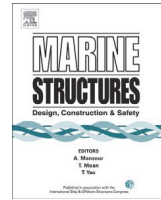
Heinvee, M., Tabri, K. (2015). **A simplified method to predict grounding damage of double bottom tankers.** *Marine Structures*, 43, 22–43.



Contents lists available at ScienceDirect

Marine Structures

journal homepage: www.elsevier.com/locate/marstruc



A simplified method to predict grounding damage of double bottom tankers



Martin Heinvee*, Kristjan Tabri

Department of Mechanics, Faculty of Civil Engineering, Tallinn University of Technology, Estonia

ARTICLE INFO

Article history:

Received 2 July 2014

Received in revised form 17 March 2015

Accepted 17 April 2015

Available online 28 May 2015

Keywords:

Ship grounding

Grounding damage assessment

Simplified analytical method

Double bottom damage

ABSTRACT

This paper presents a set of analytical expressions for the calculation of damage opening sizes in tanker groundings. The simplified formulas were given for the grounding force, longitudinal structural damage and the opening width in the inner and outer plating of a tanker's double bottom. The simplified formulas derived are based on a set of numerical simulations conducted with tankers of different dimensions- 120, 190 and 260 m in length. The simulations were performed for five penetration depths and for several rock/ground topologies.

The formula for the horizontal grounding force was derived provided the grounding force is proportional to the contact area and the contact pressure. By use of regression analysis it was shown that the contact pressure for any combination of ship and rock size can be expressed with a single normalized polynomial. The actual contact pressure was found by scaling the normalized pressure with the structural resistance coefficient. Given the formulation for the normalized contact pressure, the actual contact force for a ship can be found as a product of average contact pressure and the contact area.

The longitudinal length of the damage was evaluated based on the average contact force and the kinetic energy of the ship. The damage opening widths in the outer and inner bottom of the ship were derived separately for two ranges of relative rock sizes as they have strong influence on the deformation mode. The damage widths were given as a function of rock size, penetration depth and double bottom height. To improve the prediction of the onset of the inner bottom failure, a critical relative penetration depth as a function of the ratio of the rock size and the ship breadth was established.

* Corresponding author.

E-mail address: martin.heinvee@ttu.ee (M. Heinvee).

Comparison to the numerical simulations showed that the derived simplified approach describes the horizontal grounding force and the damage length well for the penetration depths above 0.5 m. For the range of specified relative rock sizes, the damage width in the inner and outer bottom deviates from numerical simulations approximately up to 25%, which was considered sufficient for the analyses where rapid damage assessment is needed. Comparison was also made to real accidental damage data and to the results of several simplified formulas.

© 2015 Elsevier Ltd. All rights reserved.

Nomenclature

a	rock size parameter
A	contact area between the rock and the ship
B_a	rock width
c_T	parameter describing the ship structural resistance
δ	vertical penetration depth
D_{in}	opening width in the inner bottom plating
D_{out}	opening width in the outer bottom plating
d_{in}	inner opening width obtained from numerical simulation
d_{out}	outer opening width obtained from numerical simulation
F_H	average grounding force
dif_a	difference between rock width and numerical value (outer opening width)
DIF_a	difference polynomial for rock a
h_{db}	ship's double bottom height
L	ship length
p	value of contact pressure
p^i	function of contact pressure for a ship i
$\bar{P}(a)$	function of normalized contact pressure
S_{gir}	ship girder spacing
a/S_{gir}	relative rock size

1. Introduction

Increasing cargo flows all over the world have affected the density of marine traffic and thus risks for accidents. For example, in the Gulf of Finland oil transportation has quadrupled in the past ten years [1], which makes it a region of the highest risk in the world. However, the number of collisions and groundings with oil and chemical tankers in the mentioned region has stabilized [2], indicating the efficiency of existing measures towards increased safety at seas. As the traffic continues to increase, it is necessary to further improve various measures to keep the current safety level.

The most severe environmental consequences are caused by accidents with oil and chemical tankers, which in the worst case can lead to extensive oil spill. Accidents can be prevented and their consequences reduced by implementing safety measures that can be developed through risk analyses conducted for certain transportation areas. In a risk analysis, possible impact on the environment and human lives can be evaluated for typical accidental scenarios. To develop and test the safety measures, large numbers of accidental scenarios are to be analyzed. Thus, fast and sufficiently accurate tools are needed.

When analyzing a tanker grounding accident, it is desirable to evaluate also the amount and duration of the oil spill, which requires the size of the damage opening to be evaluated. It is shown in Ref. [3] that the size of the damage opening in the inner bottom of the tanker strongly influences the duration of the oil spill. Most of the studies describing ship grounding accidents focus on the evaluation of the grounding force and the deformation energy. A simple formula was developed by Minorsky [4] who used accidental statistics and found that the dissipated energy is proportional to the volume of the damaged material. Inspired by this approach, Simonsen [5] used rock width, assumed equal to the damage width, and equivalent plate thickness to evaluate the grounding force and damage. The opening width was not explicitly discussed.

Another group of simplified models allows calculation of the structural response (collapse load or deformation energy) for the individual structural members – plates, cruciforms, stiffeners [6–10]. The total response of the assembly is obtained through the summation of the responses of all structural members [10–13]. Typically, even such simplified models require too much input information, which makes their use difficult. On the other hand, precise numerical simulations hardly suit in the risk analyses, as the simulation of a single scenario will take several hours [14–16].

The aim in this paper is to find simple formulas for rapid prediction of the grounding resistance and the size of the damage opening of double hull tankers. Such simplified formulation could be used in the risk analysis studies in case of lack of specific information regarding the structural arrangement of ships and where the main dimensions of the ships are the only parameters available.

The principle scheme of the derivation of the simplified approach is presented in Fig. 1. The simplified formulas were derived based on a set of numerical grounding simulations. Three double-bottom tankers of different length were included in the analysis – 120, 190 and 260 m. Each tanker was analysed for five different penetration depths δ and for four different rock sizes a . The aim of the numerical simulations was to analyse how the ship particulars and the rock size influence the grounding resistance and the extent of the damage at a given penetration depth. Therefore, as a simplification, actual grounding dynamics were neglected, penetration was assumed constant and the numerical simulations were conducted in a displacement controlled manner.

Based on the grounding simulations presented in Refs. [5] and [15] it can be concluded that the transverse bulkheads increase the average horizontal grounding force level approximately 15%. This contribution was omitted in the present study and the focus was on the double-bottom structures as the main contributor to the grounding resistance. Furthermore, such simplification was considered to reveal more apparent relationships between the main input parameters, grounding resistance and damage extent.

Numerical analyses provide the contact force time-history for each grounding scenario. Focus is on the horizontal grounding force as a main energy absorbing mechanism. To present the force outcome of each numerical simulation via single value, an average grounding force was evaluated over each force time-history. Evaluation of the average horizontal grounding forces for all the scenarios gave the grounding force as a function of ship parameters, penetration depth and rock size. To remove the dependency on the ship parameters and the penetration depth, the normalized contact pressure $\bar{P}(a)$ that depends only on the rock size a was derived using the regression analysis, as described in Ref. [17]. Given the formulation for the normalized contact pressure, $\bar{P}(a)$, the actual contact force F was found as a product of pressure P and contact area A :

$$F(L, a, \delta, h_{db}) = P \cdot A = \underbrace{f_{c_r}(L) \cdot \bar{P}(a)}_{\text{contact pressure } P} \cdot \underbrace{A(a, \delta, h_{db})}_{\text{contact area } A},$$

where $f_{c_r}(L)$ is a function scaling the normalized pressure $\bar{P}(a)$ for the actual ship with length L ; $A(a, \delta, h_{db})$ is a function describing the contact area between the rock and the ship; δ is the penetration depth and h_{db} is the double bottom height of the ship.

In Section 2, the equations for the size of damage opening were derived. For each numerically simulated grounding scenario, an average damage opening width was determined in the outer and inner bottom. The damage width in the outer bottom D_{out} was expressed via rock size and penetration depth, while for the inner bottom damage D_{in} also the double bottom height was included:

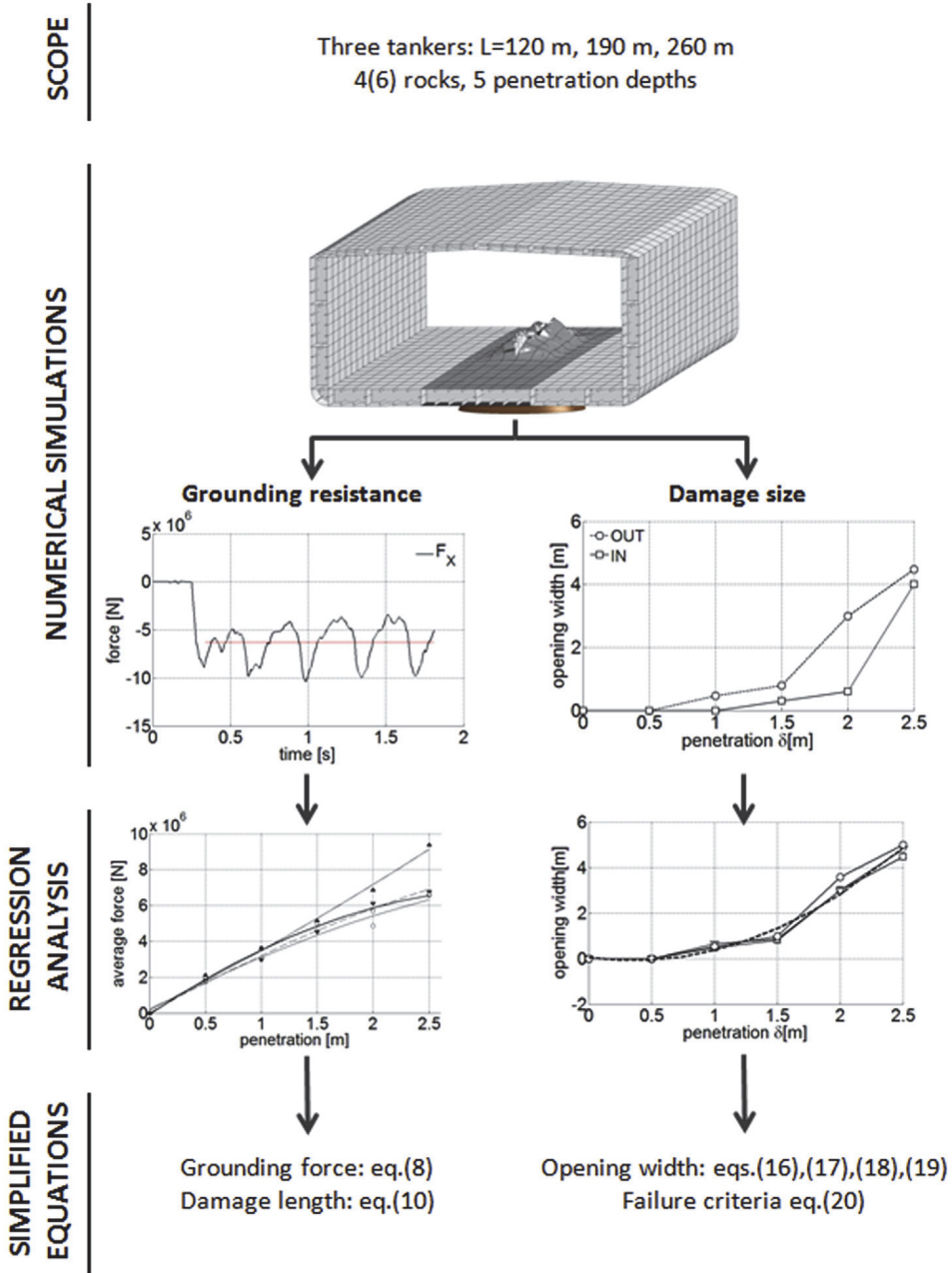


Fig. 1. Principle of the simplified approach for the derivation of grounding force.

$$D_{out} = D_{out}(a, \delta),$$

$$D_{in} = D_{in}(a, \delta, h_{db}).$$

Due to the observed different relations between the deformation mode and the relative rock size, the above formulas were presented separately for two ranges of rock sizes. Furthermore, a failure criterion for the inner bottom tearing in the form of critical penetration depth was proposed.

The derived formulas are used in Interreg IV A project MIMIC (Minimizing risks of maritime oil transport by holistic safety strategies) for a holistic approach to risks related to maritime oil transportation in the Baltic Sea.

2. Numerical grounding simulations

Simplified equations were developed based on the observations from the numerical simulations. Numerical simulations were conducted for three tankers varying in size. The effects of rock size, penetration depth and ship size were studied. In total, 60 grounding scenarios were simulated. Contact force and the size of damage recorded for each simulation form the foundation for deriving simplified equations.

2.1. FE models of tankers

Three double hull tankers with lengths 120 m, 190 m and 260 m were studied. The cross-sections and the main dimensions are given in Fig. 2 and in Table 1. Hereinafter superscripts T120, T190 and T260 are used to denote the different tankers. If the superscript is replaced by i , it means that the description is common to all three ships.

Typical ship-building steel with a yield stress of 235 MPa was used for the ship structures. For each tanker, only part of the midship region was modelled, as shown in Fig. 3. The length of the model was selected to provide sufficiently long data series for the evaluation of the average grounding force and the damage size. Moreover, the length of the models was chosen such that the influence from boundary conditions is minimal. The corresponding model lengths are given in Table 1. The longitudinal and transverse bulkheads were omitted to maintain the conservative nature of the approach. The transverse bulkheads would result in a local rapid increase of the grounding resistance, while the average grounding force increases approximately 15%, as for instance, could be seen from the numerical analysis presented in Ref. [15].

The corresponding finite element models are presented in Fig. 3. The structure was modelled using quadrilateral Belytschko-Lin-Tsay shell elements with five integration points through their thickness. As in ship grounding, the deformations are limited to the double-bottom, the finer mesh was used for the bottom structures. The prevailing element-length in the double-bottom structure was around 50–75 mm to properly account for the non-linear structural deformations. Stiffeners were modelled by using at least three elements for web and a beam element for flange. The possible material failure was modelled using the through-thickness criterion, often referred to as the Germanischer Lloyd criterion [18]. This criterion establishes element thickness and dimension dependent critical thickness strain after which an element is removed from the simulation. Standard LS-DYNA hourglass control and automatic single surface contact was used. For the contact between the sea bed and the bottom steel, the friction coefficient was taken equal to 0.3. Due to the difficulty of determining the actual value for the coefficient, the commonly implemented friction value is used [5,9,15]. In the development of simplified equations the friction coefficient was not explicitly included. The effects of friction were taken into account implicitly through the results of the finite element simulations. The nodes at the forward and aft end of the model were fixed. The rigid rock was moved first to a required penetration depth and then continued to move at a constant penetration depth along the ship at a constant velocity of 10 m/s. The finite element simulations are described in detail in Ref. [17].

2.2. Grounding scenarios

Our simulations were conducted for five different penetration depths δ (from 0.5 to 2.5 m) and for main rock sizes covering the range from sharp rock to blunt “shoal”-type rock. These rocks are axisymmetric with parabolic shape cross-sections and are defined with parabolic functions

$$z = \frac{y^2}{a}, \quad (1)$$

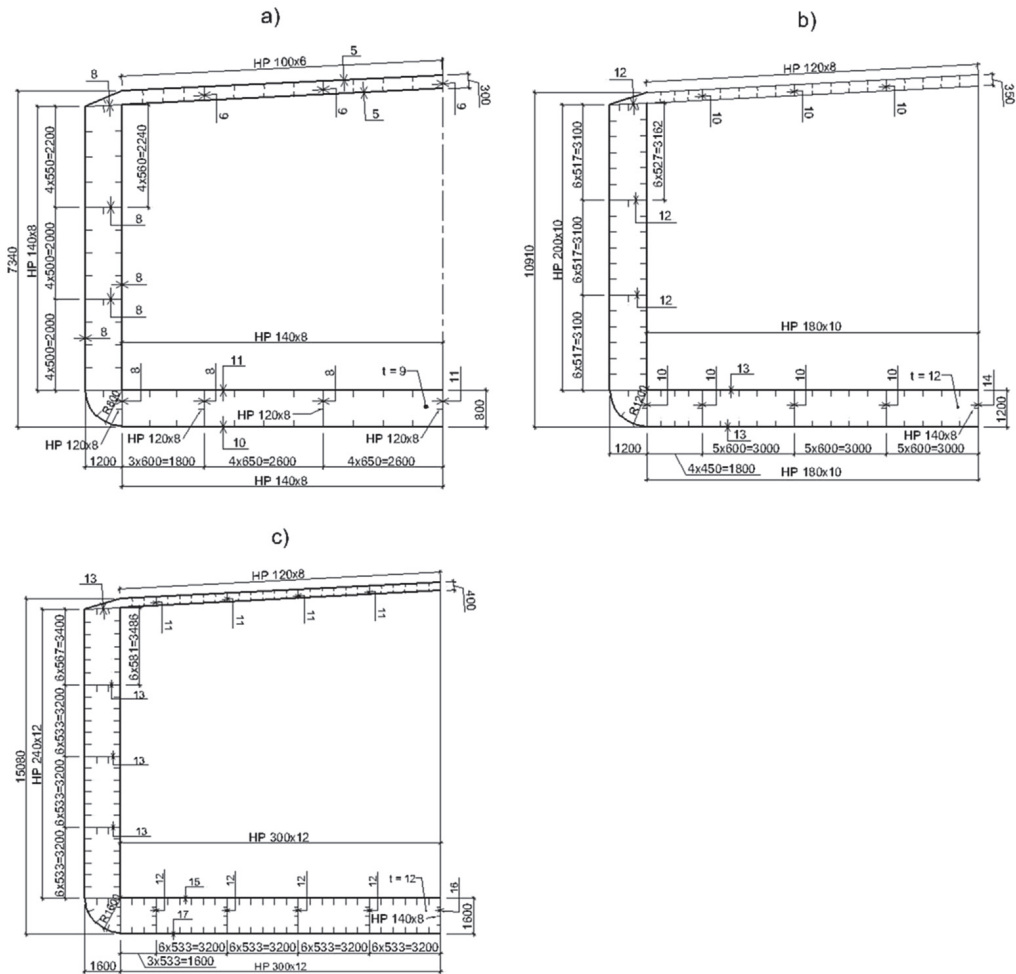


Fig. 2. Tanker cross-sections: a) tanker T120; b) tanker T190; c) tanker T260.

where the parameter a defines the actual size of the rock, whereas the values of for different rocks size are given in Table 2. The rocks are depicted in Fig. 4.

Since the dominating deformation mechanism in ship grounding is plate tearing, the simulation phase with constant vertical penetration was considered when recording the grounding force.

Table 1

Main dimensions and parameters of tankers used in numerical simulations.

Parameter/Tanker	T120	T190	T260
Length [m]	120	190	260
Breadth[m]	16	24	32
Depth [m]	8	16	18
Double-bottom height [m]	0.8	1.2	1.6
Outer plating thick [mm]	10	13	15
Tank-top thick [mm]	11	13	15
Girder spacing [m]	2.6	3.0	3.2
Floor spacing [m]	2.2	3.5	4.0
FE model length [m]	37.4	35	36

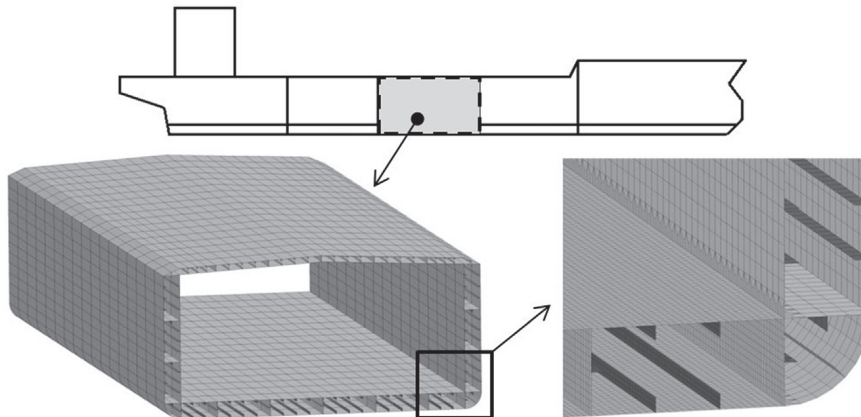


Fig. 3. Finite element model of a tanker.

To evaluate the critical penetration depth for the inner plating failure, a set of numerical simulations were conducted, using also two additional rock sizes: AB and BC in Table 2. The simulations were conducted up to the penetration depth of $\delta = 2.5$ m.

2.3. Grounding force in numerical simulations

The numerical simulations provide a response of different structural configurations for different combinations of penetration depth and bottom topology. Typically, the contact force and the description of damage are the outcomes of the simulation. Focus was on the horizontal grounding force, the typical time–history of which is presented in Fig. 5. The average grounding force was evaluated over the time in which the constant penetration depth was reached, see the constant horizontal line in Fig. 5. For brevity, hereinafter when referring to the contact force and the contact pressure, the average contact force and average contact pressure are considered, if not stated otherwise.

Average force values are presented as a function on the penetration depths in Fig. 6 with the rock size as a variable. As expected, larger ships result in a higher contact force. Rocks A and B cause a parabolic force increase for tankers T120 and T190, while forces induced by rocks C and D increase linearly. For the largest tanker T260, horizontal force increases linearly with all the rocks, as the inner hull is penetrated later. This effect is due to the relative size between the rock and the ship. The slope of the curve decreases and becomes more parabolic when the bottom plating is torn open. As the height of the double-bottom increases with the length of the ship, the inner hull fractures later in larger ships, resulting in a more linear behavior of the average force. However, it was concluded that the contact force can be considered proportional to the penetration depth in all the simulated scenarios. This is probably due to the fact that analyzed tankers follow a minimum scantlings approach given by the rules and their scantlings are thus proportional to their size.

2.4. Damage opening width in numerical simulations

The description of damage size in the outer and inner plating of the double bottom was obtained for each numerical simulation. Since the width of the damage opening varies along the ship, see Fig. 7, the average values for the damage opening width in the outer and inner plating are defined and denoted

Table 2
Rock size parameters.

	Rock A	Rock AB ^a	Rock B	Rock BC ^a	Rock C	Rock D
a [m]	3	4.4	6	8.8	12	24

^a Rock sizes AB and BC are used only for the evaluation of the inner bottom failure criterion in Section 3.5.

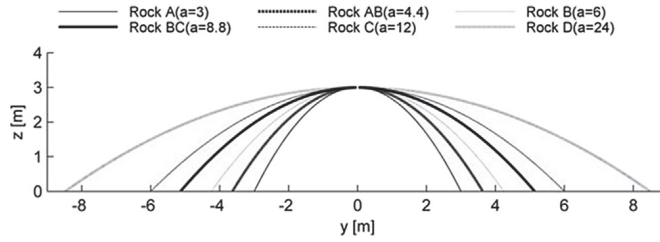


Fig. 4. Different rocks used in the simulations.

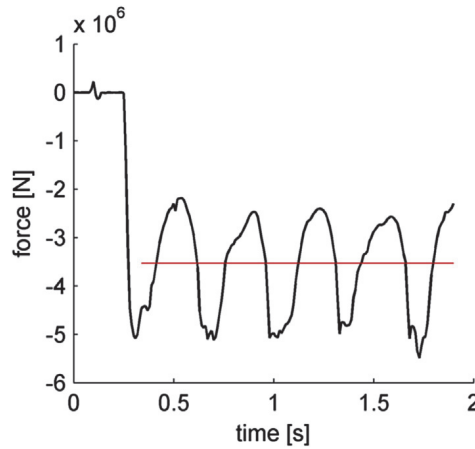


Fig. 5. Numerical simulations: horizontal contact force as a function of time.

with d_{in}^i and d_{out}^i , respectively. For brevity, hereinafter the damage opening width in the outer and inner plating is noted as “outer width” and “inner width”, respectively.

The magnitude of the outer width for rocks A and B differs from that of the much larger rock C. In the case of rocks A and B, the outer damage width was approximately five times larger than that corresponding to rock C. Due to very local contact in the case of smaller rocks, high strain concentration results in a bottom fracture at a relatively low penetration depth, i.e. the deformation mode is similar to that in Fig. 8a. Since the dominating deformation mode is local tearing, the bottom plating is torn open and the outer width increases nearly proportionally with the penetration depth. The deformations and damage are limited by the girders. In contrast, with the relatively large rock C, the contact area is large

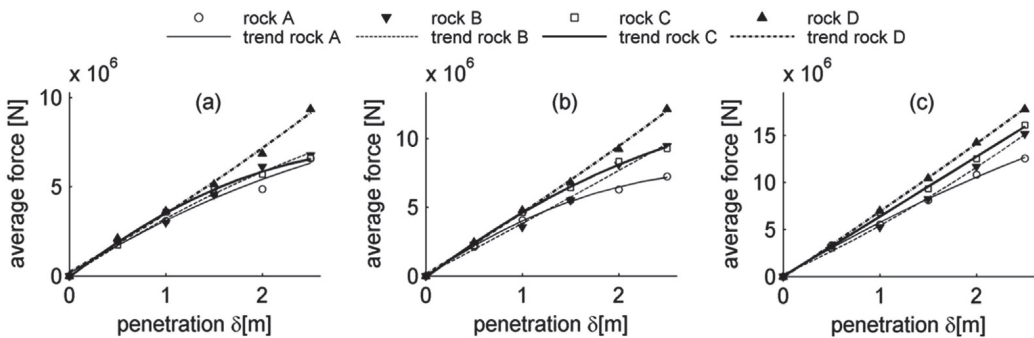


Fig. 6. Average contact force as a function of penetration depth: a) T120; b) T190; c) T260.

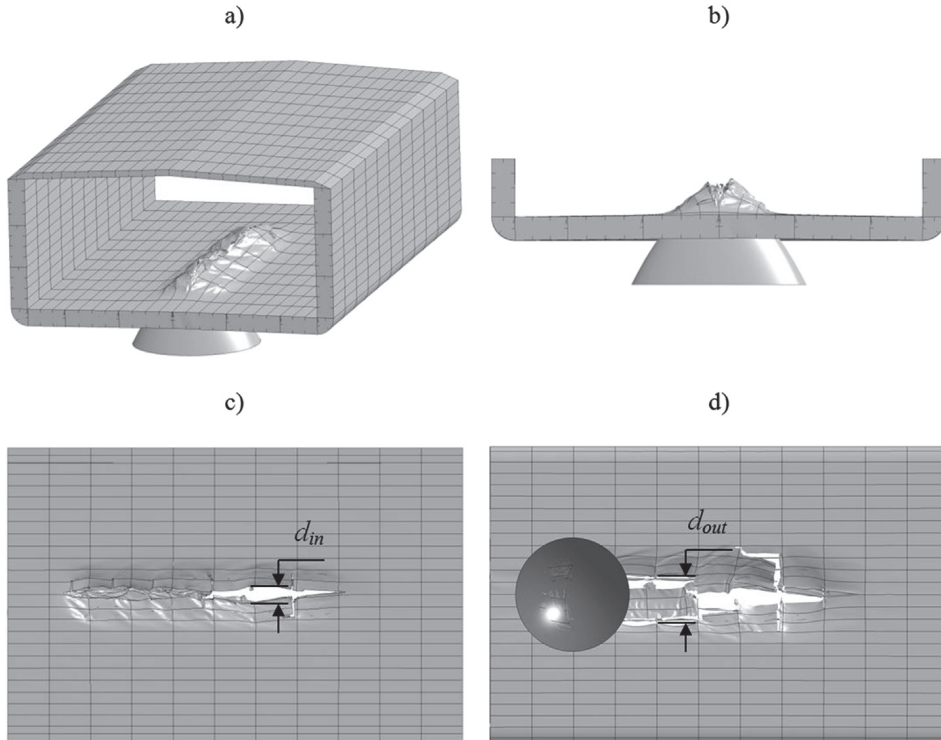


Fig. 7. Grounding damage: a) isometric view of the tanker; b) front view; c) damage opening in the inner bottom; d) damage opening in the outer bottom.

and the global crushing of the bottom structures is dominating. Thus, the plating is torn open at larger penetration depths, see Fig. 8c. In the case of average sized rock B, the deformation mode is a combination of local tearing and global crushing, see Fig. 8b. Based on these considerations, it was concluded that the rock size strongly influences the deformation mode, which can lead to wide or narrow damage openings. This can be seen in Fig. 8, where the results of rock C on a relatively narrow opening are compared to much wider local damages in the case of rocks A and B.

With the largest rock D, a large part of the ship bottom was crushed and the outer plating was fractured only at the largest penetration depths, while the inner plating was never fractured, see Fig. 9jkl. Therefore, simulations with the largest rock D were neglected in the further study. Fig. 9 also reveals that the inner width has a shift with respect to the outer width while the shapes of the curves are similar. Moreover, the outer damage is less dependent on the ship size than on the inner damage size.

3. Simplified formulas

The formulas for the grounding force and the damage length are discussed only briefly as their elaborate derivation is presented in Ref. [17]. Derivation of the formulas for the damage opening will be presented in detail.

3.1. Contact force and pressure

Average horizontal grounding force F_H was analyzed and presented through the pressure acting on the contact surface between the rock and the ship's double-bottom. The average contact pressure for rock a and ship i at the penetration depth δ was obtained with a simple expression

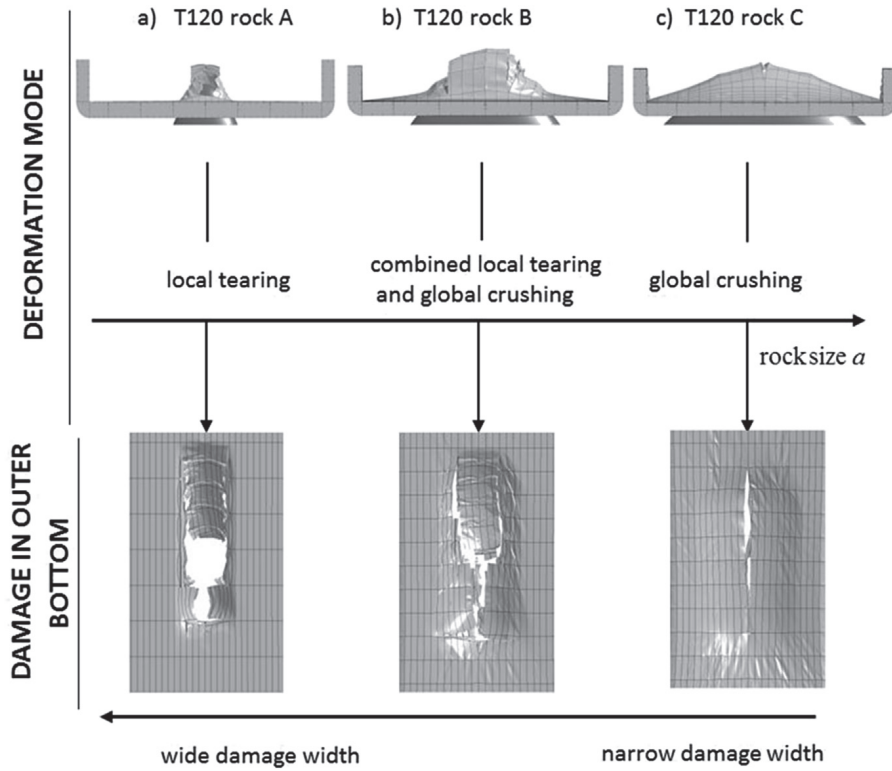


Fig. 8. Dominating deformation modes depending on the rock size: a) local tearing; b) combined tearing and crushing modes; c) global crushing mode.

$$p(a, \delta, h_{db}) = \frac{F_H}{A}, \tag{2}$$

where A is the contact area depending on the penetration depth (see Fig. 10):

$$A(a, \delta, h_{db}) = \begin{cases} \frac{4}{3} \sqrt{a} \cdot \delta^{\left(\frac{3}{2}\right)} & \text{for } \delta \leq h_{db} \end{cases} \tag{3}$$

$$\frac{4}{3} \sqrt{a} \cdot \left[\delta^{\left(\frac{3}{2}\right)} - (\delta - h_{db})^{\left(\frac{3}{2}\right)} \right] & \text{for } \delta > h_{db}. \tag{4}$$

Looking at the pressure values obtained with Eq. (2), it was found that the contact pressure variations are small at the penetration depths larger than 0.5 m [17]. Furthermore, the pressure value is almost constant with respect to the penetration depth and depends only on the rock size parameter a . Therefore, the pressure as a function of rock size was approximated with a polynomial $P^i(a)$ for each ship. Since these polynomials were found to be of similar shape but different in magnitude, the polynomials were normalized with respect to the magnitude and presented via a uniform regression polynomial \bar{P} in the following form:

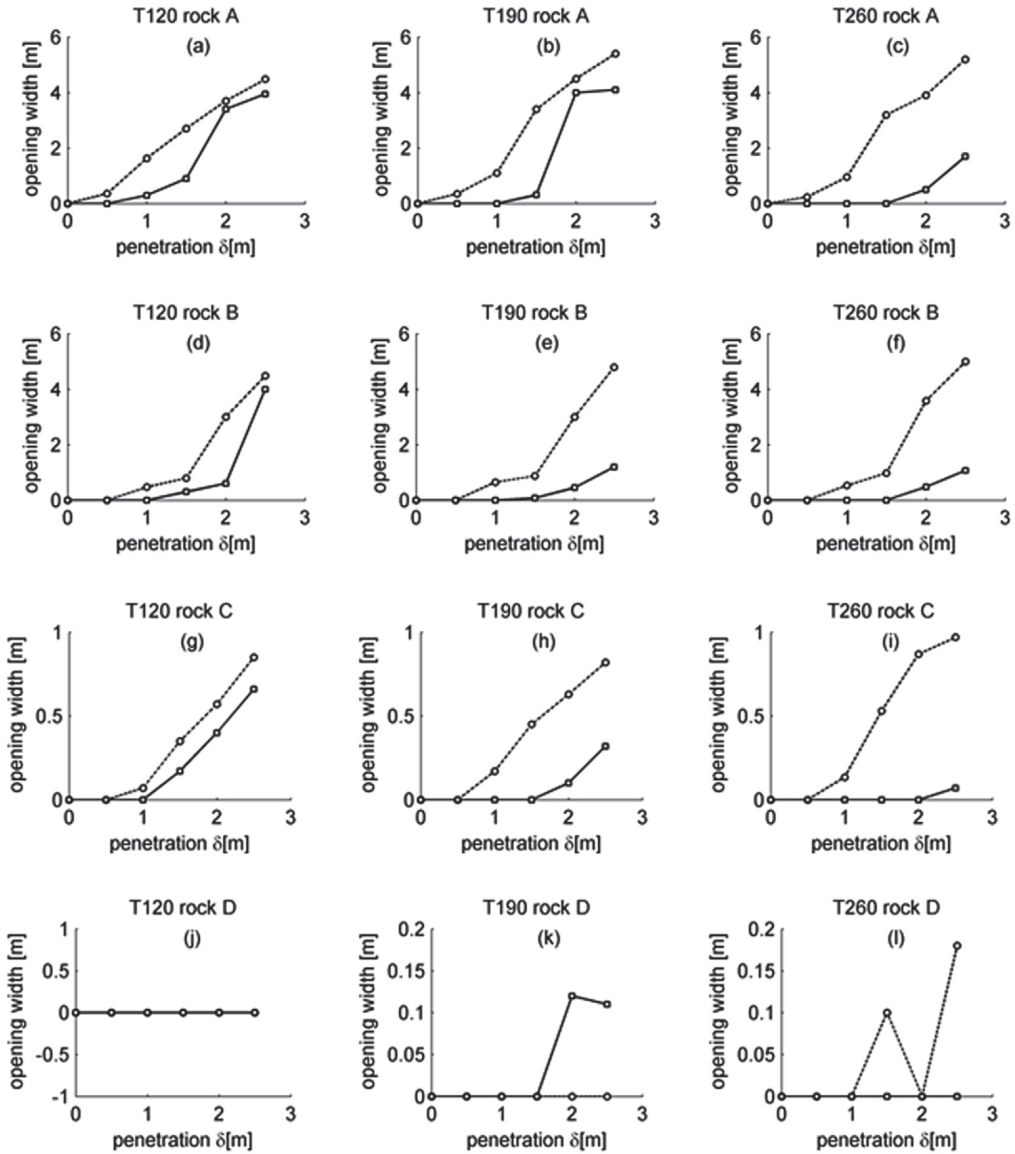


Fig. 9. Results of the FE simulations: opening width in the outer bottom (dotted line) and the inner bottom (continuous line).

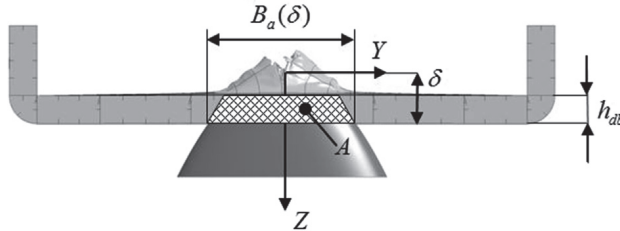


Fig. 10. Cross-section of a ship during grounding.

$$\bar{P}(a) = 1.8 \cdot 10^{-3} a^2 - 7.4 \cdot 10^{-2} a + 1.2. \quad (5)$$

To scale the uniform shape $\bar{P}(a)$ to a magnitude corresponding to the actual ship, it has to be multiplied by a coefficient \bar{c}_T^i that describes the ship's structural resistance. Thus, the actual pressure P^i for a ship i takes the form:

$$P^i(L, a) = \bar{c}_T^i \cdot \bar{P}(a) = \bar{c}_T^i \cdot (1.8 \cdot 10^{-3} a^2 - 7.4 \cdot 10^{-2} a + 1.2). \quad (6)$$

The coefficient \bar{c}_T^i for a certain ship i can be evaluated by using two options. First option is through the steps of the following procedure:

1. Select the ship and the rock:
 - a. ship i with the length L from the range $120 \text{ m} \leq L \leq 260 \text{ m}$
 - b. rock size a from the range $3 \leq a \leq 24$
2. Conduct a number of numerical grounding simulations

Each simulation with the selected ship i and the rock a at j different penetration depth δ_j is to be conducted in displacement controlled manner. Minimum number of simulations is $j=1$, however as the j increases more accurate \bar{c}_T^i is obtained.

3. Calculate the average horizontal grounding force F_H (see, Fig. 5) for each conducted simulation
4. Calculate the average contact pressure p_j^i for each simulation

Given the horizontal grounding force F_H , penetration depth δ_j , rock size a and ship's double bottom height h_{db} , the contact pressure p_j^i for each simulation can be obtained by Eq. (2), where the contact area A is to be calculated with Eq. (3) or (4).

5. Calculate the mean pressure value \bar{p}^i for the pressures p_j^i with

$$\bar{p}^i = \frac{\sum_j p_j^i(a, \delta_j, h_{db}^i)}{j}$$

6. Calculate \bar{c}_T^i for the selected ship i from Eq. (6), where the uniform pressure function $\bar{P}(a)$ is given with Eq. (5).

As an alternative to the above procedure, the coefficient \bar{c}_T^i can be approximated with bilinear functions (Fig. 11) as

$$c_T = f_{c_T}(L) = \begin{cases} 285.71 \cdot L + 1385714, & \text{for } L \leq 190[\text{m}] \\ 6857.1 \cdot L + 137143, & \text{for } L \geq 190[\text{m}], \end{cases} \quad (7)$$

which were derived using the \bar{c}_T^i values (see values in Fig. 11) corresponding to the three ships used in the current numerical simulations. However, it should be understood that Eq. (7) provides the structural resistance value similar to the ships used in the numerical analysis. Thus, the specifics of the actual ship design are not accounted for. The Eq. (7) should be used, when there is almost no information except the ship length available.

In order to calculate the horizontal force for a ship i and a rock a , Eqs. (3) and (4)(6) were combined and give the grounding force as

$$F(L, a, \delta, h_{db}) = P^i A = \bar{c}_T^i \cdot \bar{P}(a) \cdot A(a, \delta, h_{db}), \quad (8)$$

where the function $A(a, \delta, h_{db})$ is to be selected according to the condition given in Eqs. (3) and (4). The structural resistance coefficient \bar{c}_T^i for a selected ship can be evaluated by Eq. (7) or through the procedure described above.

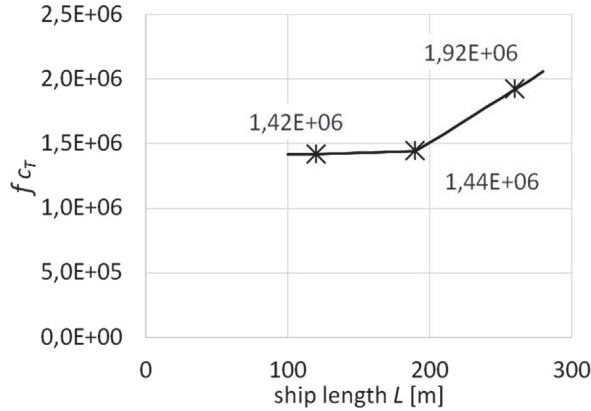


Fig. 11. Function $f_{c_T}(L)$ for structural resistance coefficient c_T .

3.2. Length of the damage opening

In the grounding analysis, one of the main aims is to evaluate the length of bottom damage, see Fig. 12. For simplicity, we assume that the ship motions, except the surge, are ignored and the kinetic energy of the ship is transformed to the work done by the grounding force. Comparing this work to the kinetic energy of the tanker, the length of damage l_{dam} can be evaluated as:

$$F_H^i l_{dam} = \frac{(1 + m_{a,x})\Delta}{2} v^2 \Rightarrow \tag{9}$$

$$l_{dam} = \frac{(1 + m_{a,x})\Delta}{2F_H^i} v^2,$$

where Δ is ship's displacement, $m_{a,x}$ is non-dimensional surge added mass usually taken as $m_{a,x} = 0.05$ and v is ship's speed. Replacing Eq. (6) into Eq. (9), a formula for the damage length can be presented as

$$l_{dam} = \frac{(1 + m_{a,x})\Delta}{2c_T(1.8 \cdot 10^{-3}a^2 - 7.4 \cdot 10^{-2}a + 1.2)A} v^2. \tag{10}$$

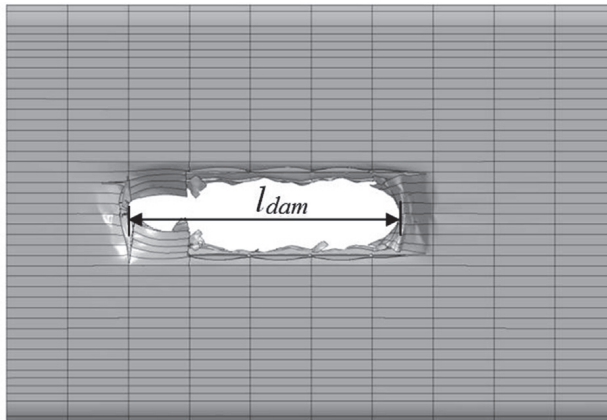


Fig. 12. Length of damage opening.

3.3. Opening width in the outer bottom

Based on the numerical simulations it was concluded that the rock size determines the deformation mode, which leads either to wide or narrow damage openings. The simulations showed that with a rock A, the plate tearing is the dominating deformation mechanism. Therefore, the damage width mainly depends on the penetration depth and the rock size. The damage width caused by rock B is of similar magnitude to the rock A, however at large penetration depths, the side girders, in addition to the central girder, influence the deformation mode. This indicates that as the rock size increases, the ship has gradually larger impact on the change of the deformation mode. The importance of tearing decreases and crushing becomes more dominant, resulting in a narrow damage opening in the outer bottom. Therefore, it was concluded that the influence of the size and structure of a ship on the damage opening width is small with sharp rocks and significant with large rocks. Due to the changing deformation mode, it is difficult to give a single expression to describe the damage width. Therefore, it is more convenient to derive damage width equations separately for two ranges of rock sizes in relation to the ship size.

The relative rock size has been used in Ref. [19], where in a ship stranding study the rock size was presented as a ratio between the rock parameter a and the ship floor spacing $-a/S_{fl}$. To determine the range of rock size for each set of formulas, the relative rock size was given as a ratio of rock size a and ship girder spacing $-a/S_{gir}$.

Fig. 13 presents the relationship between the opening width and the penetration depth. A parabolic dependence can be observed. Moreover, the rock width B_a at the outer plating (see Fig. 10) changes parabolically with the penetration depth (see also Eq. (1))

$$B_a(a, \delta) = 2\sqrt{a \cdot \delta}. \tag{11}$$

To study the dependence between the opening width and the rock geometry, the difference $dif_a^i(a, \delta)$ between the rock width B_a and the opening width d_{out}^i was calculated for each numerical simulation

$$dif_a^i(a, \delta) = B_a(a, \delta) - d_{out}^i(\delta). \tag{12}$$

These difference values dif_a^i were presented as a function of penetration depths in Fig. 14 with the ship size as a variable. For the robustness of the approach, the regression line was fitted through each set of points giving one polynomial DIF for each rock size:

$$DIF_A(\delta) = -0.0614\delta^2 - 0.76\delta + 2.68, \quad \text{for rock size } a = 3 \text{ (rock A)} \tag{13}$$

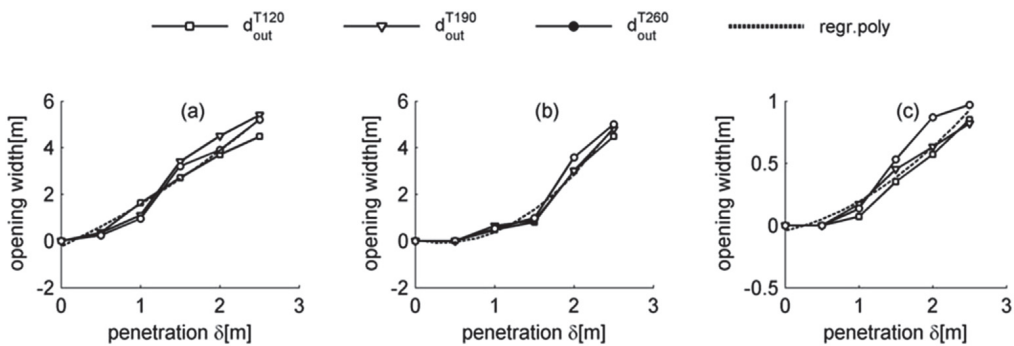


Fig. 13. Damage width of the outer bottom and corresponding regression lines (FE simulations): a) rock A; b) rock B; c) rock C.

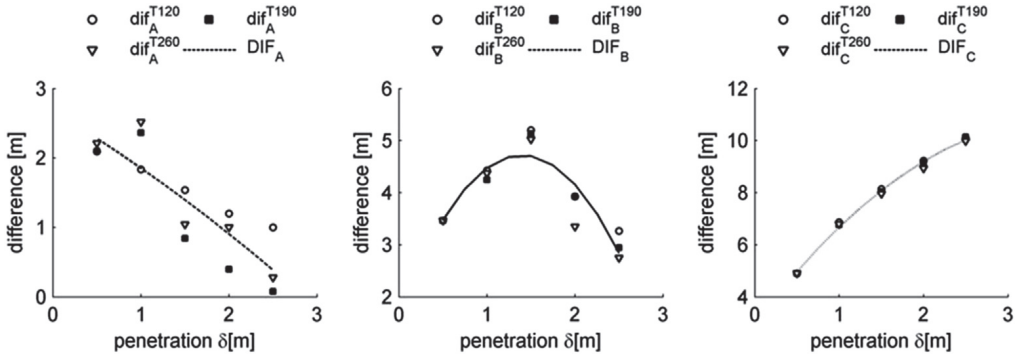


Fig. 14. Difference dif_a^i as a function of the penetration depth: a) rock A; b) rock B; c) rock C.

$$DIF_B(\delta) = -1.55\delta^2 + 4.33\delta + 1.69, \quad \text{for rock size } a = 6 \text{ (rock B)} \tag{14}$$

$$DIF_C(\delta) = -5.85^{-1}\delta^2 + 4.28\delta + 2.96, \quad \text{for rock size } a = 12 \text{ (rock C)} \tag{15}$$

The difference curves given with Eqs. (13–15) are all presented in Fig. 15. The difference was interpolated separately to two regions where the first region was determined with rocks A and B and the second region with rocks B and C.

Now the damage opening width in the outer plating can be obtained for two relative rock size regions as follows:

$$D_{out}^I(a, \delta) = 2 \cdot \sqrt{a} \cdot \delta - \left[DIF_A(\delta) + \left(\frac{DIF_B(\delta) - DIF_A(\delta)}{a_B - a_A} \right) \cdot (a - a_A) \right], \tag{16}$$

for $0.9 \leq a/S_{gir}^i \leq 2.3$, ship length $120 \text{ m} \leq L \leq 260 \text{ m}$, $a_A = 3, a_B = 6$

$$D_{out}^{II}(a, \delta) = 2 \cdot \sqrt{a} \cdot \delta - \left[DIF_B(\delta) + \left(\frac{DIF_C(\delta) - DIF_B(\delta)}{a_C - a_B} \right) \cdot (a - a_B) \right], \tag{17}$$

for $2.3 \leq a/S_{gir}^i \leq 4.6$, ship length $120 \text{ m} \leq L \leq 260 \text{ m}$, $a_B = 6, a_C = 12$

where B_a is the width of rock a at the penetration depth δ , given by Eq. (11), a_A, a_B, a_C are rock size parameters and DIF_A, DIF_B and DIF_C their corresponding difference functions given by the width

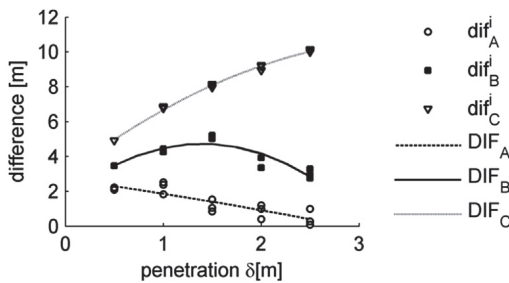


Fig. 15. Difference for rocks A, B and C.

Eqs. (13–15). Hereinafter, formulas for the first and the second rock size range are denoted by superscripts I and II respectively.

3.4. Opening width in the inner bottom

Comparing the variation of the inner width d_{in}^i with the outer width d_{out}^i , two conclusions can be made:

- 1) considering the minimum penetration depth step 0.5 m, at the penetration depth approximately $b \cdot h_{db}$ greater than for the outer bottom, where b is an unknown constant (see Fig. 9), the opening width in the inner bottom sets on continuous growth;
- 2) the opening width grows similarly to the opening width in the outer bottom, i.e. the curves are of similar shape (see Fig. 9);

The values of $b \cdot h_{db}^i$ for T120, T190, T260 are approximately 0.6 m, 1 m and 1.2 m respectively. Dividing these values $b \cdot h_{db}^i$ with corresponding double bottom heights, the average coefficient \bar{b} is obtained as

$$\bar{b} = \frac{\sum_{i=1}^3 b \cdot h_{db}^i}{3} \cong 0.75.$$

It reveals that Eqs. (16) and (17) can be used to calculate the opening width in the inner bottom by subtracting the term $\bar{b} \cdot h_{db}^i$ from the penetration depth δ . The equations for the inner width can be presented in the following form:

$$D_{in}^I(a, \delta, h_{db}) = B_a(a, \delta - 0.75h_{db}) - \left[DIF_A(\delta - 0.75h_{db}) + \left(\frac{DIF_B(\delta - 0.75h_{db}) - DIF_A(\delta - 0.75h_{db})}{(a_B - a_A)} \right) \cdot (a - a_A) \right],$$

for $0.9 \leq a/S_{gir}^i \leq 2.3$, ship length $120 \text{ m} \leq L \leq 260 \text{ m}$, $a_A = 3, a_B = 6$

(18)

$$D_{in}^{II}(a, \delta, h_{db}) = B_a(a, \delta - 0.75h_{db}) - \left[DIF_B(\delta - 0.75h_{db}) + \left(\frac{DIF_C(\delta - 0.75h_{db}) - DIF_B(\delta - 0.75h_{db})}{(a_C - a_B)} \right) \cdot (a - a_B) \right],$$

for $2.3 \leq a/S_{gir}^i \leq 4.6$, ship length $120 \text{ m} \leq L \leq 260 \text{ m}$, $a_B = 6, a_C = 12$

(19)

where B_a is the width of rock a at the penetration depth $\delta - \bar{b} \cdot h_{db}^i$, given by Eq. (11), a_A, a_B, a_C are rock size parameters and DIF_A, DIF_B and DIF_C their corresponding difference functions given by Eqs. (13–15). Eqs. (16–19) are to be used only for the ships with the length ranging from 120 to 260 m.

If a relative rock size a/S_{gir}^i is smaller than 0.9, then Eqs. (16) and (18) can be used. However, the interpolation is no longer done between the functions DIF_B and DIF_A – the upper and the lower polynomial. Instead, it is conducted between the function DIF_A and the zero level. Thus, the function DIF_A is used instead of the function DIF_B and DIF_A is taken equal to zero. If a relative rock size is larger than 4.6, then a very small damage opening may exist in the outer and inner bottom of the ship.

As the damage opening in the inner bottom results in severe consequences to the environment and to the ship, its detection is of crucial importance. However, Eqs. (16–18) can only be applied in a situation when the damage opening exists. Therefore, in the next section an additional criterion is developed that defines the onset of the inner bottom tearing.

3.5. Failure criterion for inner bottom

In order to derive a failure criterion for the inner bottom, a set of numerical simulations with the three ships and five different rock sizes, indicated as A, AB, B, BC and C in Table 2, were conducted. The simulations were conducted with two different rock positions with respect to the web frames: (i) the rock was positioned directly under the intersection of the floor and the central girder and (ii) the rock was between the floors. The vertical penetration speed of 1 m/s was selected for the rock. The criterion was sought as a function of the penetration depth, ship and rock size.

The critical penetration depth δ_f at which the inner bottom is fractured was determined for each numerical simulation. To study the dependence between the critical penetration depth and the ship size, the δ_f was divided with the corresponding double bottom height h_{db} , providing the relative penetration depth. These values are presented in Fig. 16 as a function of the ratio between the rock size and the ship breadth - a/B . If the rock was positioned between the floors a strong correlation was obtained between the relative penetration depth δ_f/h_{db} and a/B , see Fig. 16. However, if the rock was positioned under the floors the correlation is weak and the relative penetration depth is almost independent of a/B ratio.

Since no fracture occurs at the penetration depth lower than the double bottom height of the ship, the regression line was fitted through the lowest points, giving a conservative lower bound criterion. Considering the negligibly small slope, the lower bound failure criterion becomes $\delta_f/h_{db} \geq 1.05$, i.e. the fracture occurs at the penetration depth

$$\delta \geq 1.05h_{db}. \tag{20}$$

This confirms the conclusion made in Ref. [19] where the inner bottom was claimed to be fractured at the penetration depth approximately equal to the double bottom height. However, an experimental study presented in Ref. [20] found the critical penetration depth to be approximately equal to $1.4h_{db}$. The values δ_f obtained in this paper are distributed between $1.05h_{db}$ and $2.1h_{db}$. Higher relative penetration depths were obtained when the rock was positioned in between the floors. However, the conservative approach is preferred and the condition given by Eq. (20) is used in this paper.

The failure criterion given by Eq. (20) is to be used in conjunction with Eqs. (18) and (19) under the following considerations:

- If Eqs. (18) and (19) give a positive nonzero value and the failure criterion Eq. (20) confirms the fracture, then Eqs. (18) and (19) can directly be used.

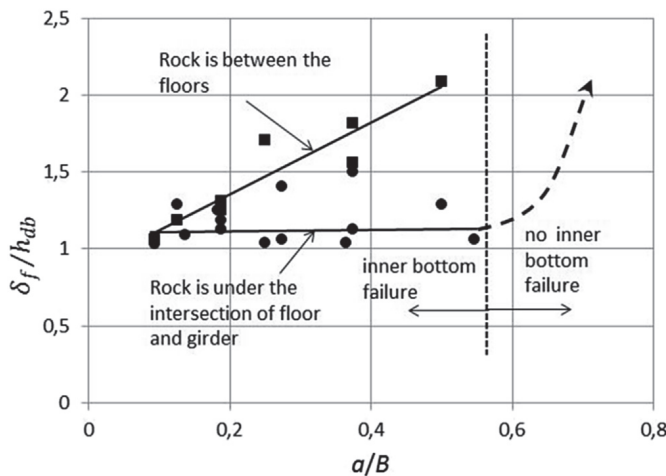


Fig. 16. Fracture criterion for the inner bottom (A, AB, B, BC, C indicate the rocks as given in Table 2).

- If Eqs. (18) and (19) give a positive nonzero value and the failure criterion Eq. (20) indicates no fracture, then $D_{in} = 0$.
- If Eqs. (18) and (19) give a negative value and Eq. (20) indicates no fracture, then $D_{in} = 0$.
- If Eqs. (18) and (19) give $D_{in} = 0$ and Eq. (20) indicates a fracture, then only very narrow damage opening is caused.

4. Validation with the numerical simulations

For the validation of the derived formulas full- or model-scale experiments or data from real accidents are most valuable. Here the comparison is made to the numerical simulations, while Chapter 6 focuses on real accidental data.

4.1. Grounding force

Fig. 17 shows the comparison for the grounding force F_H , where each graph presents the average grounding force for three different rocks. It reveals that F_H is under-predicted for penetration depths smaller than 1.0 m and slightly over-predicted for higher penetration depths. Obviously, this is due to the exclusion of pressure values at the penetration depth of 0.5 m, see Section 4.1. However, it can be seen from the figures that for penetrations $\delta \geq 1.0$ m Eq. (8) predicts F_H with good accuracy and can thus be applied to Eq. (10) to evaluate the length of the damage.

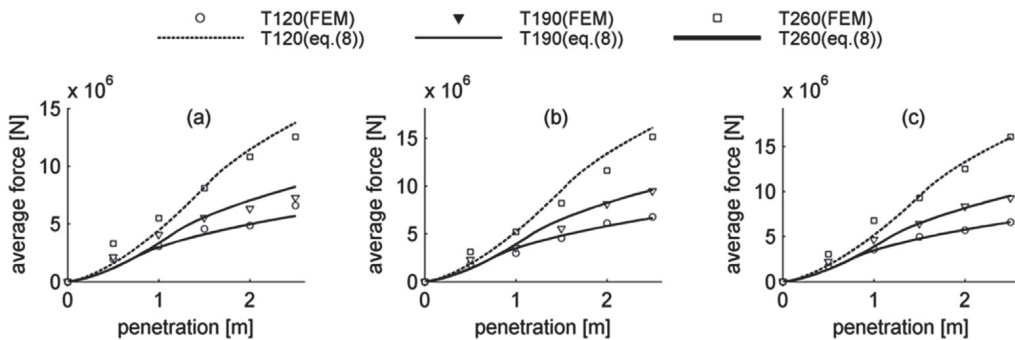


Fig. 17. Comparison of horizontal forces: a) Rock A ($a = 3$); b) Rock B ($a = 6$); c) Rock C ($a = 12$).

4.2. Opening width

To assess the applicability of Eqs. (16–19), opening widths D_{out} and D_{in} were calculated and compared to the numerical simulations. The comparison is shown in Fig. 18, where in each graph D_{out} and D_{in} are presented for a certain rock and ship size. The comparison reveals that the Eqs. (16–19) estimate the opening widths in the outer and inner bottom with relatively good accuracy and the maximum deviation from the numerical simulations is up to 25%.

5. Validation with the real accidental data

In order to assess the developed approach in more realistic circumstances, 18 grounding accidents occurred in Finnish waters [21] were studied. The report covers several ship types. However, since they all have double-bottom structures, comparison to the derived simplified equations can be made. In Ref. [21], for each accident the bottom damage is described via the extent of the replaced steel structure using four measurements - damaged area A , maximum vertical depth d of the damage, the length s of the damaged area (cannot exceed ship length) and the total damage length l , which is the sum of the lengths l_i of individual damage paths, see Fig. 19. Unfortunately, this data only allows to compare the

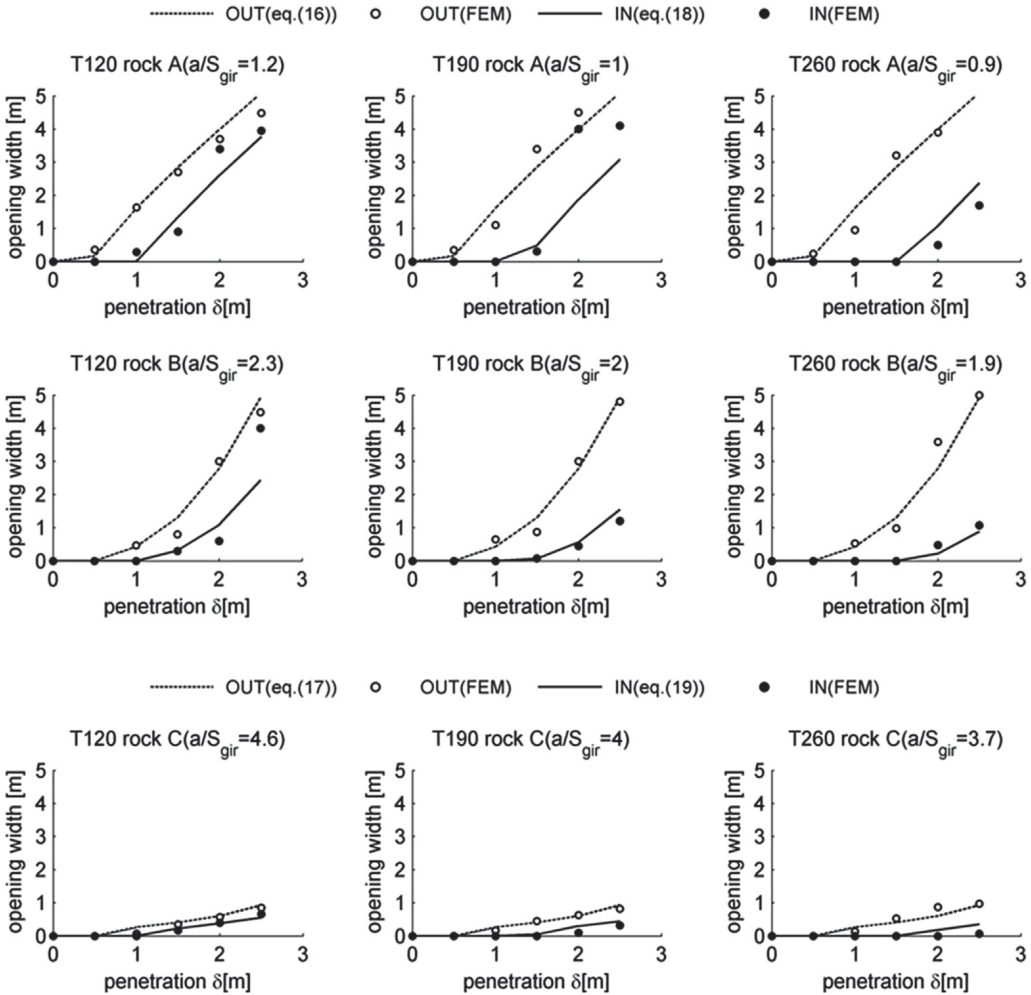


Fig. 18. Comparison of the inner and the outer opening width.

grounding force and the deformation energy as only very limited information is presented for the damage openings.

Based on the registered ship velocities, Luukkonen calculated the loss of the kinetic energy E_{kin} and compared it with deformation energy evaluated with simplified models given by Minorsky [4], Vaughan [22] and Luukkonen [21], which all are based on the volume of the damaged steel. To compare the derived equations to these results, the deformation energy was also evaluated as a product of the damage length l and the grounding force F_H , given with Eq. (8). For that the rock size parameter a was derived with the help of the equivalent damage breadth A/l and the maximum vertical depth d . The results are presented in Table 3, where the calculated deformation energy and the corresponding differences to the loss of the kinetic energy are given for each ship. Table 3 shows that with all four calculation approaches the general trends are predicted, while some results still deviate significantly. As expected, the energy is often over predicted (difference is negative) with Eq. (8), indicating that the actual penetration depth and the rock size are smaller than the maximum vertical depth d and equivalent breadth A/l of the damaged steel structure. Approximately similar level of accuracy is obtained also with the simple formulas by Minorsky, Vaughan and Luukkonen, indicating once again that

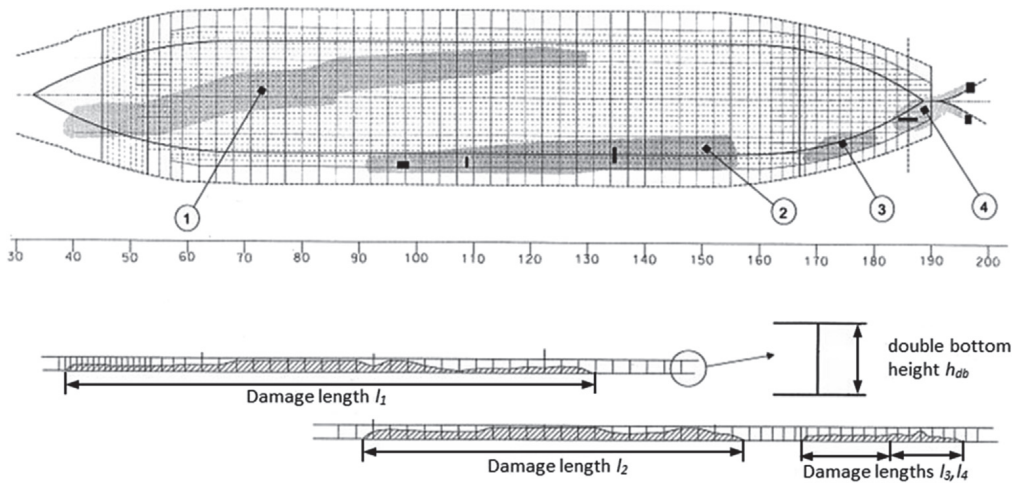


Fig. 19. Detailed bottom damage layout of a tanker #1 [21].

the interpretation of accidental damage data has a great influence on the accuracy of the energy predictions.

For tanker #1 a detailed bottom damage profile is available in Table 11 in Ref. [21], giving also the actual penetration depth in addition to the maximum vertical depth d of the damaged steel, see Fig. 19. That significantly lowered the predicted deformation energy from 667 MJ to 75 MJ while the loss of kinetic energy was 208 MJ. It is obvious that for this example the extent of damaged steel structure significantly exceeds the direct damage by rock, which is required for more precise estimates.

6. Conclusions

Simplified formulas to evaluate the damage opening size in tanker groundings were derived and presented. In the derivations, the effects of ship size and structural resistance were separated from those of rock size and penetration depth. This allows, for example, modifications of the level of ship's

Table 3
Comparison between grounding energies (data adapted form Luukkonen [21]).

Ship type	Ship length [m]	E_{kin} [MJ]	Minorsky [4]		Vaughan [22]		Luukkonen [21]		Eq. (8) $\times l$	
			E_{calc} [MJ]	Dif. from E_{kin} [%]	E_{calc} [MJ]	Dif. from E_{kin} [%]	E_{calc} [MJ]	Dif. from E_{kin} [%]	E_{calc} [MJ]	Dif. from E_{kin} [%]
Bulker#1	159,2	691	423	39	387	44	324	53	572	-18
Tanker#1	150	208	312	-50	278	-34	233	-12	667	-237
									(75,2)	(-64)
RoRo#2	130	86,9	59	32	27	69	23	74	60,8	38
RoRo#3	130	3,2	49	-1424	17	-425	15	-353	10,8	-237
RoRo#4	146	342	837	-144	798	-133	662	-93	897	-400
Bulker#2	180,5	43,6	94	-115	61	-41	52	-20	131	-183
Ferry#1	142,4	57,8	150	-159	116	-102	99	-71	61,8	-7
Ferry#2	139,8	487	825	-69	786	-61	653	-34	512	-19
RoRo#5	118,5	116	96	17	63	45	54	54	72,6	37
RoRo#6	171,6	144	171	-18	137	5	116	19	104	28
RoRo#7	146	174	246	-41	212	-22	178	-2	514	-244
Tanker#3	126,5	53,9	53	2	20	62	18	67	43,2	24
Bulker#3	134,3	300	351	-17	317	-5	265	12	475	-58
RoRo#8	128,8	245	333	-36	298	-22	250	-2	394	-61
Bulker#4	130	24,5	86	-250	53	-117	45	-85	39,2	-42

structural resistance while leaving the effect of rock size unchanged. These simplified formulas are to be used in analyses, where there is very limited information available regarding the ship structures.

Formulas for the grounding force and the longitudinal extent of structural damage are based on uniform pressure that depends on the rock size alone. This pressure is scaled to the ship level by using the structural resistance coefficient c_T of the ship and the contact area that depends on the rock size and ship's double-bottom height. Two evaluation methods are outlined for this scaling coefficient – a 6-step procedure based on numerical simulations and a regression line based formula. Since the relative rock size strongly influences the deformation mode, either local tearing or global crushing or their combination, damage width was derived separately for two ranges of relative rock size. The calculation of damage size in the inner bottom was improved by introducing the failure criterion presented as a critical relative penetration depth. This failure criterion was found to be in good agreement with the conclusions made in Refs. [20] and [19]. All the formulas were derived without any transverse or longitudinal bulkheads, thus presenting the lowest possible contact force level.

Comparison to the numerical simulations showed that the derived simplified approach describes the horizontal grounding force well for the penetration depths above 0.5 m. For smaller penetration depths, the force is under predicted. Therefore, the approach should be further developed to account for the modes associated with smaller penetration depths, such as tearing of the bottom plating. Acceptable results were also obtained for the damage size. The deviation of the simplified model from the numerical simulations was up to 25%. Comparison was also made to real accidental damage data and to the deformation energy obtained with several simplified formulas. The deformation energy, calculated as a product of horizontal grounding force and damage length, was predicted with similar accuracy compared to the other simplified methods which evaluate the deformation energy based on the volume of deformed steel structures.

The main drawback of the derived equations is a small number of different ship configurations. This is especially important when evaluating the structural resistance coefficient c_T . An additional study will be conducted, where the effects of longitudinal and transverse bulkheads are included. These simulations would significantly extend the number of data points for regression analysis and allow to evaluate the effects of bulkheads and thus, would allow for more realistic damage assessment compared to current very conservative assessment.

Acknowledgements

This research work has been financially supported by Estonian Ministry of Education and Research (grant agreements ETF8718 and IUT19-17) and by Central Baltic Interreg IV A program through MIMIC project (“Minimizing risks of maritime oil transport by holistic safety strategies”). This support is here kindly appreciated.

References

- [1] Brunila O-P, Storgard J. Oil transportation in the Gulf of Finland in 2020 and 2030. 2012. MIMIC project report. A1.
- [2] Kujala P, Hänninen M, Arola T, Ylitalo J. Analysis of the marine traffic safety in the Gulf of Finland, reliability engineering and system safety. 2009. p. 1349–57.
- [3] Sergejeva M, Laanearu J, Tabri K. Hydraulic modelling of submerged oil spill including tanker hydrostatic overpressure, analysis and design of marine structures. 2013. p. 209–17.
- [4] Minorsky VU. An analysis of ship collision with reference to protection of nuclear power plants. *J Ship Res* 1959;3:1–4.
- [5] Simonsen B-C, Törnqvist R, Lützen M. A simplified grounding damage prediction method and its application in modern damage stability requirements. *Mar Struct* 2009;22:62–83.
- [6] [Ph. D. thesis]. thesis Amdahl J. Energy absorption in ship-platform impacts. Trondheim, Norway: Norwegian University of Science and Technology; 1983.
- [7] Wierzbicki T, Culbertson-Driscoll J. Crushing damage of web girders under localized static loads. *J Constr Steel Res* 1995; 33:199–235.
- [8] Zhang S. Plate tearing and bottom damage in ship grounding. *Mar Struct* 2002;15:101–17.
- [9] Simonsen BC. Ship grounding on rock - I. Theory. *Mar Struct* 1997;10:519–62.
- [10] Wang G, Arita K, Liu D. Behavior of a double hull in a variety of stranding of collision scenarios. *Mar Struct* 2000;13: 147–87.
- [11] Wang G, Ohtsubo H, Liu D. A simple method for predicting the grounding strength of ships. *J Ship Res* 1997;41(3):241–7.
- [12] Hong L, Amdahl J. Rapid assessment of ship grounding over large contact surfaces. *Ships Offshore Struct* 2012;7(1):5–19.
- [13] Friis-Hansen P, Simonsen BC. GRACAT: software for grounding and collision risk analysis. *Mar Struct* 2002;15:383–401.

- [14] Kitamura O. FEM approach to the simulation of collision and grounding damage. *Mar Struct* 2002;15:403–28.
- [15] AbuBakar A, Dow R. Simulation of ship grounding damage using the finite element method. *Int J Solids Struct* 2012;50:623–36.
- [16] Alsos H, Amdahl J. On the resistance of tanker bottom structures during stranding. *Mar Struct* 2007;20:218–37.
- [17] Heinvee M, Tabri K, K orgesaar M. A simplified approach to predict the bottom damage in tanker groundings. In: Proceedings of 6th International Conference on collision and grounding of ships and offshore structures, Trondheim, Norway; 2013.
- [18] Lehmann E, Egge E, Scharrer M, Zhang L. Calculation of collisions with the aid of linear FE models. In: PRADS; 2001.
- [19] Nguyen T, Garre L, Amdahl J, Leira B. Benchmark study on the assessment of ship damage conditions during stranding. *Ships Offshore Struct* 2010;7(2):197–213.
- [20] Rodd J, Sikora J. Double hull grounding experiments. In: in Fifth International offshore and polar engineering conference (ISOPE), Denmark, Haag; 1995.
- [21] Luukkonen J. Damage of ship bottom structures in grounding accident [in Finnish], M-239 report. Espoo: Helsinki University of Technology; 1999.
- [22] Vaughan H. Damage to ships due to collision and grounding. DnV Technical Report No. 77-345. Oslo, Norway; 1977.

PUBLICATION III

Heinvee, M., Tabri, K., Kõrgesaar, M., Urbel, A. **Influence of longitudinal and transverse bulkheads on ship grounding resistance.** *Proceedings of International Conference on Collision and Grounding of Ships and Offshore Structures: International Conference on Collision and Grounding of Ships and Offshore Structures*, 15-18.06.2016, South Korea.

Influence of longitudinal and transverse bulkheads on ship grounding resistance and damage size

Martin Heinvee¹⁾, Kristijan Tabri¹⁾, Mihkel Kõrgesaar²⁾, Annika Urbel¹⁾

¹⁾Depth. of Mechanics, Faculty of Civil Engineering, Tallinn University of Technology, Estonia

²⁾Depth. of Applied Mechanics/Marine Technology, Aalto University, Espoo, Finland

Abstract

This paper presents improvements to the simplified ship grounding resistance and damage opening model for double bottom tankers of Heinvee et al. (2013) by including the effect of longitudinal and transverse bulkheads. The study is based on numerical simulations of 90 grounding scenarios. The scenarios were constructed for three different size tankers, three rock sizes and five penetration depths. Influence of the longitudinal bulkhead on the grounding resistance is described via additional term. The effect of the transverse bulkheads on the grounding resistance is less profound and thus, this influence is excluded from the simplified formulas. A new approach for the calculation of structural resistance coefficient, that allows scaling of the grounding resistance according to the ship size, is proposed based on the volume of deformed material. Moreover, it is shown that Minorsky's formula (Minorsky, 1959) for ships collisions is also valid for ship grounding. Formulations for the prediction of the size of the damage opening were modified to include the effect of the bulkheads.

Keywords

Ship grounding; Simplified analytical method; Grounding damage assessment.

Introduction

The paper presents a simple formula for a rapid prediction of grounding damage of double hull tankers. These simplified formulations are aimed for risk analysis studies where there is only limited amount of information available regarding the ships. Several simplified models have been developed to describe a ship grounding accidents. The models either base on a simplified closed form expressions (Cerup-Simonsen et al. 2009), (Hong & Amdahl 2012) or on numerical simulations (Alsos & Amdahl 2007). Precise numerical simulations are too time consuming for risk analyses and require detailed input information. On the other hand, simplified models are often limited to a certain sea bottom topology or to ship's structural configuration. Moreover, often the

methods require that to some extent the damage mechanics are prescribed: for example, the description of contact energy is based on the fracture propagation in the bottom plating.

Simple formulation based on a small number of parameters that describe the grounding resistance of a tanker in a grounding accident was derived by Heinvee et al. (2013). The longitudinal and transverse bulkheads contribution was omitted. The aim of the current paper was to determine the effects of the longitudinal and transverse bulkheads to the average grounding resistance and to the damage size. Large number of grounding scenarios with three tankers including longitudinal and transverse bulkheads are simulated for three rock sizes at five penetration depths. Two transverse rock positions were selected for each grounding scenario, one being directly under the longitudinal bulkhead and other between the bulkhead and the side of the ship. With both rock positions, numerical grounding simulations were conducted in displacement controlled manner at constant grounding velocity. For the each grounding simulation, average horizontal grounding force was calculated and the values corresponding to the both rock positions were compared.

The tankers used in the current paper are designed to meet higher strength requirements than tankers used in previous studies (Heinvee et al. 2013, Heinvee & Tabri 2015). Thus, the uniform pressure polynomial as the central element in the simplified approach and the function for the structural resistance coefficient c_T , that scales the resistance according to the ship size, were updated using the same approach as in Heinvee et al. (2013). The structural resistance coefficient c_T is here evaluated based on the volume of the deformed material. Furthermore, it is shown that the simple formula between the dissipated energy and the volume of damaged material given by Minorsky (1959) is applicable also for ship groundings.

The effect of transverse and longitudinal bulkheads to the damage opening size is studied and equations for the outer and inner damage widths are updated compared to Heinvee & Tabri (2015).

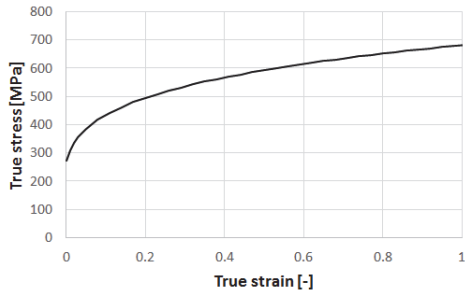


Fig. 3: True stress-strain curve.

Grounding scenarios and rock locations

The grounding simulations were conducted for five different penetration depths δ (from 1.0 to 3.0 [m] with 0.5 [m] spacing) and for three rocks. All the rocks are axisymmetric with parabolic cross-sections given by $z=y^2/a$, with a being the parameter defining the rock size (Heinvee & Tabri 2015). Rocks ranged from sharp rocks denoted as rock A ($a=3$) and rock B ($a=6$) to blunt “shoal”-type rock C ($a=12$).

The grounding simulations are done for two transverse rock locations (see Fig. 4a):

- i) location $B/4$: between the longitudinal bulkhead and the ship side i.e. at $B/4$;
- ii) location $B/2$: directly under the central longitudinal bulkhead i.e. at $B/2$.

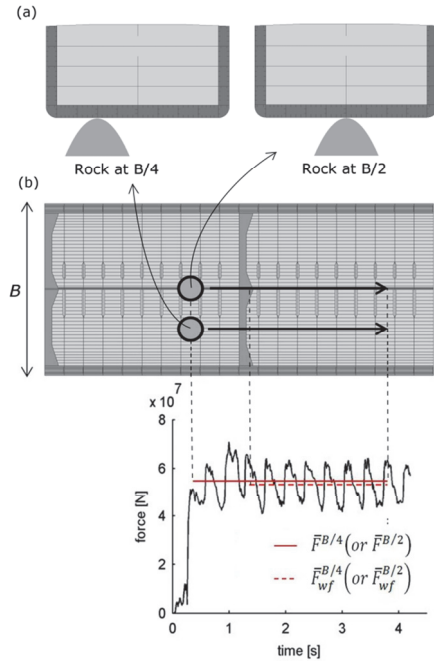


Fig. 4: Setup for FE calculations: (a) rock positions, (b) ranges for the evaluation of grounding forces.

Horizontal rock travel starts two web frame distances

before the transverse bulkhead and terminates at two web frame distances before the next bulkhead, see Fig. 4b. For each simulation, time histories for the horizontal grounding force (Fig. 4b), deformation energy and the volume of the deformed elements are obtained. From each force time histories two average force values are evaluated, Fig. 4b:

$\bar{F}^{B/2}$ (or $\bar{F}^{B/4}$) – average force over the whole horizontal travel distance including the effect of the transverse bulkhead, see red solid line in the figure;

$\bar{F}_{wf}^{B/2}$ (or $\bar{F}_{wf}^{B/4}$) – average force over the reduced horizontal travel distance excluding the effect of the transverse bulkhead, see red dashed line in the figure;

The effect of longitudinal bulkhead can be determined by comparing the average forces $\bar{F}_{wf}^{B/2}$ and $\bar{F}_{wf}^{B/4}$. Similarly, the effect of transverse bulkheads is determined by comparing the average forces $\bar{F}^{B/4}$ and $\bar{F}_{wf}^{B/4}$.

Furthermore, to study the opening widths in outer and inner bottom, the corresponding values are measured from each FE simulation.

Effect of longitudinal bulkhead

The effect of longitudinal bulkhead to the grounding force is presented in Fig. 5 via comparison of average forces $\bar{F}_{wf}^{B/2}$ (longitudinal bulkhead contributes to the grounding resistance) and $\bar{F}_{wf}^{B/4}$ (no resistance contribution by longitudinal bulkhead). Fig. 5 presents the ratio $\bar{F}_{wf}^{B/2} / \bar{F}_{wf}^{B/4}$ as a function of penetration depth for different rocks and ships. Figure reveals that at low penetration depths the longitudinal bulkhead increases the resistance about 10 % regardless of ship and rock size. The influence of the bulkhead increases at higher penetration depths. For $\delta=3$ [m] the maximum force ratios for ships T150, T190 and T260 are 1.3 (30%), 1.46 (46%) and 1.36 (36%) respectively.

It should be noted that at $\delta > 1$ [m] the ratio continues to increase for rocks A and B, while for the rock C the ratio remains almost constant. As the rock C is relatively large compared to the ship cross-sections, the double side starts to contribute to the resistance at higher penetration depths. Thus, it can be concluded that with large shoal-type rocks ($a \geq 12$) the influence of the longitudinal bulkhead is small as it is partly compensated by the contribution from the double side structure. Furthermore in Fig. 5a the ratio decreases for rock C at $\delta > 1.5$ [m] due to the crushing of the ship side that gives significant additional resistance. As the purpose was to determine the effect of longitudinal bulkhead, these scenarios are omitted in subsequent development of the term describing the effect of longitudinal bulkhead (Eq.1 and Fig. 6).

In Fig. 6 the regression curve is fitted through all the $\bar{F}_{wf}^{B/2} / \bar{F}_{wf}^{B/4}$ ratios, giving a term describing the effect of the longitudinal bulkhead:

$$\frac{\bar{F}_{wf}^{B/2}}{\bar{F}_{wf}^{B/4}} = 0.105\delta + 1.04. \quad (1)$$

In order to employ the obtained relationship, we derive formula for the average force $\bar{F}_{wf}^{B/4}$ by using the approach presented in Heinvee et al. (2013).

Thus, the rock directly under the longitudinal bulkhead, the average grounding force can be calculated as

$$\bar{F}_{wf}^{B/2} = \bar{F}_{wf}^{B/4} \cdot (0.105\delta + 1.04), \quad (2)$$

where $\bar{F}_{wf}^{B/4}$ is average grounding force without the contribution from the longitudinal bulkhead.

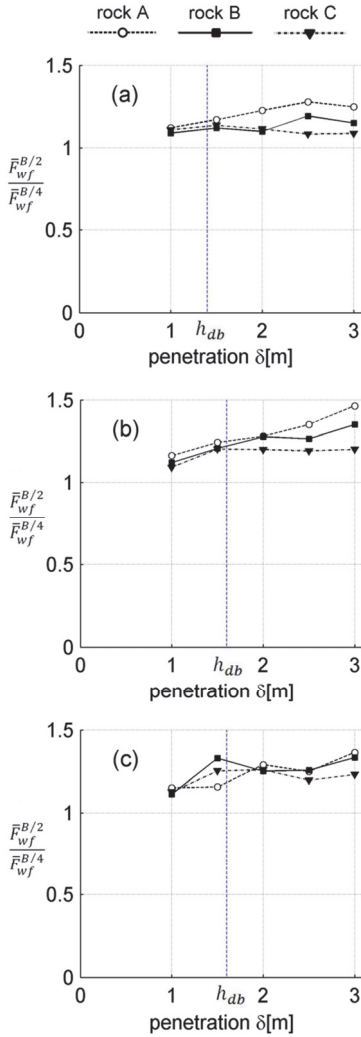


Fig. 5: Increase of average grounding force due to the longitudinal bulkhead presented as a ratio $\bar{F}_{wf}^{B/2}/\bar{F}_{wf}^{B/4}$. Dashed vertical line indicates the double bottom height.

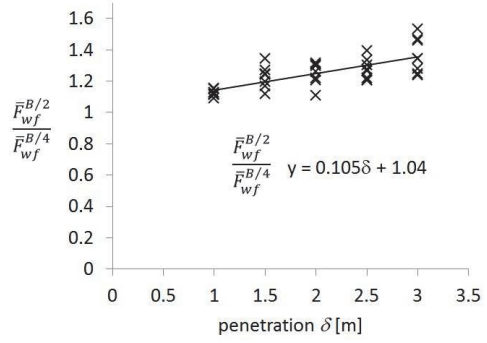


Fig. 6: The effect of longitudinal bulkhead to the average grounding force: The ratio between average forces calculated at $B/2$ and $B/4$.

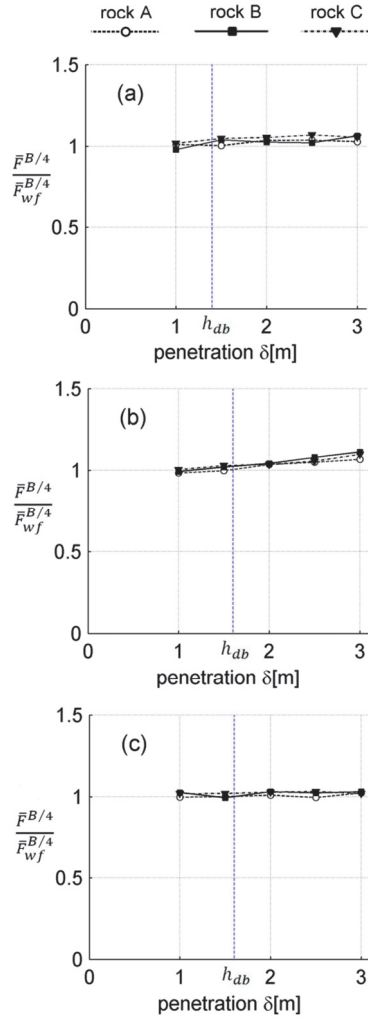


Fig. 7: The effect of transverse bulkhead to the grounding force presented as a ratio $\bar{F}_{wf}^{B/4}/\bar{F}_{wf}^{B/4}$. Dashed vertical line indicates the double bottom height.

Effect of transverse bulkhead

To study the influence of transverse bulkheads we compare two average forces $\bar{F}^{B/4}$ and $\bar{F}_{wf}^{B/4}$. The average forces ratios $\bar{F}^{B/4} / \bar{F}_{wf}^{B/4}$ are presented in Fig. 7 for three ships and for three rock sizes.

In Fig. 7 the force ratios $\bar{F}^{B/4} / \bar{F}_{wf}^{B/4}$ for both rock positions remain almost constant and are approximately equal to 1, which means that bulkhead has only small influence to the average grounding force. Similar behavior of the ratio was observed also for $\bar{F}^{B/2} / \bar{F}_{wf}^{B/2}$. As the influence of the transverse bulkhead to the average grounding force is small, its contribution is not explicitly presented in the simplified equations.

Updated formulas for the grounding force

The simplified formula for the average horizontal grounding force F_H^i was given by Heinvee et al. (2013) as

$$F_H^i = \bar{c}_T^i \cdot \bar{P} \cdot A, \quad (3)$$

where \bar{c}_T^i is a coefficient for ship i and is characterizing ship's structural resistance and defined via bilinear function of ship length L , $\bar{c}_T^i = f_{c_T}(L)$, \bar{P} is the uniform pressure polynomial describing the contact pressure as a function of rock size a and A is the projected contact area between the rock and the ship double-bottom (Heinvee et al. 2013) given in Appendix A.

The current paper updates the function for the structural resistance coefficient \bar{c}_T^i and the uniform pressure polynomial \bar{P} using the same procedure as presented in Heinvee et al. (2013). The updated structural resistance coefficient function for \bar{c}_T^i takes the form (Fig. 8a)

$$\begin{aligned} \bar{c}_T^i &= f_{c_T}(L) \\ &= \begin{cases} -1375 \cdot L + 2609107, & \text{if } 150 \leq L \leq 190 \text{ [m]} \\ 10676 \cdot L + 319322, & \text{if } L \geq 190 \text{ [m]} \end{cases}. \end{aligned} \quad (4)$$

In Fig. 8 the structural resistance coefficients \bar{c}_T^i are presented for the tankers used in this paper (Fig. 8a) and for those used in Heinvee et al (2013) (Fig. 8b) and about 1.6 times increase in recognized. Reasons for that are analyzed in the next section, where the structural resistance coefficient is connected to the volume steel material.

The updated form for the pressure polynomial was derived based on average forces $\bar{F}_{wf}^{B/4}$ and is as follows

$$\bar{P}(a) = 2.64 \cdot 10^{-3} a^2 - 6.1 \cdot 10^{-2} a + 1.16. \quad (5)$$

The contact force in grounding can now be calculated using Eq. 3. If the rock is positioned directly under the longitudinal bulkhead then Eq. 3 is to be multiplied with the term given by Eq. 1 giving the average grounding force under the longitudinal bulkhead as

$$F_H^i = \bar{c}_T^i \cdot \bar{P} \cdot A \cdot (0.105\delta + 1.04). \quad (6)$$

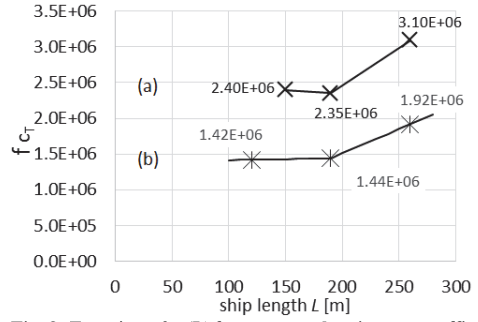


Fig. 8: Functions $f_{c_T}(L)$ for structural resistance coefficient \bar{c}_T^i : (a) based on tankers used in current paper and (b) from Heinvee et al. (2013).

Structural resistance coefficient as a function of material volume

The difference of structural resistance coefficients in Fig. 8 is due to the different design criteria used for the ships- the tankers in the current paper meet all the strength criteria according to HCSR-OT rule while the tankers in Heinvee et al. (2013) only satisfy the minimum rule scantling requirements and thus, present very conservative approach in means of structural resistance. Clearly, the latter tankers contain less steel. To determine their differences, we calculate the volume of deformed material V_{def} (material where plastic strain $\varepsilon_p > 0.01$) for four numerical simulations: two conducted with T190 tankers and two with T260 tankers, see Table 2.

Table 2: Ratios of V_{def} and \bar{c}_T^i for different tankers.

Scenario	δ [m]	V_{def} [m ³]	Ratio (V_{def})	Ratio (\bar{c}_T^i)
T190,rock A*	2.5	4.05	$\frac{6.05}{4.05} = 1.5$	$\frac{2.35}{1.44} = 1.63$
T190,rock A**	2.5	6.05		
T260,rock A*	2.5	5.55	$\frac{7.75}{5.55} = 1.4$	$\frac{3.1}{1.92} = 1.61$
T260,rock A**	2.5	7.75		

* tanker used in Heinvee et al. (2013); ** tanker used in the current study.

The results given in Table 2 show that the volume of deformed material for the current tankers is 1.5 and 1.4 times higher for T190 and T260 tankers, respectively. This indicates a possible correlation between the structural resistance coefficient and the volume of deformed steel material. If such correlation exists, the \bar{c}_T^i values presented by Eq. 4 can be used as a basis to evaluate a \bar{c}_T^j value for any ship j once the steel volumes V_{mat}^i and V_{mat}^j are determined:

$$\begin{aligned} \frac{\bar{c}_T^i}{\bar{c}_T^j} &= \frac{\bar{V}_{mat}^i(a, \delta)}{\bar{V}_{mat}^j(a, \delta)} \rightarrow \\ \bar{c}_T^j &= \frac{\bar{V}_{mat}^j(a, \delta)}{\bar{V}_{mat}^i(a, \delta)} \bar{c}_T^i, \end{aligned} \quad (7)$$

where $\bar{V}_{mat}^i(a, \delta)$ and $\bar{V}_{mat}^j(a, \delta)$ are approximations for the steel volume to be deformed per unit length in a certain grounding scenario defined via rock size a and penetration depth δ . A routine to approximate this volume is presented in detail in Appendix A, which also presents the \bar{V}_{mat}^i values for the tankers (Table. A1) used in the current paper. In the calculation procedure the volume \bar{V}_{mat}^i includes the contributions from the double bottom structural members, which are in direct contact with the rock.

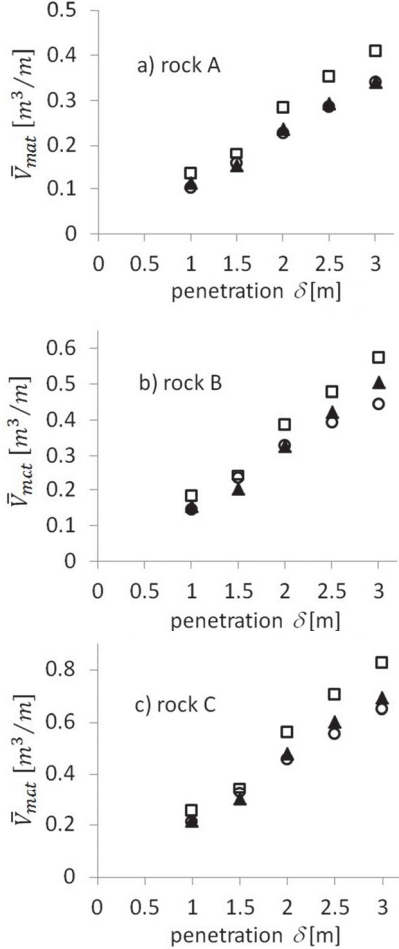


Fig. 9: Averaged volume of deformed material compared for ships T150, T190 and T260: a) Rock A; b) Rock B and c) Rock C.

In Fig. 9 averaged steel volume \bar{V}_{mat}^i is presented for all the simulated scenarios with position B/4. Two patterns can be recognized. First, for each ship the averaged volume increases proportionally with the penetration depth. This holds for all the rocks. This indicates that the ratio of average volumes at each penetration depth is constant between any two ships. This is also presented in Table 3, where the averaged steel volumes are normalized with respect to the volume of the largest tanker

T260. The Table 3 reveals that the normalized values are constant for each tanker, except for T150 at $\delta=1.5$ [m] for which the normalized value is 0.93. This is due to rapid and local increase in steel volume as the penetration slightly above the double bottom height ($h_{db}=1.4$ [m] for T150). This effect diminishes as the penetration increases further. Thus, it is suggested to use $\delta \geq h_{db}$ for the evaluation of the \bar{V}_{mat} in Eq. 7.

Table 3: Normalized material volumes.

Ship	$\bar{V}_{mat}^i / \bar{V}_{mat}^{T260}$ penetration δ [m]		
	1.0	1.5	2...3
T150	0.80	0.93	0.8
T190	0.85	0.84	0.85
T260	1	1	1

In Fig. 10 the normalized volumes from Table 3 and the \bar{c}_T^i values from Fig. 8 are presented as a function of ship size. All the values are normalized with respect to the corresponding value of the largest tanker T260. The comparison shows that the average volume behaves similar to the structural resistance coefficient. Thus, the structural resistance coefficient can be determined via the steel volumes by using Eq. 7. It should be noted, that for the comparison in Eq. 7, the same a and δ values should be used both for $\bar{V}_{mat}^i(a, \delta)$ and $\bar{V}_{mat}^j(a, \delta)$ and for $\delta \geq h_{db}$.

Moreover, as the link between the \bar{V}_{mat}^i and the structural resistance exists, there should also be a relationship between the steel volume and the deformation energy. This relationship is studied in the next section.

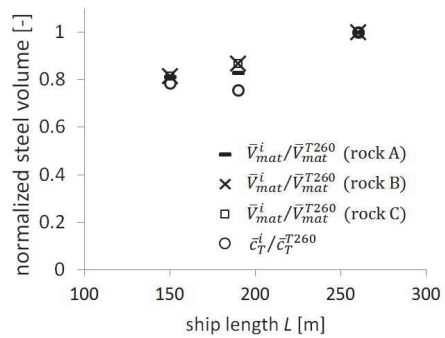


Fig. 10: Comparison of normalized steel volume and structural resistance coefficients given.

Relationship between the dissipated energy and volume of deformed material

It was shown by Minorsky (1959) that there is linear correlation between the volume of the deformed material and the energy dissipated during the ships collision.

In Luukkonen (1999) the performance of Minorsky's equation together with several other simplified models was analyzed with respect to real grounding accidents. Although the correlation between the deformed material and the dissipated energy was recognized, significant variations occurred for all the models. Obviously, the differences were partly due to poor reporting of the real accidents, e.g. the grounding velocity and the description of the grounding scenario. Here the aim is to develop linear relationship between the steel volume \bar{V}_{mat}^i and the absorbed energy based on numerical simulations, where the grounding scenario is well defined.

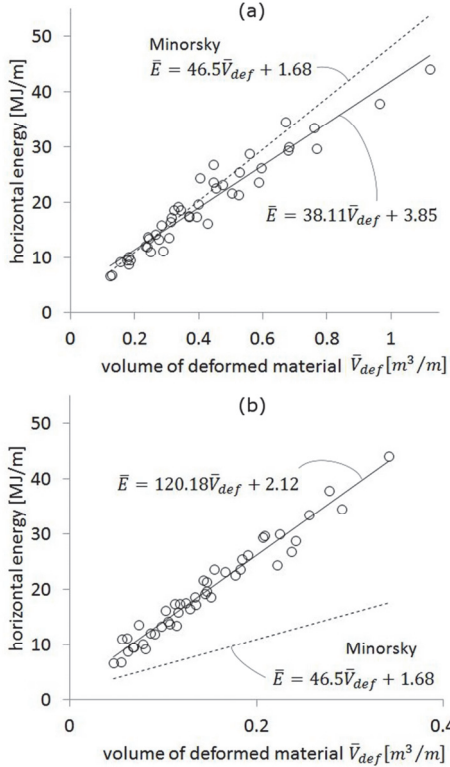


Fig. 11: Averaged energy vs volume of deformed material per unit damage length in case of B/4: (a) $\varepsilon_p > 0.01$; (b) $\varepsilon_p > 0.1$.

We use the steel volume V_{mat} (Appendix A) to approximate the volume of the deformed material V_{def} . For each grounding simulation the volume of deformed material V_{def}^i was calculated for two different levels of equivalent plastic strains: $\varepsilon_p > 0.01$ and $\varepsilon_p > 0.1$, which are plotted against the dissipated energy in Fig. 11 for the position B/4. The dissipated energy includes the contribution from friction. In the figure, both the energy \bar{E} and the steel volumes are presented per unit length. For that the deformation energy E absorbed during the rock travel over the horizontal distance L_h (Appendix A) was divided with L_h to obtain \bar{E} . For both plastic strains a strong linear correlation can be noticed. Clearly, the amount of deformed material depends how one defines

the deformed material. It is interesting to note that for $\varepsilon_p > 0.01$ the obtained dependency is very similar to the one shown by Minorsky (1959). To maintain the similarity to Minorsky's classical relationship, we derive the relationships based on $\varepsilon_p > 0.01$, giving the deformation energy \bar{E} per unit length as:

$$\bar{E} = \begin{cases} 38.11(1.07\bar{V}_{mat} + 0.021) + 3.85 \text{ [MJ/m]} & \text{for rock at } B/4 \\ 38.11(1.26\bar{V}_{mat} - 0.016) + 3.85 \text{ [MJ/m]} & \text{for rock at } B/2 \end{cases} \quad (8)$$

where \bar{V}_{mat} unit is $[m^3/m]$.

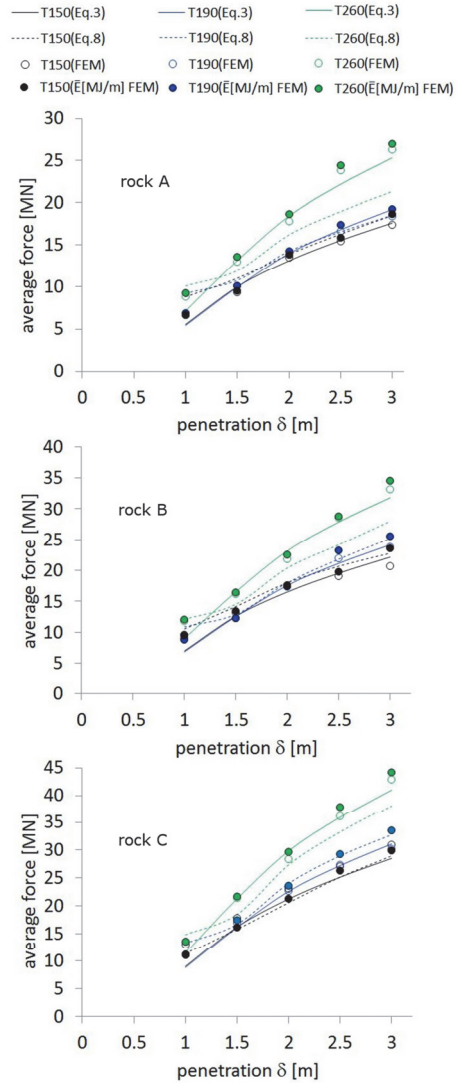


Fig. 12: Average force calculated with Eq. (3) and Eq. (8), ($\varepsilon_p > 0.01$).

It should be noted, that the energy per unit length, \bar{E}

given by Eq. 8, has a unit of [MJ/m] and actually represent the average grounding force. Thus, it can be directly compared to the average grounding force given by numerical simulations and with Eq. 3 and Eq. 6. For the position B/4, this comparison is given in Fig. 12, where empty circles present the average grounding force from numerical simulations, filled circles present the energy per unit length from numerical simulations, solid lines present Eq. 3 and dashed lines present Eq. 8. Good correlation exists between the equations and the numerical simulations, except for Eq. 8 and tanker T260, where the deviation is about 15-20%.

Depending on the available information for grounding scenario either Eq. 3, Eq. 6 or Eq. 8 can be used for the calculation of the average grounding force. If the rock size, penetration depth and the ship scantlings are available then Eq. 8 can be used to take into account the resistance of the specific ship. However, if such detailed data for ship is not available then Eq. 3 or Eq. 6 can be employed using the penetration depth, rock size, ship length and double bottom heights as variables.

Size of the damage opening

In this chapter the effect of transverse and longitudinal bulkheads to the damage opening width is studied. The damage opening formulas developed in Heinvee & Tabri (2015) are updated accordingly. The damage opening formulas give the dimensions of the opening widths and should be used together with a criteria defining whether the failure in the inner bottom occurs. First, the formulas for the opening widths are updated following the updated criteria for critical penetration depth.

Damage width in outer and inner bottom

In each numerical simulation the average opening width was measured for the outer and inner bottom and the measurements are presented in Fig. 15. Fig. 15 presents the damage widths only for the position B/4. In B/2 the behavior and the damage dimensions were similar meaning that the effect of longitudinal bulkhead to the average inner opening width is modest. Moreover, observations from FE simulations showed that a noticeable increase in opening width in the inner bottom occurred locally at the vicinity of the transverse bulkhead and this has only minor effect on the average width. The numerical simulations showed that the grounding damages with respect to the ship size were relatively local and concentrated to the vicinity of the intruding rock, see Fig.13b. It is interesting to notice that the presence of the transverse and longitudinal bulkheads contributed to the localization of the damage. In the simulations without the bulkheads (Heinvee & Tabri, 2105) the stiffness of the double bottom was lower and, especially in the case of larger rocks, the resulting damage was global deformation of the whole double bottom, see Figure 11a. When the bulkheads are included, the dominating deformation mode is a combination from local tearing and global crushing in case of all three rocks.

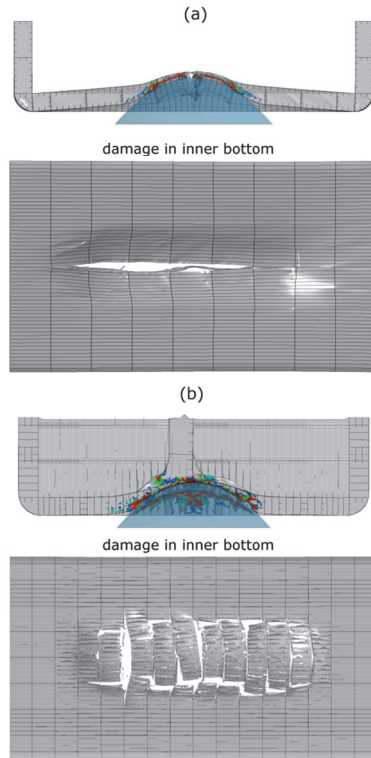


Fig. 13: Comparison of bottom damages: (a) tanker without the bulkheads (Heinvee & Tabri 2015) (b) tanker with bulkheads.

In Heinvee & Tabri (2015) the equation for the damage opening widths were given separately for two rock size ranges due to the dominant global crushing modes in the case of large rocks ($a \geq 12$). Here, the deformation modes were similar for all the covered rock sizes and the equations can be presented for a single range covering all the rocks ($3 \leq a \leq 12$). Analysis revealed that within the range of penetration depths 1.0 to 3.0 [m] the behavior of the opening width in the outer bottom generally follows the rock width. Similar observations as in Heinvee & Tabri (2015) can be made:

- i) the opening width in the inner bottom grows similarly to the opening width in the outer bottom;
- ii) onset of failure in the inner bottom is delayed by $\bar{b} \cdot h_{db}$ compared to that in the outer bottom, where constant $\bar{b} \cong 0.75$.

Simulations revealed that the outer bottom failure was observed roughly at $\delta \geq 0.5$ [m]. Thus, the simplified formulas for the prediction of opening widths in the outer and inner bottom are as follows:

opening width in the outer plating

$$D_{out}(a, \delta) = \begin{cases} 2\sqrt{a \cdot \delta} \cdot [1.6\delta - 0.8] & \text{for } \delta \leq 1[\text{m}] \\ 0.8 \cdot 2\sqrt{a \cdot \delta} & \text{for } \delta > 1[\text{m}] \end{cases} \quad (9)$$

$$\text{for } 150 [\text{m}] \leq L \leq 260 [\text{m}], 3 \leq a \leq 12$$

opening width in the inner plating

$$D_{in}(a, \delta, h_{db}) = \begin{cases} 2\sqrt{a(\delta - 0.75h_{db})}[1.6(\delta - 0.75h_{db}) - 0.8] \\ \text{for } \delta \leq 1 \text{ [m]} \\ 0.8 \cdot 2\sqrt{a(\delta - 0.75h_{db})}, \text{ for } \delta > 1 \text{ [m]} \end{cases} \quad (10)$$

for $150 \text{ [m]} \leq L \leq 260 \text{ [m]}$, $3 \leq a \leq 12$.

Comparison between the measured opening widths and the calculations using the above equations are presented in Fig. 15. The figure shows that Eq. 9 slightly underestimates the width of the damage opening in the outer plating especially in the case of larger penetration depths. The deviation is about 20%. For the inner plating opening, the Eq. 10 alone, see dashed lines in Fig. 15, significantly overestimates the damage width for lower penetration depths, while for higher values the prediction is reasonable. Thus, a criterion is required to define the onset of the failure in the inner plating. This criteria is presented in the next section.

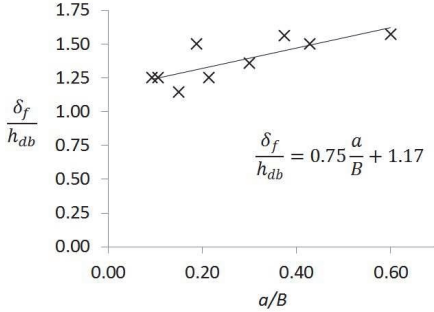


Fig. 14: Fracture criterion for the inner bottom.

Critical penetration depth for the inner bottom failure

The critical penetration depth δ_f defines whether the inner bottom is torn open as Eq. 10 alone might predict inner bottom failure prematurely, see Fig. 15. Updated form for the critical penetration depth is derived in a similar manner to Heinvee & Tabri (2015). In the derivation, the simulations with the rock position $B/2$ are used. The critical penetration depth δ_f obtained from the numerical simulation was divided with the corresponding double bottom height h_{db} , providing the relative critical penetration depth. These ratios are presented in Fig. 14 as a function of the ratio between the rock size and the ship breadth - a/B . The regression line through the measured points forms the criterion as follows:

$$\begin{aligned} \frac{\delta_f}{h_{db}} &= 0.75 \frac{a}{B} + 1.17 \rightarrow \\ \rightarrow \delta_f &= \left(0.75 \frac{a}{B} + 1.17\right) h_{db}. \end{aligned} \quad (11)$$

The inner bottom damage occurs once the penetration

depth is higher than given by Eq. 11. After the critical penetration depth is reached, the width of the opening in the inner bottom can be evaluated using Eq. 10, see Fig. 15.

Conclusions

Simplified formulas for the calculation of average grounding force given in Heinvee et al. (2013) have been updated to consider the contribution from the transverse and longitudinal bulkheads. The contribution is studied via series of numerical grounding simulations. The analysis of numerical simulations showed that the longitudinal bulkhead substantially increases the average grounding force. If the intruding rock is directly under the longitudinal bulkhead the grounding force can be up to 50 % higher compared to the situation when the rock is between the bulkhead and the ship side. This influence is included in the simplified formulas via additional term depending on the penetration depth. Analysis also revealed that, in general, the transverse bulkhead has small influence to the average grounding force and thus its contribution is not explicitly included in the equations, while its influence is implicitly included in the structural resistance coefficient.

A new approach was proposed for the prediction of resistance coefficient \bar{c}_T^i based on the approximation of the volume of the deformed material. It was shown that the structural resistance coefficient is proportional to the volume of deformed material. Even though the calculation requires detailed information of ship's double bottom structure, it provides analytical measure to develop more ship-specific estimate for \bar{c}_T^i . Moreover, simulations revealed that a linear relationship exists between the volume of the deformed material and the energy absorbed in grounding i.e. Minorsky's relationship, though slightly modified, is applicable also for ship groundings. Equations to predict the volume of the deformed material in a certain grounding scenario were derived based on the structural configuration of the double bottom.

The longitudinal and transverse bulkheads influence also the damage opening size during the grounding over large rocks. In the case of smaller rocks, the influence of the bulkheads on the opening size was modest.

Acknowledgement

This research work has been financially supported by the BONUS STORMWINDS (Strategic and Operational Risk Management for Wintertime Maritime Transportation System) project, by the research grant IUT1917 from Estonian Science Foundation and by Tallinn University of Technology project B18 (Tool for direct damage calculations for ship collision and grounding accidents). This help is here kindly appreciated.

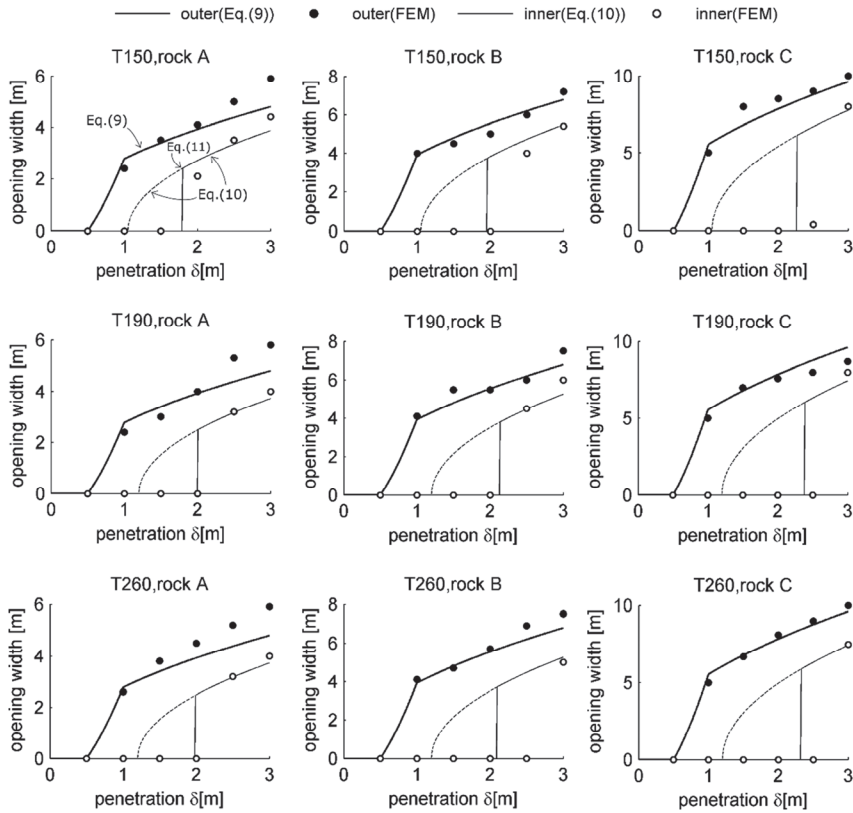


Fig. 15: Opening width in the inner and the outer bottom: FE simulations vs. equations.

References

- Alsos, H and Amdahl, J. 2007. On the resistance of tanker bottom structures during stranding. *Marine Structures* 20: pp 218-237.
- Heinvee, M., Tabri, K and Kõrgesaar, M. 2013. A simplified approach to predict the bottom damage in tanker groundings., Proc. 6th International Conference on Collision and Grounding of Ships and Off-shore Structures, Trondheim, Norway.
- Heinvee, M and Tabri, K. 2015. A simplified method to predict grounding damage of double bottom tankers. *Marine Structures* 43: pp 22-43.
- Hong, M and Amdahl, J. 2012. Rapid assessment of ship grounding over large contact surfaces. *Ships and Offshore Structures* 7(1): pp 7-19.
- Kõrgesaar, M. 2015. Modelling ductile fracture in ship structures with shell elements. Ph.D. thesis, Aalto University, Helsinki, 2015.
- Luukkonen, J. 1999. Damage of ship bottom structures in grounding accident [in Finnish], M-239 report. Espoo: Helsinki University of Technology.
- Minorsky, V.U. 1959. An analysis of ship collision with reference to protection of nuclear power plants. *Journal of Ship Research* 3: pp 1-4.

- Simonsen, B.C., Törnqvist, R and Lützen, M. 2009. A simplified grounding damage prediction method and its application in modern damage stability requirements. *Marine Structures* 22: pp 62-83.

Appendix A

Procedure for the calculation of steel volume:

In transverse and longitudinal direction, the structural members contribute to the total steel volume only if in direct contact with the rock, see red area in Fig. A1. In longitudinal direction the steel volume is evaluated over the horizontal length L_h that is the length of one tank compartment and is symmetric with respect to the transverse bulkhead.

The steel volumes are calculated with the following steps:

- (i) Equivalent thicknesses for the *inner* and *outer* plate, girders and floors are calculated as follows

$$t_{eq} = t_{pl} + \frac{n \cdot A_{stif}}{D},$$

where t_{pl} is the plate thickness, n is the number of stiff

eners on the plate and D is the plate width. If the plating consists of several plates with different thicknesses then the equivalent value for the t_{pl} is calculated as

$$t_{pl} = \frac{\sum_i d_i \cdot t_i}{D},$$

where d_i is the width of i -th plate and t_i is the corresponding thickness.

(ii) Determine the length for the longitudinal members and the number for the transverse members:

The length of *longitudinal members* (inner and outer plate, girders) is taken as L_h .

Number of the *transverse members* is equal to the number of floors inside the length L_h .

(iii) Taking into account the position of the rock with respect to the structural members, calculate the total volumes for the structural members:

Outer plate

$$V_{out_pl} = 2\sqrt{a} \cdot \delta \cdot t_{eq} \cdot L_h,$$

Inner plate

$$V_{in_pl} = 2\sqrt{a} \cdot (\delta - h_{db}) \cdot t_{eq} \cdot L_h,$$

Girders

$$V_{gir} = \sum_i \delta_d \cdot t_{gir}^i \cdot L_h,$$

where, t_{gir}^i is the equivalent thickness of a girder i , δ_d is the height of the “deformed” part of a girder which is given as:

$$\delta_d = \delta - \frac{\Delta Y^2}{a},$$

where, ΔY is the horizontal distance from the tip of the rock to the girder i , see Fig. 1A. If entire girder is “damaged” then $\delta_d = h_{db}$.

Floors

$$V_{floor} = n \cdot t_{eq} \cdot A_{floor},$$

where n is the number of floors, t_{eq} is equivalent thickness of the floor and A_{floor} is equal to the contact area A between the floor and the rock given by

$$A_{floor} = A = \begin{cases} \frac{4}{3}\sqrt{a} \cdot \delta^{(3/2)}, & \text{if } \delta \leq h_{db} \\ \frac{4}{3}\sqrt{a} \cdot [\delta^{(3/2)} - (\delta - h_{db})^{(3/2)}], & \text{if } \delta > h_{db} \end{cases}.$$

(iv) Total volume of material V_{mat} for a scenario is sum of all individual volumes of structural members

$$V_{mat} = V_{out_pl} + V_{in_pl} + V_{gir} + V_{floor} \quad [\text{m}^3].$$

(v) Volume per meter is calculated as

$$\bar{V}_{mat} = V_{mat}/L_h \quad [\text{m}^3/\text{m}].$$

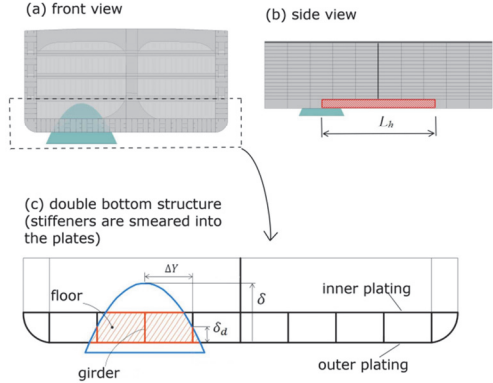


Fig. A1. The principle scheme for the calculation the steel volume of deformed material V_{mat} .

Table A1 present the \bar{V}_{mat}^i and \bar{V}_{def}^i values for the grounding scenarios simulated in this paper. The presented values are calculated for B/4.

Table. A1: Steel volumes [m^3/m], ($\epsilon_p > 0.01$).

δ [m]	\bar{V}_{mat}^i	\bar{V}_{def}^i	\bar{V}_{mat}^i	\bar{V}_{def}^i	\bar{V}_{mat}^i	\bar{V}_{def}^i
	Rock A ($a=3$)	Rock B ($a=6$)	Rock C ($a=12$)			
T150						
1	0.10	0.12	0.15	0.19	0.21	0.29
1.5	0.16	0.18	0.23	0.28	0.32	0.43
2	0.23	0.24	0.33	0.37	0.46	0.52
2.5	0.29	0.30	0.40	0.40	0.56	0.60
3	0.34	0.32	0.45	0.45	0.65	0.68
T190						
1	0.11	0.13	0.15	0.18	0.21	0.25
1.5	0.15	0.18	0.20	0.23	0.30	0.39
2	0.24	0.27	0.33	0.37	0.48	0.59
2.5	0.29	0.31	0.42	0.48	0.60	0.68
3	0.34	0.34	0.50	0.53	0.69	0.76
T260						
1	0.13	0.16	0.18	0.24	0.25	0.31
1.5	0.18	0.25	0.24	0.31	0.34	0.50
2	0.28	0.34	0.39	0.45	0.56	0.77
2.5	0.35	0.40	0.48	0.56	0.70	0.96
3	0.40	0.45	0.57	0.67	0.82	1.12

PUBLICATION IV

Tabri, K., Aps, R., Mazaheri, A., Heinvee, M., Jönsson, A., Fetissov, M. (2015). **Modelling of structural damage and environmental consequences of tanker grounding.** *In: Analysis and Design of Marine Structures V: 5th International Conference on Marine Structures, 25–27.03.2015, Southampton UK.* Ed. C. Guedes Soares and R. Ajit Sheno. Taylor & Francis, 703–710.

Modelling of structural damage and environmental consequences of tanker grounding

Kristjan Tabri

Department of Mechanics, Tallinn University of Technology, Tallinn, Estonia

Robert Aps

Estonian Marine Institute, University of Tartu, Tallinn, Estonia

Arsham Mazaheri

Department of Applied Mechanics, Aalto University, Espoo, Finland

Martin Heinvee

Department of Mechanics, Tallinn University of Technology, Tallinn, Estonia

Anette Jönsson

Swedish Meteorological and Hydrological Institute, Norrköping, Sweden

Mihhail Fetissov

Estonian Marine Institute, University of Tartu, Tallinn, Estonia

ABSTRACT: Paper presents a simulation environment for a fast assessment of ship grounding accidents in means of structural damage and environmental consequences. The simulation environment consists of (i) statistical analysis to evaluate the relevant accidental scenarios; (ii) accidental damage and oil spill assessment and (iii) SmartResponse Web based environmental consequence evaluation. The damage evaluation module defines the size and the position of the structural damage that is input for the oil spill analysis. The amount and time duration of oil spill is simulated using a model based on internal hydraulics theory. Amount of spilled oil and its propagation in time and space allows to estimate the environmental impact for the region of the accident presented via spilled shoreline length classified according to environmental sensitivity index. The performance of this integrated simulation environment is exemplified by simulating a number of grounding accidents close to the Port of Muuga in the Gulf of Finland.

1 INTRODUCTION

Ship grounding and collision accidents are one of the major types of accidents in maritime transportation. To increase the safety of shipping, the ships or the shipping routes should be analysed for possible accidental scenarios. Accidental scenarios can be defined via risk analysis taking into account the traffic routes and flows. For holistic overview of the accidental consequences, the consequence analysis should not only focus on the immediate outcomes such as structural damage, but also include the consequences to the human lives and environment. Therefore, this paper introduces an enhanced methodology for dynamic situation assessment in the case of grounding accidents that allows establishing a link between the maritime traffic flows and possible accidental damage due to maritime accidents. In predicting the environmental impact the actual weather conditions and potentially polluted shoreline environmental sensitivity are considered.

The simulation environment consists of (i) statistical analysis to evaluate the relevant accidental scenarios; (ii) Accidental Damage and oil Spill Assessment Model (ADSAM) and (iii) Smart-Response Web based environmental consequence evaluation. Such environment can be used for risk analysis studies or as tool to provide response related awareness during an actual accident. In building the oil spill response related dynamic situation awareness the Smart-Response Web application is used to integrate the information from 1) ADSAM model that is linking external impact conditions, and tank arrangement to an assessment of structural damage, spill duration and volume, for a range of ship types, 2) spilled oil trajectory and behaviour simulations by Seatrack Web-system for forecasts and backtracking of drift and spreading of oil, chemicals and substances in water (SMHI, 2012), and 3) Environmental Sensitivity Index (ESI) map layers comprising three general types of information—shoreline classification, biological resources and human-use resources

imported into the system as the Web Services. With all these simulation tools combined the accidental outcome can be presented not only as amount of oil spill, but the outcome becomes dependent on the weather conditions that affect also the location and the length of the impacted shoreline.

As a case study several imaginary grounding accidents are simulated for the vicinity of the port of Muuga in the Gulf of Finland. For the case study a simplified risk analysis is conducted that defines one of the most probable ships for the accident and defines the possible grounding locations. Different possible bottom topologies and penetration depth are assumed without deeper insight on the actual topology.

2 SYSTEM DESCRIPTION

2.1 Statistics

In order to generate scenarios for a typical tanker grounding accident in the studied area, three sources of data are utilized; 1- The traffic data of the tankers navigating in the studied area is based on the AIS (Automatic Identification System) data of the Gulf of Finland from the year 2012, obtained from HELCOM-statistics (Baltic Marine Environment Protection Commission—Helsinki Commission), from which the distributions of length and speed of the tanker traffic are extracted; 2- The characteristics of the tankers navigating in the Gulf of Finland, such as DWTs, are extracted from the IHS Fairplay® database; 3- The likely locations for grounding accident scenarios are chosen based on the previously occurred grounding accidents in the Gulf of Finland, which are obtained from the accident database of HELCOM-statistics for the years 1989 till 2011.

The raw AIS data normally have faulty inputs like erroneous geographical coordinates, speeds, Course Over Grounds (COG), and heading as well as missing inputs like the ship dimensions. These problems need to be addressed before one to be able to use the data for any statistical analysis.

The received AIS data from the HELCOM was thus first filtered based on the speed, COG, and headings of the records. The records of vessels with speed more than 40 kn and less than 2 kn are removed from the dataset. Commercial vessels in the studied area cannot reach to speed of 40 kn, thus speeds of that magnitude and above are considered faulty. Additionally, vessels with speed less than 2 kn are considered as stationary and in anchor position; therefore their records are removed from the dataset too to ease the analysis.

The records of vessels with negative COGs, and COGs more than 360 are also considered faulty and removed. Same boundaries are set for the headings. Thereafter, using the algorithms suggested by (vanDorp and Merrick 2009), the filtered data are cleaned from the possible erroneous coordinates. This was done by defining a logical maximum distance between two sequential transmitted AIS records from a single vessel, given the maximum speed of the vessels in the area. Thus, using the instant speed of a vessel and the time of the AIS records, any AIS record that has been transmitted within a larger distance of the defined threshold from either of its previous or following AIS records was detected as faulty and thus removed from the dataset. The missing records regarding the size of the ships are compensated as much as it was possible with other available records in the data, using crosschecking with MMSI and IMO numbers of the vessels. The filtered data are then sorted into a route-based database based on the origin and destination of the ship-tracks, using the algorithm suggested in (Goerlandt and Kujala 2011). The final route-based database is stored in a MATLAB® cell-array, which gives the possibility of easily extracting any desired traffic statistics like distributions of speed and size related to specific ship type and to-from a desired location.

The IHS Fairplay® database is used to obtain the statistical dependency between the various characteristics of the typical tankers navigating in the area. Figure 1 shows the statistical relations between length and DWT and draft of the tankers

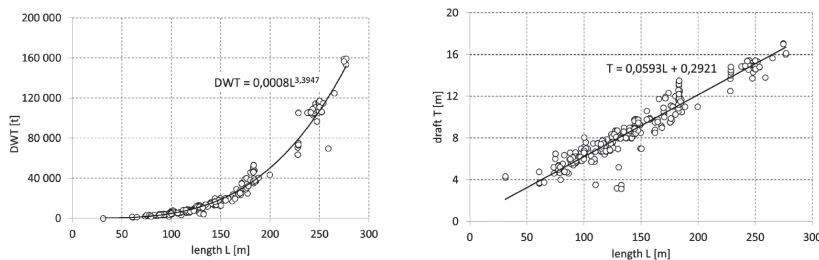


Figure 1. Statistical relations between length and DWT and draft of the tankers navigating in the Gulf of Finland.

navigating in the Gulf of Finland as examples. The obtained relations are utilized with Monte Carlo method to create grounding scenarios.

The HELCOM-statistics accident database is used to find the location of the previously occurred grounding accidents in the studied area (see Figure 4). In total, eight grounding accidents between the years 1989 and 2011 for the studied area are recorded in HELCOM-statistics, in which only one was a tanker.

2.2 Structural damage assessment

Rapid structural damage assessment is based on a model described by Heinvee et al. (2014). The reference presents closed-form solutions for the grounding force, longitudinal structural damage and the opening width in inner and outer plating of the tanker double bottom. The simplified formulas are derived based on a set of numerical simulations that are conducted with tankers of different dimensions. The closed form equations require only limited amount of input such as ship length L , double-bottom height h_{db} , rock size a , penetration depth δ and some other general values. During the grounding only the sway motion of the tanker is considered in order to maintain the simplified nature of the model and to reduce the required input parameters.

The formula for the horizontal grounding force is derived with the consideration that the grounding force is proportional to the contact area and the contact pressure. With using regression analysis it is shown that the contact pressure for any combination of ship- and rock size can be expressed with a single normalized polynomial. The actual contact pressure is found by scaling the normalized pressure with structural resistance coefficient. Given the formulation for the normalized contact pressure $\bar{P}(a)$, the actual contact force $F(L, a, \delta, h_{db})$ for a ship can be found as a product of average contact pressure and contact area $A(a, \delta, h_{db})$:

$$F(L, a, \delta, h_{db}) = P^i A = \bar{c}_T^i \cdot \bar{P}(a) \cdot A(a, \delta, h_{db}) \quad (1)$$

with the contact area between the rock and the double bottom calculated from (see also Figure 2).

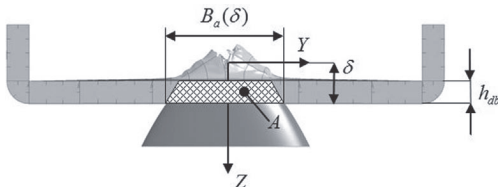


Figure 2. Contact area between the rock and the double-bottom.

$$A(a, \delta, h_{db}) = \begin{cases} \frac{4}{3} \sqrt{a} \cdot \delta^{\left(\frac{3}{2}\right)} & \text{for } \delta \leq h_{db} \\ \frac{4}{3} \sqrt{a} \cdot \left[\delta^{\left(\frac{3}{2}\right)} - (\delta - h_{db})^{\left(\frac{3}{2}\right)} \right] & \text{for } \delta > h_{db}. \end{cases} \quad (2)$$

The structural resistance coefficient \bar{c}_T^i for a selected ship can be evaluated with

$$c_T = f_{c_T}(L) = \begin{cases} 285.71 \cdot L + 1385714, & \text{for } L \leq 190 \text{ [m]} \\ 6857.1 \cdot L + 137143, & \text{for } L \geq 190 \text{ [m]} \end{cases} \quad (3)$$

Equalizing the kinetic energy of a tanker to the work done by the grounding force allows to evaluate the damage length l_{dam} :

$$l_{dam} = \frac{(1 + m_{a,x}) \Delta}{2c_T(1.8 \cdot 10^{-3} a^2 - 7.4 \cdot 10^{-2} a + 1.2) A} v^2 \quad (4)$$

where $m_{a,x}$ is dimensionless surge added mass and Δ is ship's displacement.

The damage opening widths in outer and inner bottom of the ship are derived separately for two ranges of relative rock sizes, as it has strong influence on the deformation mode either local tearing, global crushing or their combination. The damage widths are presented as a function of rock size, rock penetration depth and double bottom height. Damage opening size in outer and inner hulls is calculated with eqs. (16–19) in Heinvee et al. (2014).

2.3 Oil spill assessment

The oil outflow model is based on the model presented by Sergejava et al. (2013). This model is based on the internal hydraulics theory and can evaluate the oil spill from side and bottom damage in single- and double-hull tankers.

In the case of grounding damage, the total oil outflow volume for uni-directional flow is fixed due to the difference in the hydrostatic pressure of the oil and water columns relative to the tank bottom. The total oil outflow duration for uni-directional flow is dependent on the discharge coefficient C_{db} and the shortest duration is associated with the inviscid case i.e. $C_{db} = 1$ (Sergejava et al. 2013).

For the double-bottom damage, see Figure 3, the oil outflow duration T_{oil} and volume V_{oil} can be calculated by analytical formulae:

$$T_{oil} = \frac{2S}{A\sqrt{2g}} \frac{1}{C_d} \sqrt{V_{oil}^*/S} \quad \& \quad (5)$$

$$V_{oil}^* = \left(\Delta_j^* - \frac{\rho_2}{\rho_1} \Delta_o \right) S.$$

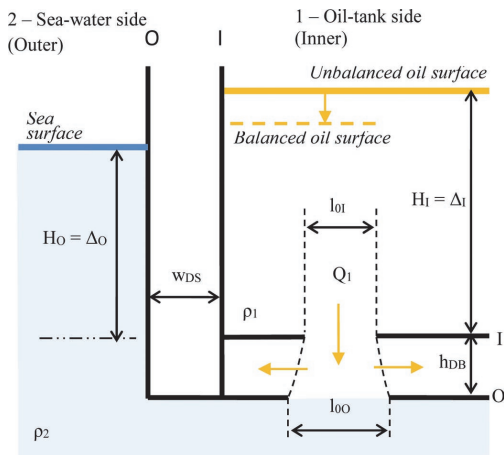


Figure 3. Sketch of the uni-directional flow through the double-hull bottom damage hole and notations. Bottom ballast volume V_{DB} is available for the initial oil volume loss.

where A is the area of the damage opening, S is the surface area of the damaged tank, g is gravitational acceleration, C_d is the discharge coefficient, ρ_1 and ρ_2 are the pressure levels at the opening inside the tank and at the ship bottom, Δ_o is the difference between the sea level and the tank top, Δ_I is the internal height of the tank, and Δ_I^* is fixed by the relationship $\Delta_I^* = \Delta_I - V_{DB}/S$ with V_{DB} being the double-bottom volume under the damaged tanks. It should be mentioned here that no oil outflow occurs from the tanker if the bottom ballast volume V_{DB} is large as compared to the oil outflow volume available due to the internal overpressure. It is assumed that half of the oil contained initially in the double-bottom will be spilled to the sea.

2.4 Environmental impact assessment based on environmental Sensitivity Index

According to NOAA (National Oceanic and Atmospheric Administration, 2002), the Environmental Sensitivity Index (ESI) maps have been an integral component of oil-spill contingency planning and response since 1979 serving as quick references for oil spill responders, comprising three general types of information: 1) shoreline classification, 2) biological resources and 3) human-use resources. The classification of Estonian shoreline geology is elaborated by K. Orviku (Orviku et al. 2010), and is later converted into Estonian shoreline ESI classification (Aps et al. 2014). The environmental sensitivity data represent three different ecosystem elements (Aps et al. 2009): the EU Habitat Directive Annex 1 habitats and associated habitat forming species, the EU Birds Directive

Annex 1 birds and seals. Information on bird, seal and habitat GIS map layers are integrated into a single measure of ecosystem sensitivity—ecological sensitivity index. For this purpose the maximum value of different map layers was calculated in each raster cell. Higher index values correspond to higher ecological sensitivity. GIS map layers of human use values are imported from Estonian Land Board Geoportal and obtained from Estonian maritime administration.

3 CASE STUDY: GROUNDING NEAR THE PORT OF MUUGA

The case study exemplifies the simulation environment by analysing grounding accidents near the Port of Muuga in the Gulf of Finland, see Figure 4. There have been eight reported grounding incidents near the harbour during 1989–2011 as indicated with red dots in Figure 4. None of the grounding incidents have so far resulted in significant oil spill, but however indicate the grounding risks associated with the region. Based on the statistics of the tankers visiting the port, a typical tanker is selected and a number of grounding accidents is simulated for different bottom topologies and penetration depths. Large number of possible oil spills is obtained and for a selected spills the spill trajectory and environmental impact is evaluated and presented in means of polluted shoreline length.

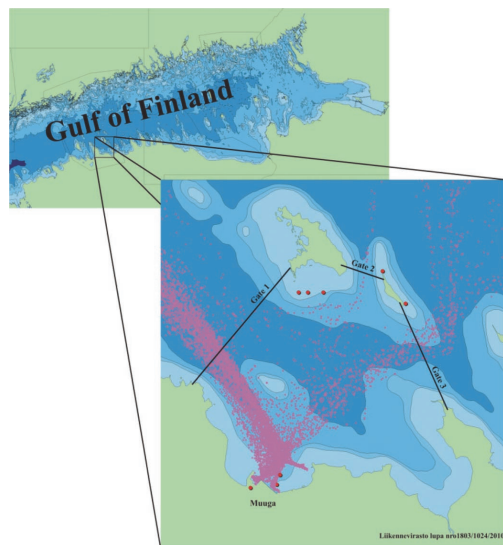


Figure 4. Port of Muuga in the Gulf of Finland, with the defined virtual gates. The locations of the grounding accident occurred between years 1989–2011 near Port of Muuga are shown with red dots.

3.1 Tankers in the port of Muuga

In order to generate the required scenarios for tanker grounding accident in the studied area, the created database is used to extract the traffic of all the tankers to/from port of Muuga. To do so, three virtual gates are defined (see Figure 4) in the way that all the ship traffic to and from port of Muuga have to pass through them. Thereafter, the tankers (i.e. AIS type code of 80 till 89) that their tracks have intersection with the defined gates are considered as traffic to/from port of Muuga. In this way of traffic extraction, the internal traffic of, for instance bunker tankers, inside the port area is not caught and thus is not considered into the statistics that are used for scenario generation.

Based on the extracted tanker traffic, the distributions for the dimensions of the tankers that visited port of Muuga in 2012 are extracted and presented in Figure 5. The length of the tanker is selected as a main parameter and 180 m long tanker is selected for the analysis as being one of the most frequent in the harbour.

3.2 Equivalent tanker and the grounding scenarios

The grounding scenarios are created by a stochastic process that generates random length and speed from the distributions that are extracted from the tanker traffic in the studied area. Then, based on the statistical relation of the length and other characteristics of the tankers such as DWT, the other required data for consequence assessment of the scenario are generated and presented in Table 1.

Table 1. Main dimensions of the tanker used in the grounding analysis.

Length, m	180
Breadth, m	28
Draft, m	11
Depth, m	14
Double-bottom height, m	1.2
Structural resistance coefficient c_T (see Eq. (3))	$1.35e6$

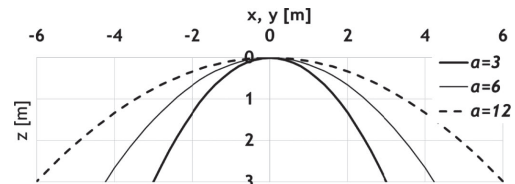


Figure 6. Different rocks used in the simulations.

It is assumed that the ship has a single longitudinal bulkhead.

The exact bottom topology in the region is not known and thus, the grounding accidents are simulated for different rock sizes defined by rock size parameter a , that is given a value $a = 3, 6, 12$ [m]. Each rock is of polynomial shape ($z = y^2/a$) as presented in Figure 6.

For each rock the penetration depth varies from 0.4 to 4 m with 0.5 m spacing. Grounding velocities range from 10 to 18 kn with 2 kn spacing. The accident is assumed to occur at the south of Äksi island as shown in Figure 8.

3.3 Results

Amount of spilled oil (m^3) in simulated scenarios is presented in Figure 7 as a function of damage length. Large number of scenarios resulted in oil spill while some, especially those with small penetration depth or with very large rocks ($a = 12$ or 24), did not yield to spill. In groundings with high speed the damage length became equal to the ship length indicating that the kinetic energy of the ship exceeded the energy absorbed by structural deformations. Figure 7 also reveals two distinct levels for spill amounts at the same damage length depending on whether the bottom under longitudinal bulkhead is damaged and the oil spill occurs from two transverse adjacent tanks.

Table 2 presents the oil spills that are selected for the evaluation of the environmental impact. The accidents are assumed to take place in 2nd of October 2013 and the actual weather conditions for the selected time period are used.

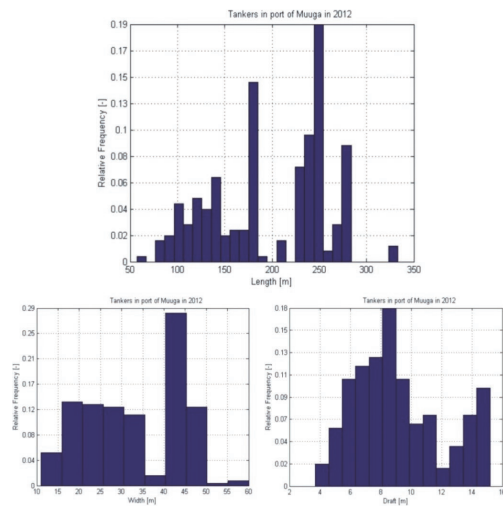


Figure 5. Histogram of tankers' dimensions in the port of Muuga in 2012. The used bin size is 10 m for length, 5 m for width, and 1 m for draft.

According to simulated oil spills (Table 2) the coupled Seatrack Web and SmartResponse Web system was used to assess the level of threat spills poses to the coastal sea sensitive environment (Table 3). Seatrack Web is used to simulate the spill movement according to actual weather conditions, see Figure 8. Once the spill movement analysis is complete, it is used as an input to the SmartResponse Web for the evaluation of the

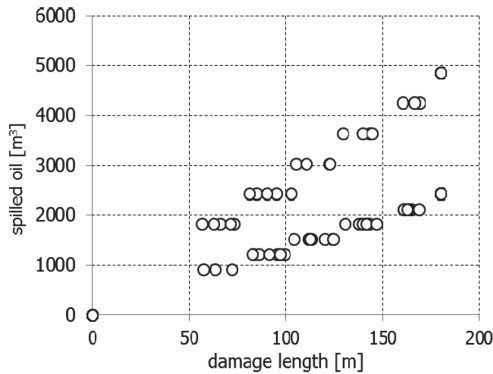


Figure 7. Simulated scenarios, spilled oil vs damage length.

Table 2. Oil spills used for the evaluation of potential environmental impact.

v	a	Penetr. d	l_{dam}	Oil spill
kn	m	m	m	m ³
14	3	4,0	163	2125
14	6	3,0	166	4249
14	6	4,0	139	3642

environmental impact (Figure 9 and Figure 10). Figure 8 shows that under the given weather conditions, the oil spill moves south-east until it reaches to Rammu island and pollutes its shoreline. The environmental damage is presented as the length of the impacted shoreline and as impacted sea area classified by different environmental sensitivity indices in Table 3.

According to first scenario oil is impacting 1.23 km of highly sensitive silty shore (sheltered flats, ESI high sensitivity shore class 9) while second and third scenarios are resulting accordingly in pollution of 1.77 and 1.95 km of medium sensitive gravel-pebble shore (gravel beaches—granules and pebbles, ESI medium sensitivity shore class 5a).

Oil spill simulations showed also that according to particular local weather conditions of 3–5 October 2013 the spilled oil stranding time was in interval 22.5–45 hours and oil was threatening both Natura and Natura & Bird areas (Table 4).

Table 3. Impacted shore ESI type and length (km) and sea area (km²) by environmental sensitivity index intervals (Estonian Aksi and Rammu islands, 2–3 October 2013).

Spill, m ³	ESI shore type	Impacted shore length km	Impacted sea area (km ²) by environmental sensitivity index intervals			
			0–25	26–50	51–75	76–100
2125	Silty shore	1.23	0.07	0.16	0	0
3642	Gravel-pebble shore	1.77	0.24	0.03	0	0
4249	Gravel-pebble shore	1.95	0.35	0.08	0	0

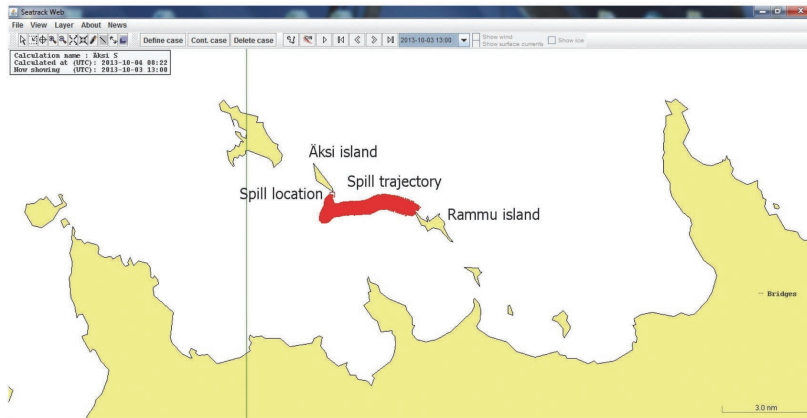


Figure 8. Spilled oil movement simulated by Seatrack Web.

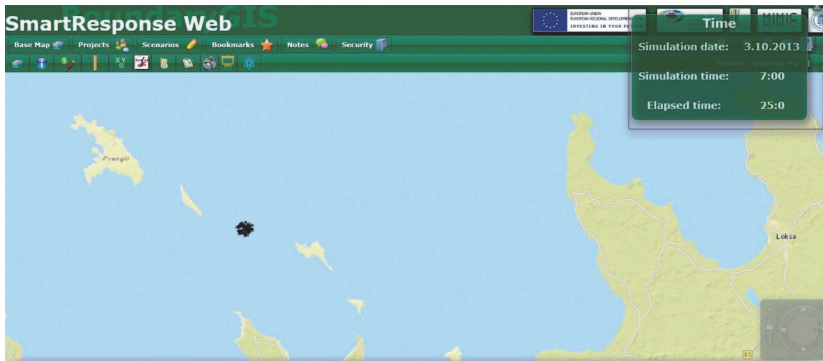


Figure 9. Oil slick size and position simulated by Seatrack Web and imported into SmartResponse Web for potential environmental impact assessment (25 hours after the spill).

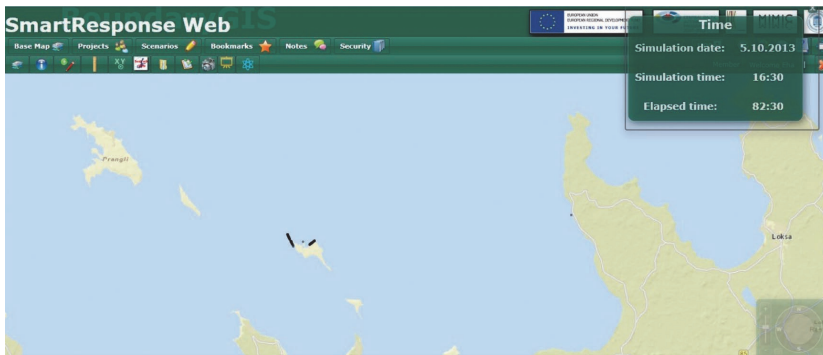


Figure 10. Stranded spilled oil simulated by Seatrack Web and imported into SmartResponse Web for potential environmental impact assessment (end of the spill propagation).

Table 4. Calculated oil stranding time (hours) and impacted Natura and Natura and Bird areas (km²)—Estonian Aksi and Rammu islands, 3–5 October 2013.

Spill m ³	Oil stranding time (hours)	Impacted Natura area (km ²)	Impacted Natura and Bird area (km ²)
2125	45	0.97	0.49
3642	22.5	0.49	0
4249	25	0.56	0

4 DISCUSSION AND CONCLUSIONS

Paper introduced an enhanced methodology for building dynamic situation awareness in maritime accidental oil spill response operations based on oil spill related dynamic situation assessment. The presented model can be used to conduct risk analysis or to provide situation awareness during actual accidents. Proposed holistic approach

allows connecting the traffic flows to possible environmental damage due to maritime accidents.

The case study revealed that in the case of tanker grounding accident near the Port of Muuga both Natura and Natura & Bird areas can be polluted. Oil spill propagation to these areas takes up to 45 hours under the given weather conditions. With the predictions for the spill trajectory, necessary preventive and recovery actions can be undertaken to prevent the pollution in environmentally sensitive areas.

Developed integrated modelling framework for weather forecast driven oil spill related dynamic environmental situation assessment is used already now by Estonian response authorities to better understand the inherent uncertainty in forecasting the outcomes of oil spill, and the likely variability in actual results seen. Further, participation in a process of oil spill related dynamic environmental situation assessment facilitates communication, common understanding, and consensus building within the team of response authorities. Finally, the

simulations of dynamic environmental situation assessment can promote the oil combat training in several ways. The scenario cases can help response authorities to learn the likely impacts of common decisions, and to realize the eventual unreliability of initial expectations.

ACKNOWLEDGEMENTS

This research work has been financially supported by Estonian Science Foundation (grant agreement ETF8718) and by Central Baltic Interreg IV A program through MIMIC project (“Minimizing risks of maritime oil transport by holistic safety strategies”). This support is here kindly appreciated.

REFERENCES

- Aps, R.; Fetissov, M.; Herkül, K.; Kotta, J.; Leiger, R.; Mander, Ü.; Suursaar, Ü. (2009). Bayesian inference for predicting potential oil spill related ecological risk. In: Guarascio, M., Brebbia and Garzia, F. (Eds.) Safety and Security Engineering III. WIT Transactions on the Built Environment (149–159). WIT Press.
- Aps, R.; Tõnisson, H.; Anfuso, G.; Perales, J.A.; Orviku, K.; Suursaar, Ü. (2014). Incorporating dynamics factor to the Environmental Sensitivity Index (ESI) shoreline classification—Estonian and Spanish example. *Journal of Coastal Research*, SI 70, 235–240.
- Goerlandt, F.; Kujala, P. (2011). Traffic simulation based ship collision probability modeling. *Reliability Engineering and System Safety* 96 (1): 91–107.
- Heinvee, M.; Tabri, K.; Kõrgesaar, M. (2013). A simplified approach to predict the bottom damage in tanker grounding. In: *Proceedings of International Conference on Collision and Grounding of Ships and Offshore Structures*. Trondheim, Norway. Taylor & Francis, 2013.
- NOAA, (2002). *Environmental Sensitivity Index Guidelines, Version 3*. NOAA Technical Memorandum NOS OR and R11. Hazardous Materials Response Division, National Ocean Service, Seattle, WA, 192 p.
- Orviku, K.; Kont, A.; Tõnisson, H. (2010). Estonia. Bird, E. (Eds.). *Encyclopedia of the World's Coastal Landforms* (605–611). Dordrecht, Heidelberg, London, New York: Springer.
- Sergejeva M.; Laanearu J.; Tabri K. (2013). Hydraulic modelling of submerged oil spill including tanker hydrostatic overpressure. In: *Proceedings of 4th International Conference on Marine Structures, MARSTRUCT 2013: 4th International Conference on Marine Structures*, Espoo, Finland. Taylor & Francis, 2013, pp. 209–217.
- SMHI. (2012). Manual Seatrack Web—a user-friendly system for forecasts and backtracking of drift and spreading of oil, chemicals and substances in water. <https://stw-helcom.smhi.se/>.
- vanDorp, JR.; Merrick, JRW. (2009). On a risk management analysis of oil spill risk using maritime transportation system simulation. *Annals of Operations Research*, 1–29. doi: 10.1007/s10479-009-0678-1.

PUBLICATION V

Sormunen, O-V., Kõrgesaar, M., Tabri, K., Heinvee, M., Urbel, A., Kujala, P.
Comparing rock shape models in grounding damage modelling. *Marine Structures*. Accepted for publication on 08.07.2016.

COMPARING ROCK SHAPE MODELS IN GROUNDING DAMAGE MODELLING

Sormunen, Otto-Ville Edvard; Kõrgesaar, Mihkel; Tabri, Kristjan; Heinvee, Martin; Urbel, Annika and Kujala, Pentti

Abstract

Groundings are among the most common and destructive maritime accidents. Sea bottom shape influences greatly what kind of damage the ship structure suffers and whether this leads to loss of water tightness.

Sormunen et al. (2016) presented and statistically compared rock models used in grounding damage analysis with detailed bottom shape data from two Finnish harbour fairways. The results were promising in terms of statistical fit especially for the binormal rock model, which also showed a wide range of flexibility in representing different types of sea bottom shapes. However, this measure does not explicitly tell if the model rock in grounding damage analysis results in similar damage size as real rocks cause. To test this, this paper develops a framework for studying, testing and evaluating rock models in terms of resulting grounding damage. FEM is used to analyse and compare grounding damage of rock models to the actual rock using otherwise identical grounding scenarios. Analysis is performed for four different real rocks with each rock being modelled with four different analytical rock models as well.

The results show that rock models with good statistical fit did not necessarily result in similar grounding energy compared to results using the real rock. Differences in energy are caused especially by the rougher surface of the real rocks. For the similarity in rock area and the damaged ship structure element volume the results are much better, especially for the binormal model. As such another criteria for evaluating rock models for grounding damage analysis is needed. The results show that the damaged material volume is strongly linearly dependent on the rock area- and volume metrics. A similar linear dependency exists between the damaged volume and the energy dissipated in grounding. Knowledge of these relationships can be used towards estimating grounding damage of ships in future investigations, but rock surface unevenness should be evaluated as well.

1. Introduction and aim

Groundings are among the most common and destructive maritime accidents that can lead to loss of ship, cargo, life as well as potentially long-term environmental damage if noxious liquid cargo is spilled. To model grounding risk several studies have been conducted, see e.g. Pedersen (2010), Mazaheri et al. (2014) and Goerlandt and Montewka (2015) for an overview. Understanding the risk is the first step towards mitigating it.

There are different approaches and tools for predicting grounding damage on ships ranging from simplified analytical methods to detailed non-linear finite element analysis (Brown et al. 2000, Sormunen, 2014). In general, these tools require a number of inputs related to the ship (mass, velocity, structural scantlings, etc.) as well as inputs related to the sea bottom shape and ship draft during grounding. The sea bottom shape is one of the important factors that determine whether a grounding leads to loss of watertightness and consequently to a spill (Alsos and Amdahl, 2007). Currently the sea bottom during grounding is most often assumed to be a symmetrical conical object, see e.g. Naar et al. (2002) and Rodd (1997). Heinvee and Tabri (2015) and Heinvee et al. (2013) use a polynomial rock while in Sormunen et al. (2016) a binormal rock model was proposed. A discussion of the sea bottom shape models can be found in Sormunen et al. (2016). To which extent these rock models represent real sea bottom shapes is unknown. Therefore Sormunen et al. (2016) tested four different analytical rock models and their goodness-of-fit to real data in terms of coefficient of determination (R^2). This gives a quantitative metric to how closely the rock model shape matches the data. The analysis was carried out using real bottom shape data from Finnish Transport Agency covering the two busiest Finnish tanker harbour fairways. The tested model rocks included proposals from the literature as well as novel models proposed in that paper: two different polynomial equations, a cone and a binormal function. The results show that the binormal function gives overall the best results and for most cases a good statistical fit in terms of coefficient of determination (R^2). However, this mathematical fit does not necessarily mean that the rock model would result in similar grounding damage as the real rock in identical grounding scenarios.

Therefore, the main aim of this paper is to develop a framework for systematically studying, testing and evaluating rock models in terms of resulting grounding damage. This includes quantifying the most important parameters and comparing whether a rock model with a good statistical fit results in similar grounding damage as the real rock. The insight gained by comparison of structural damages and

absorbed energies is vital for assessing the overall performance of analytical rocks and thus sets a stage for improvements in damage stability rules and regulations.

2. Framework

The authors propose a four-step framework for comparing grounding damage differences using rock models and actual rock data:

- **Step 1: Selection of real bottom data and bottom shape models for analysis.**

Current rock shape assumptions in literature are cone- or polynomial shaped models, which show a relatively poor statistical fit to real data. Furthermore, there is a large variation in size and shape of real bottom shapes, which needs to be reflected in the rocks and rock models that are used for studying grounding damage. (Sormunen et al., 2016) Therefore, four different rocks representing various sea bottom shapes and four rock models are selected for analysis, see eq. 1-4.

- **Step 2: Grounding damage estimation with selected rock models and real rocks.**

Knowing the exact shapes of the rocks, non-linear FEM is used to calculate the grounding damage for each case. In these comparative simulations, the same ship is used and the only changing input variable is the sea bottom shape, i.e. rock.

- **Step 3: Comparison of obtained grounding damage.**

Knowing the results from step 2, the grounding damage due to different rock models is then compared with the results obtained using the real rocks. Furthermore, the main parameters affecting the differences in damage results are determined and analysed. This has currently not been studied systematically in the literature.

- **Step 4: Acceptance or revision of bottom shape models.**

Based on the findings in step 3, the goodness of the bottom shape models is evaluated and the degree to which they can be used to replicate real rocks is assessed. In this paper this is done by using a similar grounding scenario for the real rock and for each of the rock models, for which the differences in damage are compared. The differences in damage results are evaluated and compared to the degree of geometrical similarity between the rock model and the real rock. This is measured in terms of

coefficient of determination (R^2), which has an upper limit of 1 for a perfect fit of the model to the data. The assumption is that as R^2 goes towards 1 the grounding damage difference goes to 0 between the model and the real rock. If the results show a poor fit in terms of grounding damage, recommendations for improving the accuracy of the rock models are given.

This framework is applied on case study bottom data from selected Finnish fareways, which is described as follows.

3. Case study

Step 1: Bottom data and bottom shape models

The bottom topography data used here is Finnish Transport Agency (Liikennevirasto) data presented in Sormunen et al. (2016). The data is multibeam (MBES) and multi transducer echo sounder (MTES) readings as xyz-points taken from fairway surveys from Finnish harbors. From this data four example rocks were selected for further analysis to investigate whether good R^2 would indicate a good congruency in terms of grounding energy in grounding damage analysis.

The real bottom shape data is represented by a point cloud of coordinates xyz. This means that the real rock surface shape was obtained through interpolation as shown see Figure 1. The surface geometries for different rocks were generated with Siemens NX software. The first step in the geometry creation was the import of the point cloud into NX. Next, the rock surfaces were created using either surface fitting or *through points* method. Most of the surfaces were created with parametrized surface fitting. This fitting smooths out potential outliers and interpolates gaps in data. Due to the relatively smooth change of curvature of the rocks, this fitting was considered to be the most appropriate. The exception to this approach were the peaks of the cone model (equation 1), where rapid geometry change was achieved by connecting the points with straight lines i.e. the *through points* method was used. This allowed maintaining the sharp peak of the cone models, see Appendix 1-2 for more details.

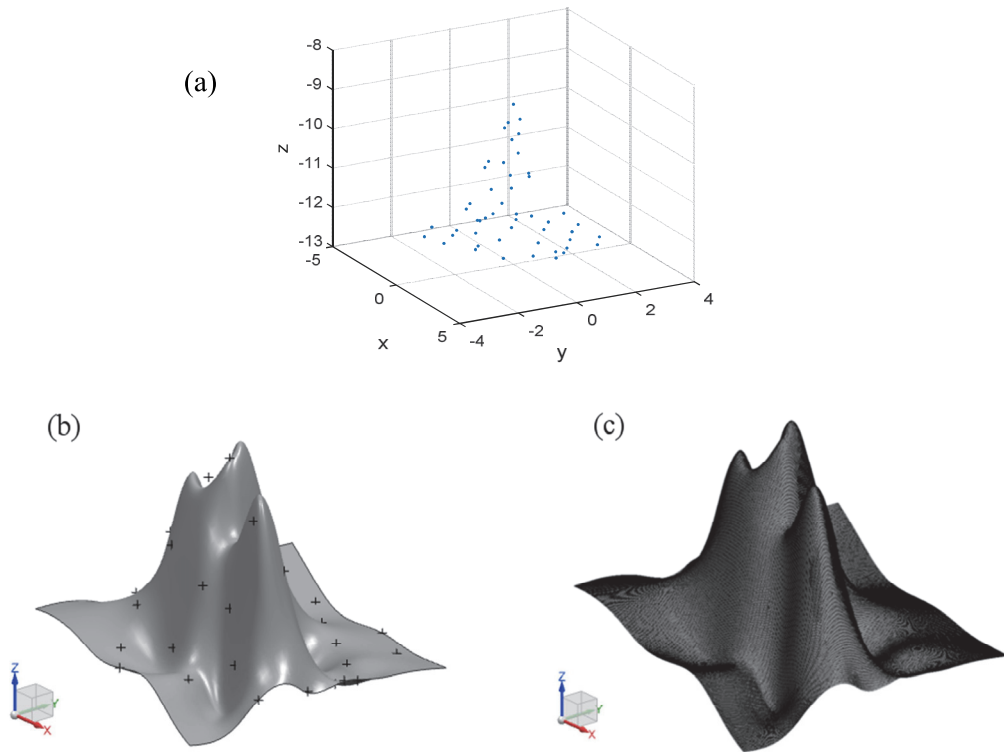


Figure 1 Example of raw sea bottom data of rock 10a as xyz-point cloud (a) with interpolated surface (b) and the meshed version (c).

The small number and unevenly scattered points combined with the subjectivity of modelling makes surface creation for this kind of data a demanding task. In NX software the fitted surface consisted of finite number of patches, each represented via 3^{rd} degree polynomial, i.e. a cubic spline. The best fit was achieved with the number of patches approximately equal to 2-3 times the number of data points. For alternative methods and an overview of the modelling error, see Appendix 1-2.

Furthermore, the complete rock surfaces were divided into elements for FEM analysis: the finite element models of rocks were meshed so that the accuracy of the geometry is retained, see Figure 1. The Sormunen et al. (2016) rock numbering system is used in this paper as well, see also Table 2. Rocks 10a (Figure 2), 4e (Figure 4) and S_a (Figure 5) were meshed with 50 mm shell elements because of their more complicated shape. The real rock 11f (Figure 3) and all the mathematical models with relatively smooth geometries were meshed with shell elements with side length of approximately 100 mm. In the grounding simulations the rock was modelled as a rigid body. Besides the interpolated

surface added to the raw xyz-data to create a continuous version of the “real“ rock, the following models were used. Their coefficients were obtained by fitting the models to the raw xyz-point data.

3.1. Bottom shape models

In the grounding damage modelling literature the rock is most commonly assumed to be a cone with some variation as to how the tip is constructed, see e.g. Klanac et al. (2006), Naar et al. (2002), Rawson et al. (1998) and Rodd (1997). Heinvee et al. (2013) present a polynomial model, which was extended in Sormunen et al. (2016). Sormunen et al. (2016) also present a binormal model for modelling sea bottom shapes. An overview of the models is presented in Table 1.

Table 1 Sea bottom shape model overview.

Sea bottom shape model	References	Parameters	Important aspects
Cone	e.g. Cerup-Simonsen et al. (2009), Klanac et al. (2006), Naar et al. (2002), Rawson et al. (1998), Rodd (1997)	Cone tip (sharp, cut-off or rounded) and opening angle and/or radius and height	Most commonly used sea bottom model in the literature
Polynomial	Heinvee et al. (2013), Heinvee and Tabri (2015), Sormunen et al. (2016)	Degree of polynomial, coefficients for x (and y)	Going from a small rock to a large rock changes the main deformation mode from local tearing of ship bottom to global crushing
Binormal	Sormunen et al. (2016)	Scaling parameters, variance and mean of x and y	Flexible model with overall best mathematical fit to real sea bottom data, can mimic cones and polynomials
Shape not mathematically specified	e.g. Alsos and Amdahl (2007)	Different sea bottom sizes and shapes	Going from a sharp rock to a wide, blunt shoal drastically increases energy required to break inner hull

The binormal model was found to have the best overall fit in terms of R^2 in Sormunen et al. (2016), where the goodness of the fits in statistical terms are also discussed. In this paper, four rock models are used alongside with the real rock data. The equations for the models are:

1. Cone equation

$$z = \frac{(x-x_0)h}{r \cos(\arctan((y-y_0)/(x-x_0)))} + h - b_1 \quad (1)$$

Where h is the height of the fitted cone and r the radius of the cone at $h = 0$. Note that this equation represents a pure cone without a blunted apex, where the origo is potentially shifted by x_0 and y_0 as the origo in the data presented in Sormunen et al. (2016) is only approximate. Note that the coefficients in Equations 1-4 are re-evaluated separately for each rock and each rock model equation.

2. Scaled and shifted binormal function

$$z = b_0 \frac{1}{2\pi\sigma_x\sigma_y\sqrt{(1-\rho)^2}} \exp\left(-\frac{1}{2(1-\rho^2)} \left(\frac{(x-\mu_x)^2}{\sigma_x^2} + \frac{(y-\mu_y)^2}{\sigma_y^2} - \frac{2\rho(x-\mu_x)(y-\mu_y)}{\sigma_x\sigma_y}\right)\right) - b_1 \quad (2)$$

Where b_0 is the scaling multiplier, b_1 a constant that counters out that all observed z are negative, σ the standard deviation, μ the mean and ρ the correlation between x and y . Note that binormal functions resemble blunted cones with certain parameters, see Sormunen et al. (2016).

3. 2nd order polynomial equation

$$z = b_0 + b_1x + b_2y + b_3x^2 + b_4xy + b_5y^2 \quad (3)$$

4. Heinvee et. al (2013) model extended in the x-axis direction

$$z = b_0 + b_1(x - x_0)^2 + b_2(y - y_0)^2 \quad (4)$$

with an added origo shift by x_0 and y_0 .

To obtain the rock-specific parameters for all four equations above, non-linear least square fitting of the models was done to the xyz-raw data. The statistical goodness of the fit of the models to the data was evaluated using the coefficient of determination R^2 , which has a maximum of 1.

The four analysed rocks to which these models were fitted were selected according to the following criteria: Obtaining a variety of different rock types as specified in Sormunen et al. (2016) and Table 2.

The selected rocks had to offer 360° data points around the apex and have a relatively good R^2 for at least one rock model. Lastly, the rock model(s) had to show a good visual fit with the data: This check is important as in isolated cases it is possible to obtain a good R^2 but have the model rock's apex at +100 m above sea level. To each of these four rocks the following four models were fitted. The rocks are numbered according to their labelling in Sormunen et al. (2016).

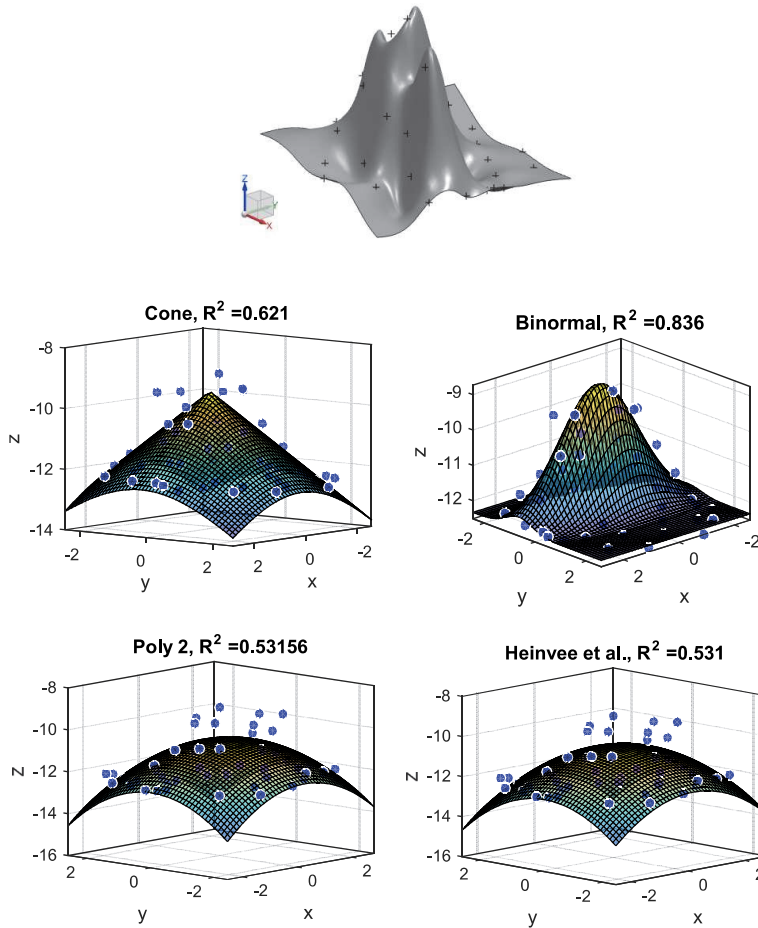


Figure 2 Rock 10a with the approximated real rock surface and the four fitted models.

Figure 2 shows the real raw data as blue dots in a xyz -space and the model fits as surfaces. The right part of the figure shows the real data and the reconstructed “real” rock surface constructed using the

approach described in step 1. It is an example of a small, sharp peak (type 1 rock in Sormunen et al. 2016); however as the peak seems to be divided into several apexes it also has traits from rock type 4: multiple smaller formations.

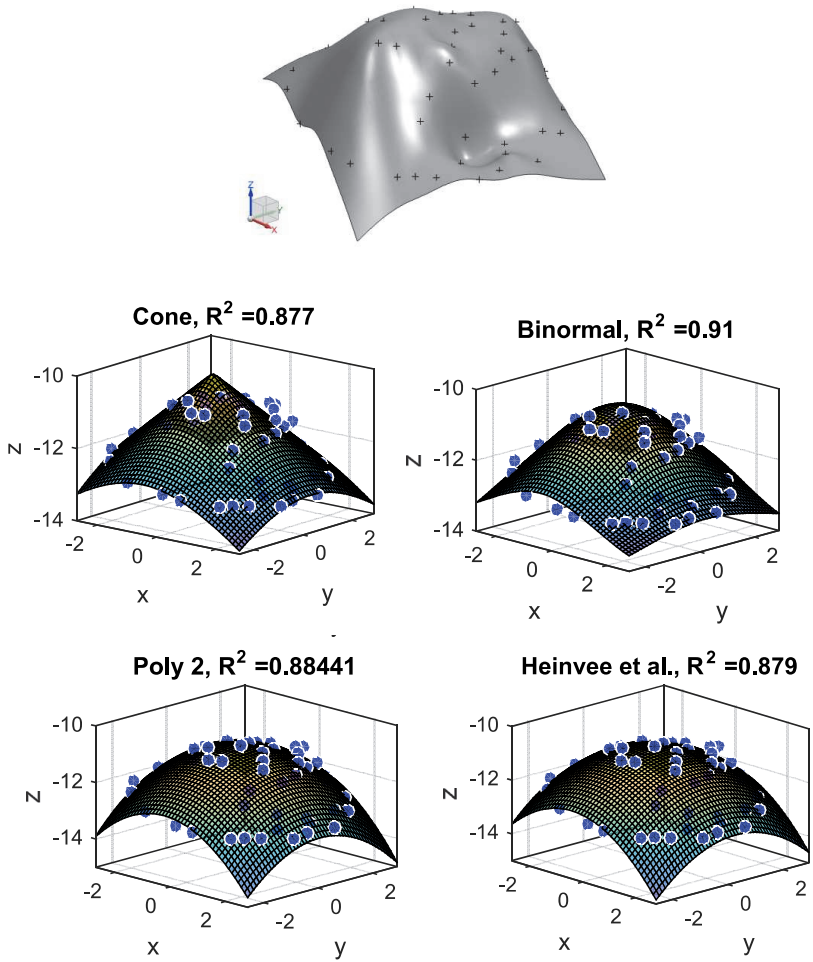


Figure 3 Rock 11f with the approximated real rock surface and the four fitted models.

Figure 3 shows rock 11f, which is a small peak somewhat similar to 10a but with a high R^2 for all models (0.8-0.9) and is much wider compared to the height. As such it has characteristics of a type 1 (sharp and small) and a type 2 (wide and blunt) rock.

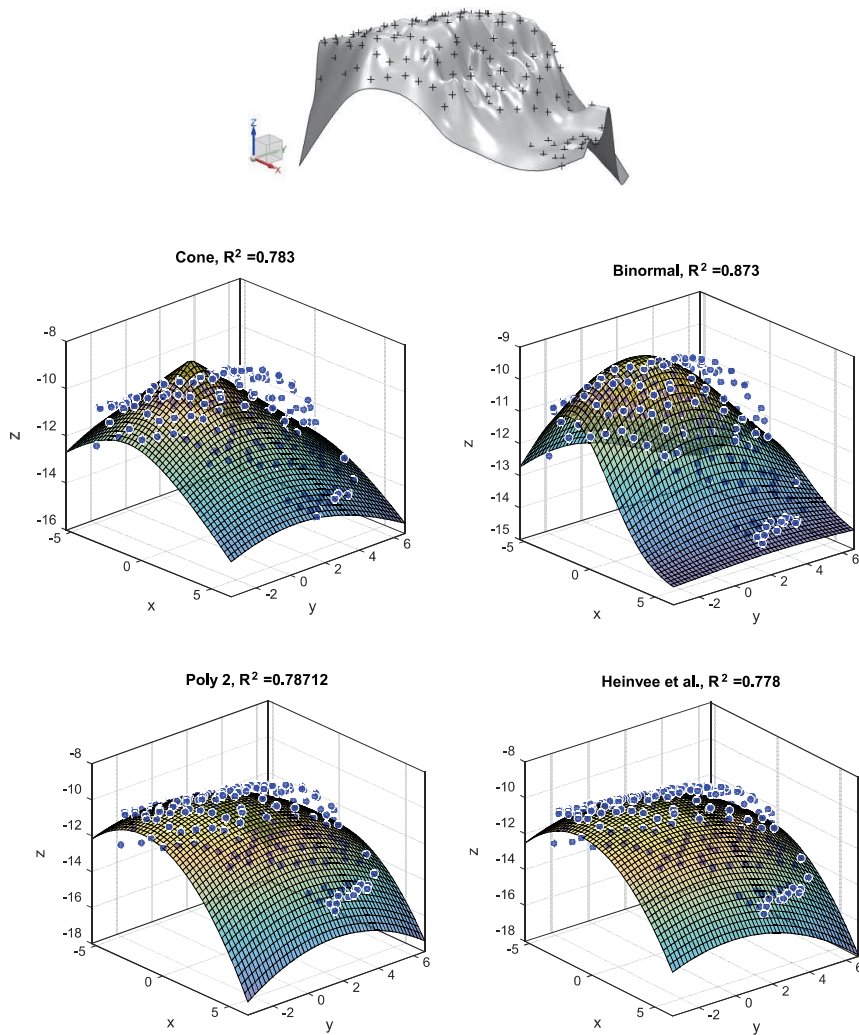


Figure 4 Rock 4e with the approximated real rock surface and the four fitted models.

Figure 4 shows rock 4e. This rock is an example of a wide, blunt bottom shape (type 2) with an overall good fit for all 4 models in terms of R^2 .

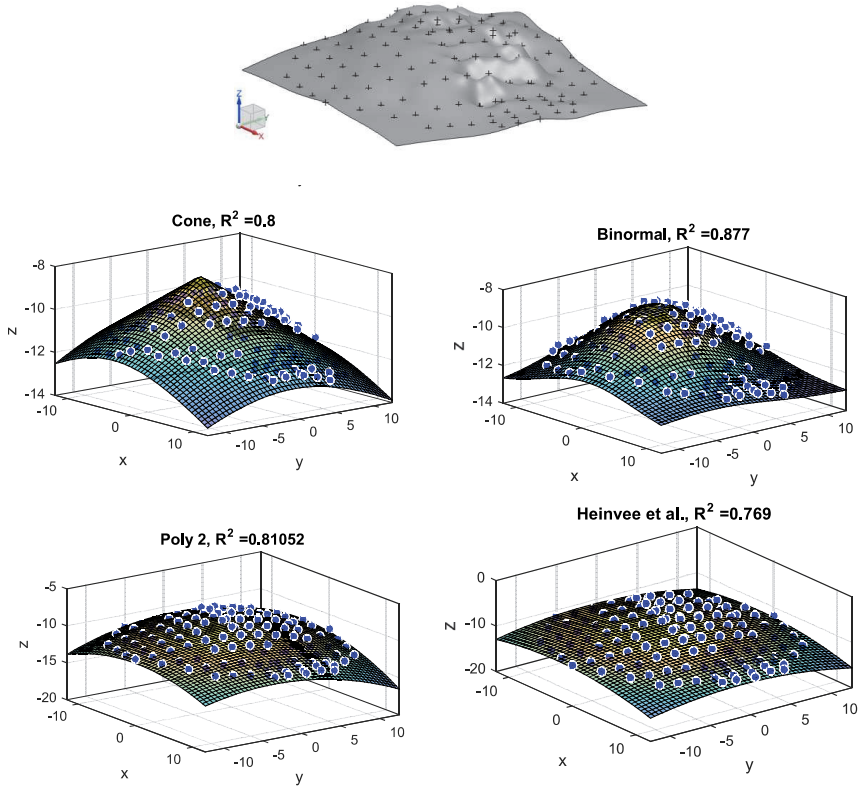


Figure 5 Rock S_a with the approximated real rock surface and the four fitted models.

Figure 5 shows rock S_a , which is an example of a large, rounded rock (though with some bumps), with a reasonable R^2 for all 4 models. It represents a type 2 rock in Sormunen et al. (2016) - a wide and blunt peak. The characteristics of the four rocks are summarized in Table 2.

Table 2 Rock statistics.

Rock label	Type	Radius r [m]	Depth change Δz [m]	Resolution d [points/m ²]
10a	1 (4)	3	3.58	1.77
11f	1-2	3	2.35	1.84
4e	2	7	4.84	1.47
S_a	2	13	3.84	0.55

The rock type classification of Sormunen et al. (2016) is as follows: Type 1: Sharp small peak, 2: Wide and blunt peak, 3: Ridge, 4: Compilation of smaller formations. r is the radius of the rock as measured from the apex, Δz the depth difference between the lowest and highest point and d the resolution of the raw sea bottom data counted in number of data points per m^2 in the xy -plane (i.e., as seen from the water surface).

Step 2: Grounding damage estimation with selected rock models and real rocks.

The principles of the numerical grounding simulations performed with the real rocks and the rock models as well as the post-processing of the analysis results are presented as follows. A double hull tanker with overall length of 190 m was used in the grounding damage analysis. DNV-GL software Poseidon (version 10) was used to dimension the tanker according to Harmonized Common Structural Rules for Oil Tankers (HCSR-OT) by IACS (2014). As Poseidon only allows Ansys output, the model was translated into LS-Dyna (release 7.1.2) through Ansys. The main dimension and parameters of the tanker are presented in Table 3 and its cross-section in Figure 6. The tanker has a central longitudinal bulkhead and six cargo tanks in longitudinal direction.

Table 3 Main dimensions and parameters of a tanker used in numerical simulations.

Parameter	T190
Length [m]	190
Breadth [m]	28
Draught [m]	12
Depth [m]	14
Design speed [kn]	15.4
Deadweight [tdw]	~30 000
Double-bottom height [m]	1.6
Outer plating thick [mm]	15-17 (varies)
Tank-top thick [mm]	14
Girder spacing [m]	3.25
Floor spacing [m]	3.5
Classification rules	HCSR-OT

establishes an element thickness and dimension dependent critical thickness strain after which an element is removed from the simulation. To evaluate the critical through-thickness strain at the moment of fracture, an empirical criterion is presented by Lehmann et al. (2001) defining the computational failure strains for different element sizes at the point of failure as

$$\varepsilon_{1,f}(l_e) = \varepsilon_g + \varepsilon_e \cdot \frac{t}{l_e} \quad (5)$$

and the critical through-thickness strain follows from the incompressibility condition $(1+\varepsilon_1)(1+\varepsilon_2)(1+\varepsilon_3)-1=0$ and assuming constrained transverse strains ($\varepsilon_2=0$) as

$$|\varepsilon_{3,f}(l_e)| = \frac{\varepsilon_{1,f}}{1+\varepsilon_{1,f}} \quad (6)$$

where ε_g is the uniform strain and ε_e is the necking strain, t is the plate thickness and l_e is the individual element length. It is commonly recommended that the ratio l_e/t is not less than 5 for a shell element. The values of uniform and necking strain are 0.056 for the uniform strain and 0.54 for the necking strain in the case of shell elements. This is obtained from thickness measurements related to the calculated stress states given in Lehmann et al. (2001)

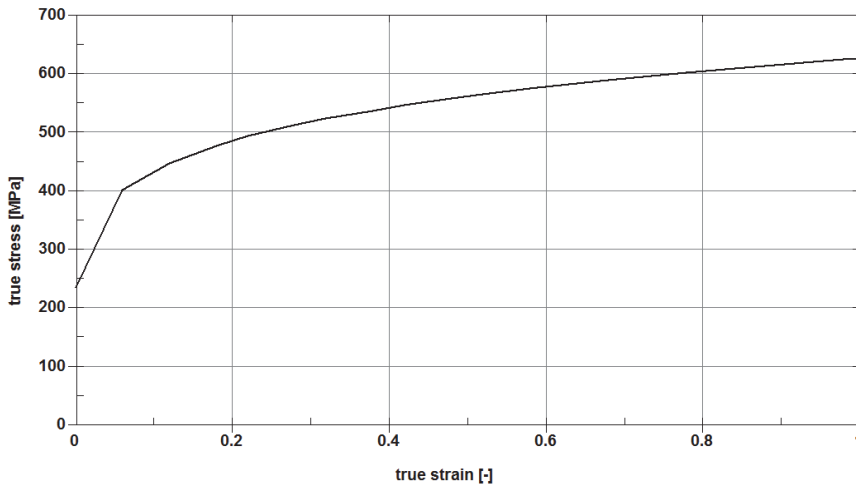


Figure 7 Plastic true stress-strain curve for S235 steel.

The grounding simulations are conducted in a displacement controlled manner as the focus is on the inner mechanics and not on the external dynamics. The rigid rock first moves to a pre-defined penetration depth and continues to move at constant penetration depth along the ship at a constant velocity of 10 m/s until simulation timer reaches 1 second, see Figure 8 and Figure 9.

This velocity is somewhat larger than typical design speed of such tanker. This constant velocity was selected as it allows to perform the simulations with reasonable calculation time while it is still small enough not to cause unrealistic inertia effects, see Konter et al (2004). The strain rate effects were neglected as the constant velocity of 10 m/s does not present realistic velocity throughout the grounding process. In real grounding the ship's velocity decreases rapidly. Fully dynamic simulations are required to take into account the correct velocity. Such simulations were considered unreasonable in such study. Furthermore, it is suggested by Storheim and Amdahl (2015) that it is conservative to neglect strain rate effects if the goal is to assess the maximum structural damage.

Two aspects were considered when defining the maximum penetration values: i) extent of data points (i.e. rock has to be fully defined within the contact) and ii) the double bottom structure has to be engaged as much as possible. Thus, the following maximum penetration values were defined for different rocks: 4e –1.9 m; 10a – 2.5 m; 11f – 1.2 m and Sa – 2.3 m. The same penetration depth was used for real rocks and the corresponding fitted models.

In the longitudinal direction the contact region lays in between two transverse bulkheads. In the transverse direction the contact region is in between the central longitudinal bulkhead and the ship side (B/4), see Figure 8. The nodes at the forward and aft end of the models are fixed. Standard LS-DYNA hourglass control and automatic single surface contact (friction coefficient of 0.1/0.3 for dynamic/static friction with exponential decay coefficient 0.01, see LSTC (2013) for friction modelling in LS-DYNA) is used.

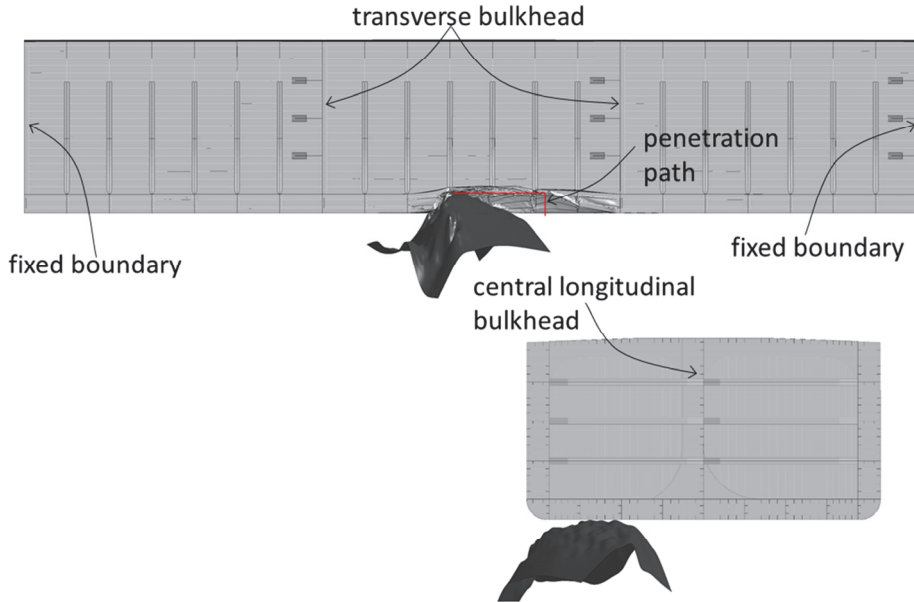


Figure 8 Setup for grounding simulations.

4. Numerical results

This section analysis the finite element results to determine any differences between response of the real and the analytical rocks. Figure 9 shows the pure deformation energy (excluding the frictional component) dissipated during the grounding simulation with different rocks and rock models. The figure shows a distinction between the vertical indentation and the horizontal penetration stages. The figure highlights the distinctive features between analysis using the real rocks versus using the rock models. The energy dissipated due to the analytical rocks correlates with the size of the rock as all rocks are displaced at the equal amount without considering the dynamics of the problem. In comparison, the real rock with its distinctive non-smooth surface evokes a different damage mechanism in the bottom structure and thus, despite the lower rock volume, relative energy dissipation is higher in both simulation stages. This particular feature will be discussed more in detail with a qualitative damage analysis later on; the time instants when this qualitative damage analysis was performed are shown on Figure 9. The particular time instances were chosen to best reveal the differences between damage mechanics between analytical and real rocks, see Figure 11, Figure 12 and Figure 13.

Step 3: Comparison of obtained grounding damage.

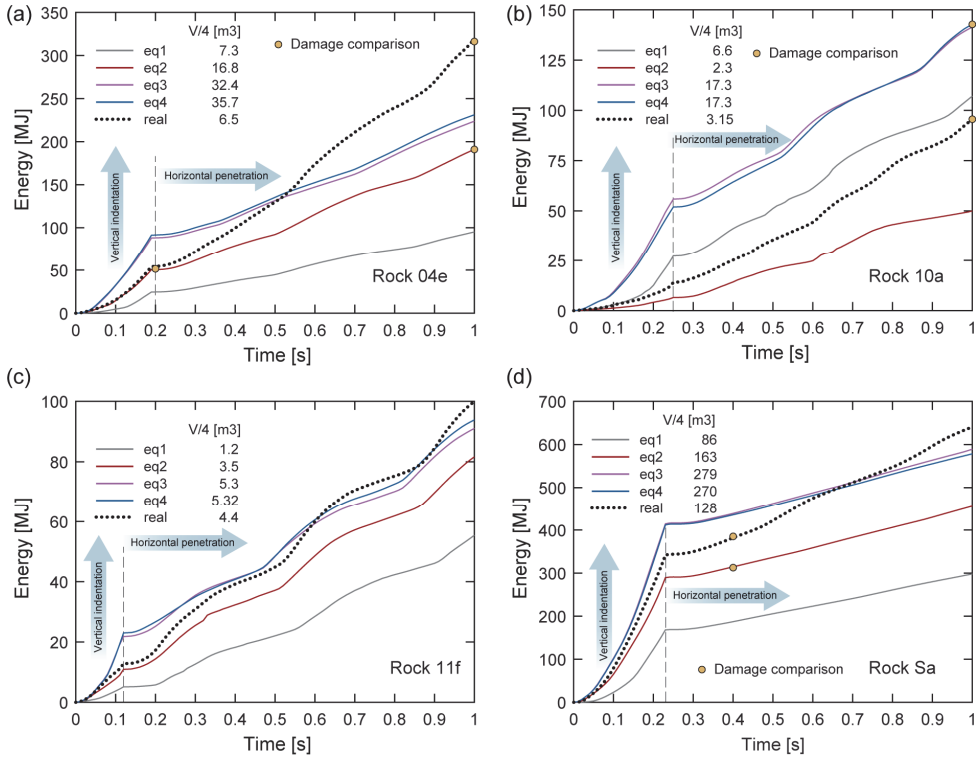


Figure 9 Deformation energy (excluding friction) absorbed during grounding for (a) Rock 04e; (b) Rock 10a; (c) Rock 11f; (d) Rock Sa. V is the approximate volume of the rock, see also Figure 15.

The marker “damage comparison” denotes the time instant at which qualitative damage analysis was performed, see Figure 11, Figure 12 and Figure 13 at the end of this section. To gain further insight into differences between real and model rocks the energy dissipation is normalized and plotted as a function of the rock shape statistical fit in terms of R^2 in Figure 10 (a). Here the R^2 describes how accurately the analytical rock approximates the real rock shape (Sormunen et al., 2016). Figure 10 (a) also illustrates assumed linear slopes of a 1-to-1 relationship between R^2 and the energy ratio. In the figure most observations lie within $\pm 10\%$ of these linear slopes in the light grey zone. In terms of R^2 the rock model accuracy is relatively good with most of the analytical rocks having R^2 higher than 0.75 but the

similarity in energy is not as only few models show a normalized energy value close to 1). In case of Rock 11f (triangular marker), the close resemblance between analytical and model rocks (high R^2) leads also to similar energy dissipation levels between the real and model rocks (normalized energy close to 1). On the other hand, most of the other observations lie below the slope of 1, and despite the high R^2 value, this mathematical resemblance in shape does not guarantee that the mechanics is accurately captured. For instance, the cone model (markers with red fill) captures the rock shape well with $R^2 \sim 0.8$ (with the exception of rock 10a), but the energy dissipated by the structure is underestimated by $\sim 50\%$ or more. The underlying difference between the Rock 11f shown in Figure 10 (b) and all the other rocks is the smoothness of rock surface. Herein, smoothness or rock surface is defined by the amount of peaks, valleys and general roughness of the surface. Following qualitative damage analysis it is shown that the rock surface plays a central role in evoking different failure mechanisms and thus, leading to different energy dissipation levels in the structure. Moreover, one of the trends emerging from Figure 10 is that the most of the analytical rocks result in lower energy dissipation levels compared with the real rocks. From the design perspective this is on the non-conservative side and thus, should be considered by the analyst. On the other hand, if the analysis is performed so that energy is used as an input and simulation stops when the energy is dissipated, the analytical rock would yield a longer damage length since energy dissipation rate is lower when analytical rocks are used. Hence, the analysis results would in that case be more conservative.

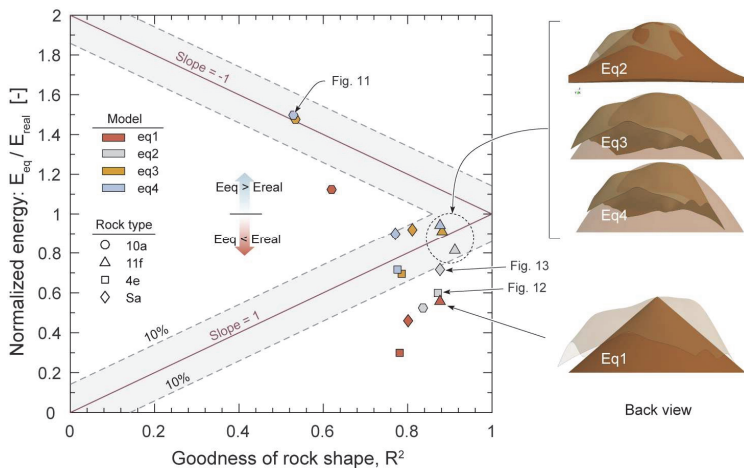


Figure 10 Relation between total (horizontal + vertical) energy absorbed during grounding simulation and rock model fit in R^2 (left). (b) Comparison of rock 11f and its analytical approximation (right).

Moving on to qualitative damage analysis of selected cases; Figure 11 (a) and (b) juxtapose the damage due to the rock 10a and Figure 11 (c) clearly shows that the approximated rock is considerably larger in volume (about 5 times) than the real rock. As revealed already by Figure 9 the rock volume is one of the most important factors affecting the absorbed energy during initial vertical indentation stage. Nevertheless, during horizontal penetration the surface roughness of the rocks plays an important role upon invoking different type of failure mechanisms in the structure and thus, leading to different energy dissipation levels. Therefore, in spite of the larger volume of eq. 4 analytical rock in Figure 11 (c), the real rock 10a dissipates the similar amount of energy during horizontal penetration stage as shown in Figure 9 (b). During horizontal penetration the real wedge-shaped rock in Figure 11 (a) cuts through the structure with its leading edge. Initially the sheet metal in front of the rock deforms by crushing, but is eventually pushed towards the sides of the rock where the metal flaps bend and curl back and forth to conform to the rock surface. In contrast, the model rock with its smooth surface pushes the structure upwards gradually during the horizontal movement, whereupon high membrane stresses develop until fracture occurs along relatively straight paths. Beyond fracture, the interaction between the structure and rock terminates with little or no crushing and bending. This difference in failure mechanics explains why significantly smaller real rock in comparison to analytical rock causes the structure to dissipate equal amount of energy during horizontal penetration.

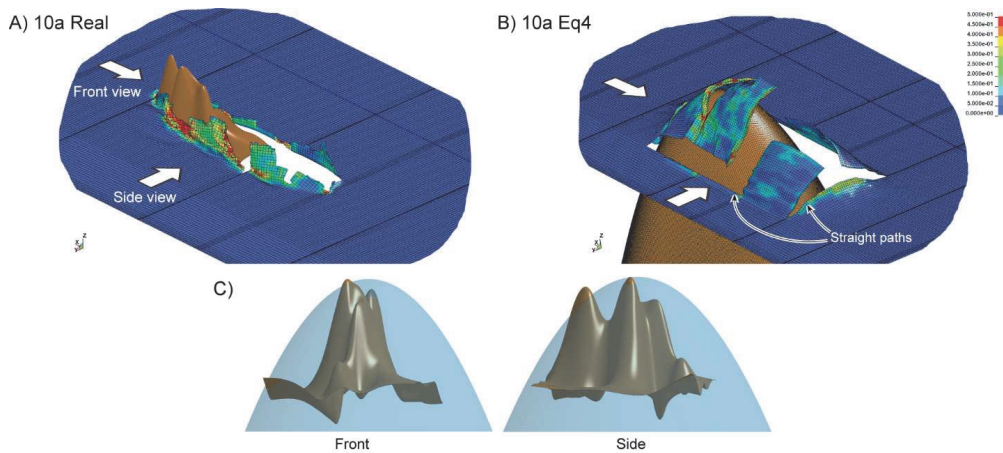


Figure 11 FE simulation results with rock 10a. Equivalent plastic strain contours of the ship bottom outer shell are shown with rest of the structure removed from the figure. Analysis with (a) real and (b) approximated (eq4) rock. Figure (c) compares the two rocks.

The second analysed case in Figure 12 - which can be considered an opposite to the first case - compares the damage due to the rock 4e and its approximation with model eq. 2 (i.e. the binormal

function). In other words, the analytical rock approximates the real rock with good accuracy according to the relatively high R^2 value of ~ 0.9 and thus, the dissipated energy during the initial indentation stage is equal, see Figure 9 (a). However, the same figure also shows that the energy dissipated during horizontal penetration compared to the real rock is almost twice as large. Figure 12 (a) and (b) compare the damage between the two rocks at two distinctive time instances: at the end of the indentation stage and at the end of horizontal penetration, i.e. at the end of the simulation. Similar failure mechanisms corresponding to the analytical rock presented in Figure 11 (b) are present in the analytical rock in Figure 12 (b). Material is gradually pushed upwards where it conforms with the smooth analytical rock surface. Fracture propagates mainly due to the high membrane tension resulting in relatively straight fracture paths with little crumpling and bending of the material neighbouring the failed elements. On the contrary, ridge-like real rock with its abrupt footing crushes the material in front of it, see Figure 12 (a). Upon contact with the rough and bumpy top surface of the rock undergoing horizontal penetration, material develops multiple regions of strain localizations. This is shown by the high plastic strain contours in Figure 12 (a) that cover almost the whole contact region; while in comparison Figure 12 (b) shows that plastic strains due to the analytical rock are less spatially distributed.

Same discussion can be extended to damage due to Sa rock and its approximation with eq. 2, which is shown in Figure 13. The model rock matches the size of the real rock, but the rough surface of the real rock provokes different failure mechanisms in a structure leading to higher energy dissipation by the structure.

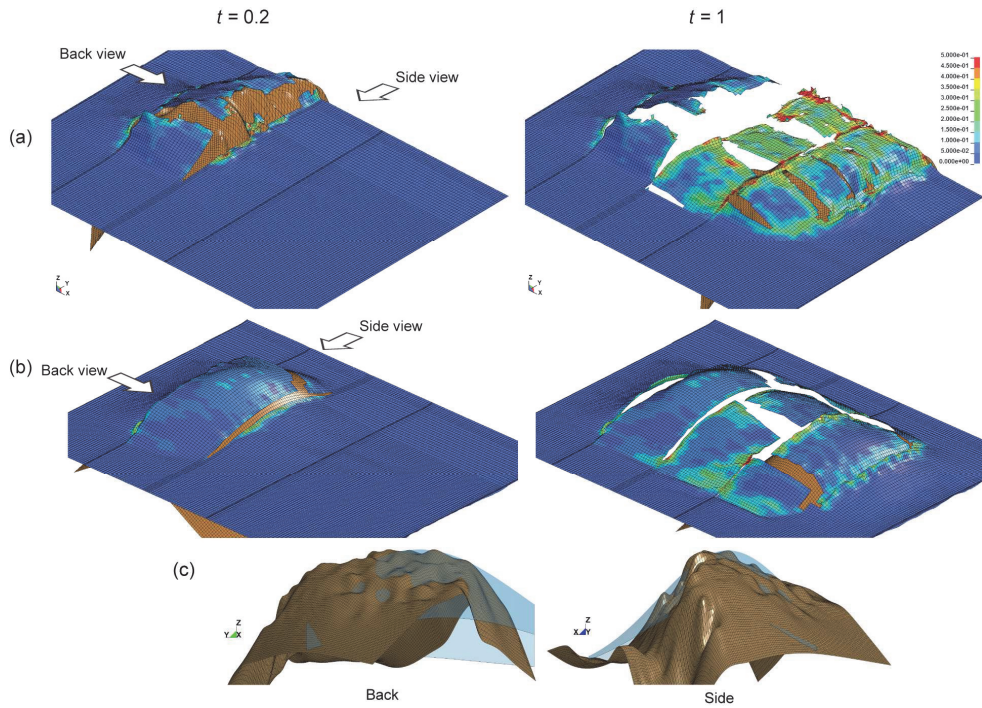


Figure 12 FE simulation results with rock 4e at two time instances. Equivalent plastic strain contours of the ship bottom outer shell are shown with rest of the structure removed from the figure. Analysis with (a) real rock and (b) approximated (eq2) rock. Figure (c) compares the two rocks.

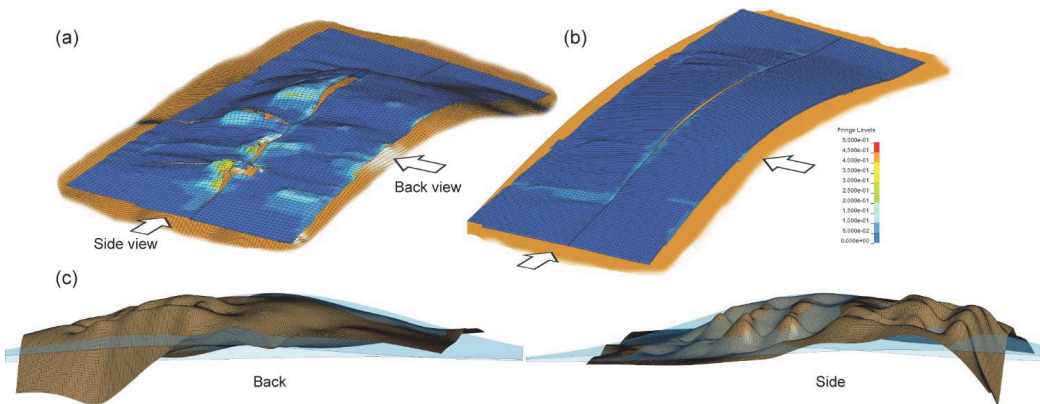


Figure 13 FE simulation results with rock Sa at $t = 0.4$. Equivalent plastic strain contours of the ship bottom outer shell are shown with rest of the structure removed from the figure. Analysis with (a) real and (b) approximated (eq4) rock. Figure (c) compares the two rocks.

The relationship between energy and the volume of damaged elements was investigated in Figure 14. R^2 was found to be 0.93 for the linear relationship between energy and total damaged element volume, meaning that the relationship between the two can be considered to be linear. For the damaged elements in the horizontal phase only R^2 was only 0.44. The difference is mainly caused by two outliers, which are the real rocks of 4e and Sa that are the only observations that exceed 20 MJ. Without them R^2 would be 0.73. The qualitative explanation to this difference is analysed in Figure 12 and Figure 13, which is the rougher surface of the real rock compared to the model rocks.

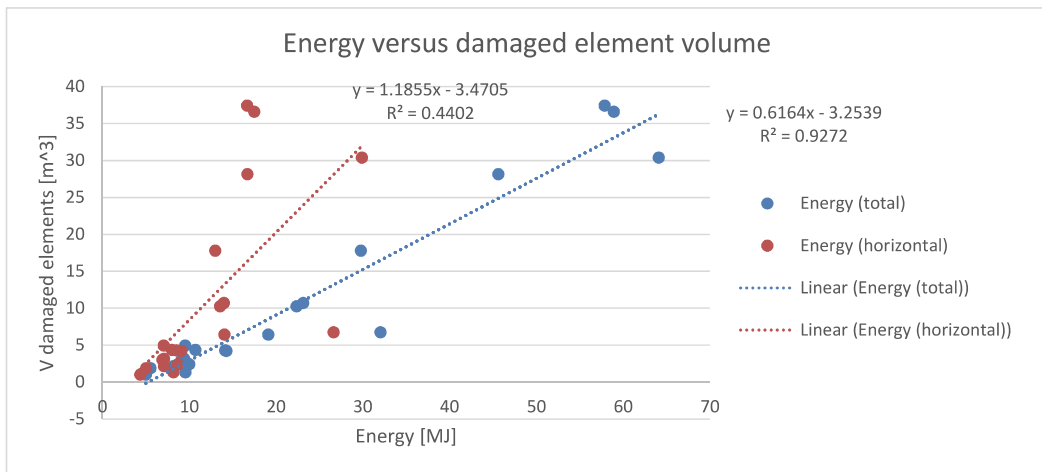


Figure 14 Relationship between energy and damaged element volume for $\epsilon_{\text{plastic}} > 0.01$. Calculated separately for total damage and energy as well as damage and energy for the horizontal phase only.

Beyond only investigating the relationship between R^2 and the energy ratio, other relationships were analysed. For each real rock and rock model, the volume, surface area and projected area in the YZ-plane were calculated, see Figure 15. From the rocks the parts were removed which are too deep and/or on the other side of the rock seen from the angle of attack of the ship (x-axis), see Figure 15 (a). The purpose was to remove the parts of the rock that were not in contact during the horizontal phase of the grounding.

The procedure goes as follows: The highest point from model was assigned to create vertical plane (YZ plane), see Figure 15 (a). After cutting model by the vertical plane second plane was created – the horizontal plane (XY- plane) which lies on the maximum penetration depth δ counted vertically from highest point, see Figure 15 (a). This plane represents the plane of the ship bottom. Once the model was cut by both planes the volume, surface area and projected areas were measured, see (b)-(c).

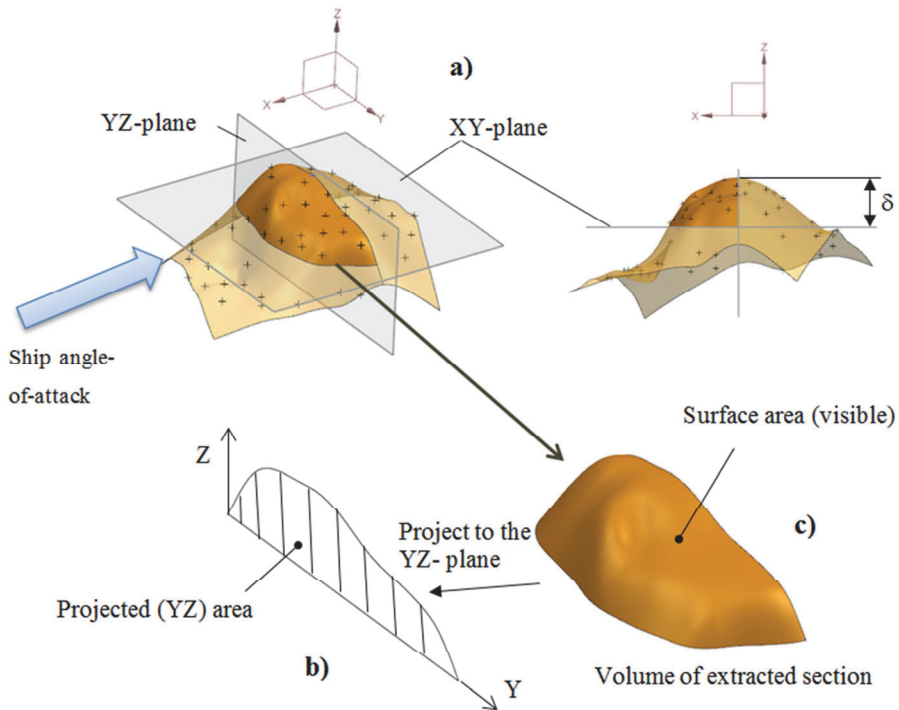


Figure 15 Procedure to measure areas and volumes for the real rock models. a) Extraction of volume section, b) projected area and c) measured volume and surface area.

These three rock area- and volume metrics are compared to the volume of damaged elements in Figure 16.

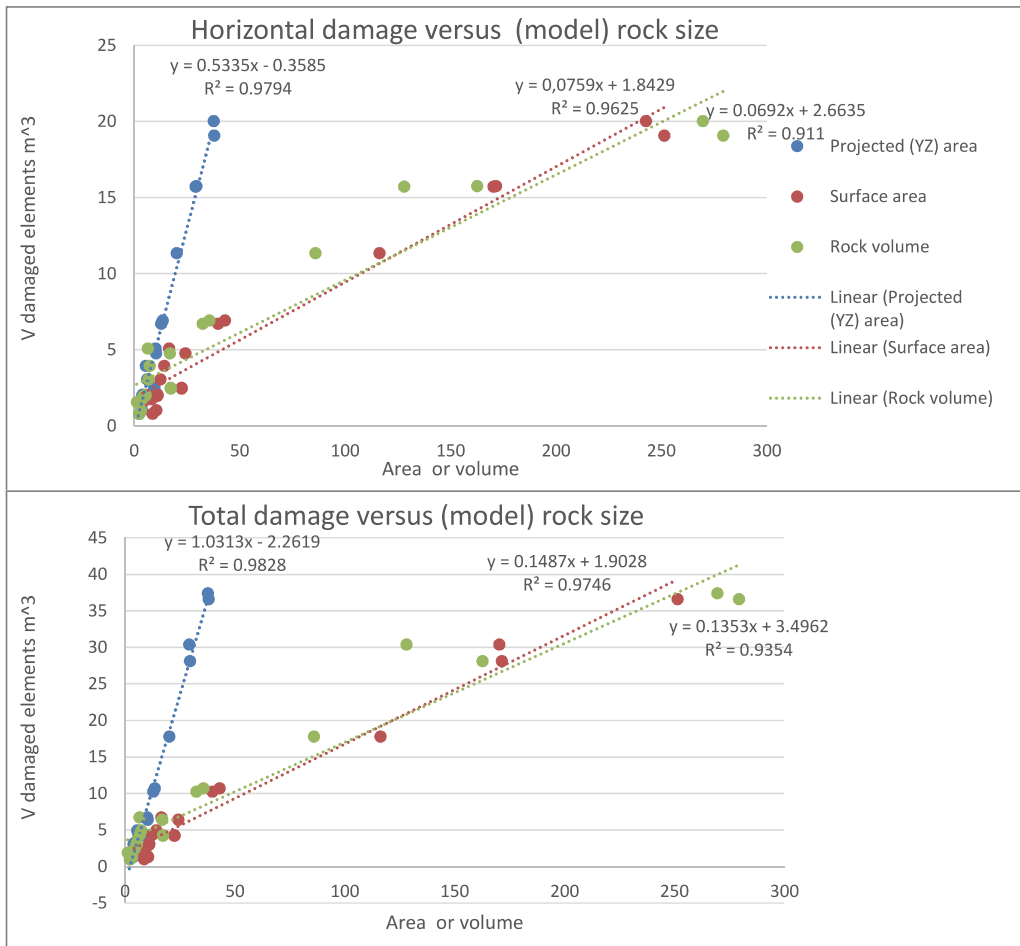


Figure 16 Rock area and volume metrics compared to the damaged element volume for $\epsilon_{\text{plastic}} > 0.01$, including real and model rocks. Top: horizontal grounding phase damage only, bottom: vertical and horizontal phase of grounding damage total.

The volume of damaged material follows very well linearly both area measurements (surface and projected) as well as the rock volume, see Figure 16. Note that the slope of the linear relationship between grounding energy and damaged material volume depends heavily on the damaged volume definition in terms of $\epsilon_{\text{plastic}}$, which is shown here for a threshold of 0.01. The best explanatory variable is the rock projected area into the YZ- plane. The R^2 remain almost identical for the three equations in Figure 16 also when considering the only damage volume during the horizontal phase of the grounding.

5. Discussion

Having mathematically relatively simple rock models with just a few parameters that need to be estimated is desirable. This would make result sharing and utilization easy for other researchers; in order to model rocks in a given sea area one would only need an estimate for the rock parameters. Furthermore, it would allow for easy generalizations about rock shapes that could then be applied for sea areas without access to detailed sea bottom data, thus making it possible to run detailed grounding damage risk analysis for whole sea areas.

Step 4: Acceptance or revision of bottom shape models

It was expected that as R^2 goes towards 1.0 the grounding simulation results obtained using the real rock and the model rock would also converge. This relationship was found to be much weaker than initially anticipated: Even at relatively high R^2 of 0.8-0.9 (which is about as good as possible with the given data) there would be large deviations in the grounding energy between the model rock and the real rock, see Figure 10. Paradoxically, when analysing the models separately for all four rocks the linear trend between R^2 and the normalized energy has a negative slope for all models except the binormal rock model (eq. 2), see Figure 17.

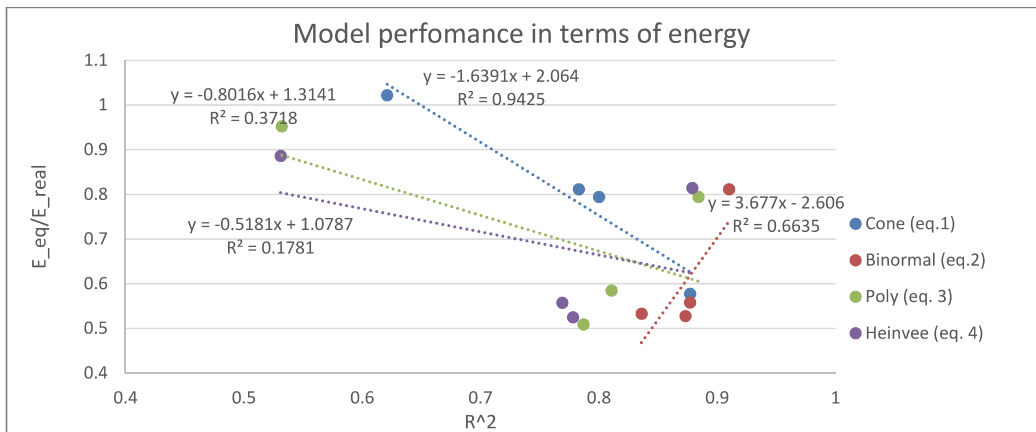


Figure 17 Comparison of R^2 and the normalized energy on a model-by-model basis for all four rocks for the horizontal damage phase only.

The cone model (eq. 1) shows the best linear relationship between R^2 and the energy, unfortunately the better the fit in terms of R^2 the more the grounding energy deviates from the results obtained using the real rock.

For the normalized damage volume the results are significantly better, in particular for the binormal model, which deviates “only” 0.4-0.23 from the real rock results, see Figure 18.

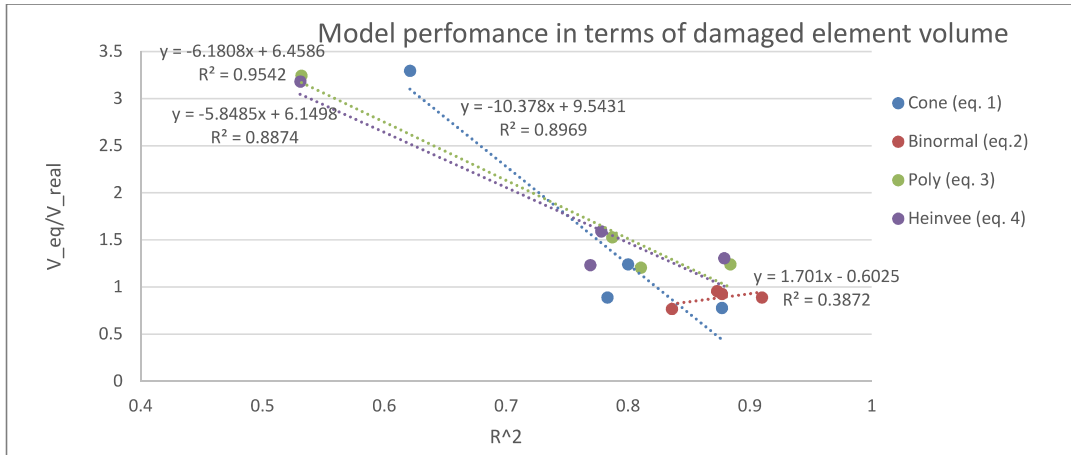


Figure 18 Comparison of R^2 and the normalized total damaged element volume energy on a model-by-model basis for all four rocks.

The results and conclusions are similar when taking into account damaged material volume of the horizontal phase only. Due to the linear relationship between the area- and volume metrics of the rocks shown in Figure 16, the conclusions are the same for the relationship between R^2 and the normalized model rock YZ-area.

It should be noted that the sample size is quite low but as the analysed rocks were specifically better cases found in the data, it can be concluded that such R^2 is not a sufficient measure by itself to verify that the sea bottom models being tested are realistic in terms of similar grounding energy. However, in the simulation it was possible to achieve similar damaged element volumes in particular with the binormal model.

Moreover it was found that even the simplistic, non-blunted cone model would achieve relatively similar grounding energies in isolated cases; Cone model for rock 10a (eq. 1) on Figure 10 shows a relatively low R^2 of 0.62 but a high normalized energy of 0.88. That means that depending on the research question even a simple cone model will occasionally be roughly correct in grounding damage analysis.

To obtain a similar volume of deformed material in this grounding simulation with a model rock, the single most important factor is having a similar surface/projected area or volume between the real rock

and the model rock for the part that is contact with the ship. Especially the projected area has a good coefficient of determination. The area/volume metrics can be used as a surrogate variable instead of calculating grounding damage with FEM: The FEM calculations are tedious and time-consuming; the calculations done here take tens of hours to run and therefore only four rocks were analysed. When suggesting new rock models, the differences in projected area can initially be compared to evaluate the goodness of the model instead of using FEM, but the uneven nature of the rock surface needs to be considered in modelling if one wants similar grounding energy: The current models are shown here to have a too smooth surface. These findings are subject to some uncertainty as the exact shape of the real rock had to be interpolated, see Appendix 1, Appendix 2 and Figure 1. Note that in order to correctly model the real rock surface roughness high-resolution xyz-bathymetric data is required. Alternatively, this could perhaps be mimicked by adding random deviations (i.e. noise) to the z-values of the rock models to create a less smooth surface.

Other models or exact sea bottom data is needed for reliable and detailed grounding damage analysis given the current understanding of sea bottom shape modelling. As suggestions for future research more complex models should be tested for modelling sea bottom shapes such as splines and Gaussian processes.

Other grounding damage estimation approaches exist as well such as the statistical approach of IMO (1995), which however does not link grounding energy, local sea bottom shape or ship structure specific conditions with the resulting damage, see also Sormunen (2014). These models are recommended to be used for regional maritime risk analysis until more realistic sea bottom shape models are introduced. The authors propose re-running the analysis on different ship models as well, including dynamic grounding effects. Of further interest is determining rules-of-thumb for when the rock is so wide that it cannot realistically rupture the inner hull in groundings. For statistical analysis on the exact relationship between grounding energy and different variables, a larger sample is desirable. Furthermore, it would be beneficial to analyse more data of sea bottom shapes from Finland as well as other sea areas.

6. Conclusions

For designing safe ship structures and analysing the risk caused by ship groundings, comparison of grounding damage and the effects of the sea bottom shape are important. The comparative analyses

demonstrate that grounding damage greatly depends on rock surface. Different failure mechanics were observed between the real rocks and the rock models: the smooth model rocks resulted in less crushing and energy absorbed within the same timeframe. Therefore, the energy difference between the model and real rock is often significant despite high R^2 of the model rock. On the other hand for damaged element volume and rock YZ-area in particular the binormal model was found to mimic the real rock quite well, especially for cases with $R^2 > 0.85$.

The relationship between the damaged material volume and the real rock or rock model projected area was found to be near-perfectly linear for the whole grounding simulation but much less so for the vertical phase of the grounding only. Thus given the limitations in the simulation, knowing the area or volume of the rock part which is in contact with the ship is enough for damage volume calculations. This can then be further used for estimating damage when the rock penetration depth and shape is known. For obtaining similar energies the current sea bottom shape models are too smooth and more complex models should be implemented to accurately model the uneven surface of the rock. This means that currently the simplified rock models do not model the real sea bottom shape accurately enough to obtain similar grounding damage with energy based damage equations.

Acknowledgements

The authors would like to thank Jani Romanoff for valuable feedback and suggestions during the writing of the paper as well as anonymous reviewers. This paper has received funding from Kotka Maritime Research Center Merikotka. The research conducted in Tallinn University of Technology has been financially supported by project B18: Tool for direct damage calculations for ship collision and grounding accidents and by BONUS Stormwinds project. This help is kindly appreciated.

References

- Alsos H, Amdahl J. On the resistance of tanker bottom structures during stranding, *Mar Struct* 2007; 20: 218–237.
- Brown, A.J., Tikka, K., Daidola, J., Lutzen, M., Choe, I., "Structural Design and Response in Collision and Grounding", *SNAME Transactions* 108, pp. 447-473, 2000.
- Cerup-Simonsen B, Törnqvist R, Lützen M. A simplified grounding damage prediction method and its application in modern damage stability requirements, *Mar Struct* 2009; 22(1): 62–83.
- Ehlers S, Broekhuijsen J, Alsos HS, Biehl F, Tabri K. Simulating the collision response of ship side structures; a failure criteria benchmark study. *International Shipbuilding Progress* 2008;55:127–44.
- Goerlandt F, Montewka J. Maritime transportation risk analysis: Review and analysis in light of some foundational issues, *Reliability Engineering & System Safety* 2015; 138: 115-134.
- Heinvee M, Tabri K. A simplified method to predict grounding damage of double bottom tankers, *Mar Struct* 2015; 43: 22-43.
- Heinvee M, Tabri K, Körgesaar M. A simplified approach to predict the bottom damage in tanker grounding, In: *Proceedings of the 6th International Conference on Collision and Grounding of Ship and Offshore Structures*, Trondheim 17-19. June 2013. Available online at: <http://www.ntnu.no/iccgs>. Accessed: 23.1.2014.
- IACS. 2014. *Common Structural Rules for Bulk Carriers and Oil Tankers*. International Association of Classification Societies. London.
- International Maritime Organization (IMO). Interim guidelines for approval of alternative methods of design and construction of oil tankers under regulation 13F(5) of Annex I of MARPOL 73/78. *Technical Report, Resolution MEPC, 66(37)*, pp. 1-40, IMO, 1995, London.
- Klanac A, Jalonen R, Varsta P. Multi-stakeholder decision-making in the risk-based design of a RO-PAX double bottom for grounding. *Proc. IMechE Part M: J. Engineering for the Maritime Environment* 2006; 221: 1-15.

Konter A, Broekhuijsen J, Vredevelde A. 2004. A quantitative assessment of the factors contributing to the accuracy of ship collision predictions with the finite element method. In: Proceedings of the third international conference collision and grounding of ships. Japan: 2004; 17–26.

Körgesaar M, Tabri K, Naar H, Reinhold E. 2014. Ship collision simulations using different fracture criteria and mesh size. In International Conference on Ocean, Offshore and Arctic Engineering OMAE2014, San Francisco, USA, Paper no: OMAE2014-23576, June 8-13 2014.

LSTC. 2013. LS-DYNA Keyword User's Manual. Livermore Software Technology Corporation.

Lehmann E, Egge ED, Scharrer M, Zhang L. Calculation of collisions with the aid of linear FE models, PRADS 2001, 2001.

Mazaheri A, Montewka J, Kujala P. Modeling the risk of ship grounding - A literature review from a risk management perspective, WMU Journal of Maritime Affairs 2014; 13: 269-297.

Naar H, Kujala P, Cerup-Simonsen B, Ludolph H. Comparison of the crashworthiness of various bottom and side structures, Mar Struct 2002; 15 (4–5): 443–460.

Pedersen PT. Review and application of ship collision and grounding analysis procedures, MarStruct 2010; 23 (3): 241-262.

Rawson C, Crake K, Brown A. Assessing the Environmental Performance of Tankers in Accidental Grounding and Collision, SNAME Transactions 1998; 106: 41-58.

Rees DWA. Basic engineering Plasticity. An Introduction with engineering and manufacturing applications. First edition. 2006. Elsevier Ltd. ISBN-13: 978-0-7506-8025-7.

Rodd J. Frame Design Effects in the Rupture of Oil Tankers During Grounding Accidents. In: Proceedings of 3rd Int. Conf. on Advances in Marine Structures, 1997, DERA, Rosyth, UK.

Sormunen, O-V., Castrén, A., Romanoff, J. and Kujala, P. Estimating sea bottom shapes for grounding damage calculations, MarStruct 2016; 45: 86–109.

Sormunen, O-V. 2014. Ship Grounding Damage Estimation Using Statistical Models. Proceedings of PSAM12 conference, 22-27 June 2014, Honolulu, USA.

Storheim M, Amdahl J. 2015. On the sensitivity to work hardening and strain-rate effects in nonlinear FEM analysis of ship collisions. *Ships and Offshore Structures*; 1–16. doi:10.1080/17445302.2015.1115181.

Zhang S. Plate tearing and bottom damage in ship grounding, *Mar Struct* 2002; 15 (2): 101–117.

Appendix 1 The error values for the “real” rock modelling

The real rock surface was constructed based on the sounding observations recorded as xyz-points. The sea bottom resolution and accuracy vary on the depth and technology used, giving us a vertical uncertainty of less than 0.3 meters using a 95 % confidence interval, usually much less. However, the uncertainty of the relative position in the data is much smaller, which is the most important factor in this case.

The “real rock” had to be reconstructed based on the xyz-point cloud for FEM analysis, adding a layer of subjectivity/uncertainty about the true form of the rock. Looking e.g. at rock S_a, the bumps on the surface might real - caused by glacial activity during the last ice age – or just echo sounding distortions.

Minimizing the “real” rock maximum error and average error values is used as a starting point for the real rock construction . Final rock surface modelling is checked by visual inspecting differences between the surface and highest points in point cloud as rock peak area is more important in grounding simulations then bottom area. If the point cloud density is very heterogeneous this affects greatly the modelling process.

As an example, rock 10a error values are quit high because most of the points are in bottom area and few points in peak area, see Figure 1. Modelling only by error values would give better error values but rock surface would then not fit that well to the rock the peak area points.It was observed that better point cloud density will give better error values; see Table 4 and Figure 1-5. Taking polynomial degrees of higher than 3 do not give much better results.

Table 4 Real rock modelling error and the degree and number of the polynomial functions used in the splines.

Rock	Model	Penetration	Degree		Patches		Maximum error[mm] ¹	Average error[mm] ²
			U	V	U	V		
10a	Real rock	2.5	4	2	9	14	1851.25	127.00
	eq1	2.5	10	10	40	40	39.74	0.13
	eq2	2.5	10	10	40	40	2505.34	10.22
	eq3	2.5	10	10	40	40	1.09	0.17
	eq4	2.5	10	10	40	40	1.09	0.17
11f	Real rock	1.2	2	2	15	13	15.00	2.56
	eq1	1.2	7	7	40	40	13.08	0.15
	eq2	1.2	10	10	30	30	0.88	0.17
	eq3	1.2	8	8	40	40	0.88	0.13
	eq4	1.2	8	8	40	40	0.76	0.13
4e	Real rock	1,9	8	10	30	30	1406.77	54.03
	eq1	1,9	7	7	40	40	28.85	0.15
	eq2	1,9	7	7	40	40	0.51	0.13
	eq3	1,9	7	7	40	40	0.53	0.14
	eq4	1,9	7	7	40	40	0.57	0.14
Sa	Real rock	2.3	7	7	40	40	237.74	27.71
	eq1	2.3	3	3	40	40	0.60	0.10
	eq2	2.3	3	3	40	40	0.64	0.10
	eq3	2.3	3	3	40	40	0.62	0.12
	eq4	2.3	3	3	40	40	0.63	0.11

¹Maximum distance between the actual data point and the fitted surface²Evaluated as mean absolute error

Appendix 2: Alternative method for rock modelling

One of the alternative method for rock modelling is to create model from triangular network, see Figure 19. With high number of points that method would allow to model a naturalistic rock which goes exactly through the observed data points. Unfortunately, in this case the point density is not sufficient to model natural looking rocks, instead overly edge rock are obtained with this method.

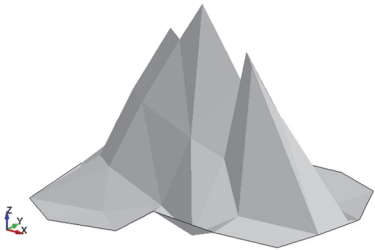


Figure 19 “Real” rock triangular network model.

Due to the limitation of the triangular network, “Fit surface” and “Through point surface” functions were used in Siemens NX software. The difference between them is illustrated in Figure 20.

<p style="writing-mode: vertical-rl; transform: rotate(180deg);">Fit surface</p>	<p>Interpolated model (number of patches and degrees are defined)</p> <p>Freeform surface – necessarily does not go through the points</p>	
<p style="writing-mode: vertical-rl; transform: rotate(180deg);">Through points</p>	<p>Interpolated model (patch type, column and row degree are defined)</p> <p>Surface goes through the points (but points are not connected with straight line)</p>	

Figure 20 Cone model for rock 11f using “Fit surface” vs “Through point surface”.

**DISSERTATIONS DEFENDED AT
TALLINN UNIVERSITY OF TECHNOLOGY ON
CIVIL ENGINEERING**

1. **Heino Mölder**. Cycle of Investigations to Improve the Efficiency and Reliability of Activated Sludge Process in Sewage Treatment Plants. 1992.
2. **Stellian Grabko**. Structure and Properties of Oil-Shale Portland Cement Concrete. 1993.
3. **Kent Arvidsson**. Analysis of Interacting Systems of Shear Walls, Coupled Shear Walls and Frames in Multi-Storey Buildings. 1996.
4. **Andrus Aavik**. Methodical Basis for the Evaluation of Pavement Structural Strength in Estonian Pavement Management System (EPMS). 2003.
5. **Priit Vilba**. Unstiffened Welded Thin-Walled Metal Girder under Uniform Loading. 2003.
6. **Irene Lill**. Evaluation of Labour Management Strategies in Construction. 2004.
7. **Juhan Idnurm**. Discrete Analysis of Cable-Supported Bridges. 2004.
8. **Arvo Iital**. Monitoring of Surface Water Quality in Small Agricultural Watersheds. Methodology and Optimization of monitoring Network. 2005.
9. **Liis Sipelgas**. Application of Satellite Data for Monitoring the Marine Environment. 2006.
10. **Ott Koppel**. Infrastruktuuri arvestus vertikaalselt integreeritud raudtee-ettevõtja korral: hinnakujunduse aspekt (Eesti peamise raudtee-ettevõtja näitel). 2006.
11. **Targo Kalamees**. Hygrothermal Criteria for Design and Simulation of Buildings. 2006.
12. **Raido Puust**. Probabilistic Leak Detection in Pipe Networks Using the SCEM-UA Algorithm. 2007.
13. **Sergei Zub**. Combined Treatment of Sulfate-Rich Molasses Wastewater from Yeast Industry. Technology Optimization. 2007.
14. **Alvina Reihan**. Analysis of Long-Term River Runoff Trends and Climate Change Impact on Water Resources in Estonia. 2008.
15. **Ain Valdmann**. On the Coastal Zone Management of the City of Tallinn under Natural and Anthropogenic Pressure. 2008.
16. **Ira Didenkulova**. Long Wave Dynamics in the Coastal Zone. 2008.
17. **Alvar Toode**. DHW Consumption, Consumption Profiles and Their Influence on Dimensioning of a District Heating Network. 2008.

18. **Annely Kuu.** Biological Diversity of Agricultural Soils in Estonia. 2008.
19. **Andres Tolli.** Hiina konteinerveod läbi Eesti Venemaale ja Hiinasse tagasisaadetavate tühjade konteinerite arvu vähendamise võimalused. 2008.
20. **Heiki Onton.** Investigation of the Causes of Deterioration of Old Reinforced Concrete Constructions and Possibilities of Their Restoration. 2008.
21. **Harri Moora.** Life Cycle Assessment as a Decision Support Tool for System optimisation – the Case of Waste Management in Estonia. 2009.
22. **Andres Kask.** Lithohydrodynamic Processes in the Tallinn Bay Area. 2009.
23. **Loreta Kelpšaitė.** Changing Properties of Wind Waves and Vessel Wakes on the Eastern Coast of the Baltic Sea. 2009.
24. **Dmitry Kurennoy.** Analysis of the Properties of Fast Ferry Wakes in the Context of Coastal Management. 2009.
25. **Egon Kivi.** Structural Behavior of Cable-Stayed Suspension Bridge Structure. 2009.
26. **Madis Ratasapp.** Wave Scattering at Discontinuities in Plates and Pipes. 2010.
27. **Tiia Pedusaar.** Management of Lake Ülemiste, a Drinking Water Reservoir. 2010.
28. **Karin Pachel.** Water Resources, Sustainable Use and Integrated Management in Estonia. 2010.
29. **Andrus Räämet.** Spatio-Temporal Variability of the Baltic Sea Wave Fields. 2010.
30. **Alar Just.** Structural Fire Design of Timber Frame Assemblies Insulated by Glass Wool and Covered by Gypsum Plasterboards. 2010.
31. **Toomas Liiv.** Experimental Analysis of Boundary Layer Dynamics in Plunging Breaking Wave. 2011.
32. **Martti Kiisa.** Discrete Analysis of Single-Pylon Suspension Bridges. 2011.
33. **Ivar Annus.** Development of Accelerating Pipe Flow Starting from Rest. 2011.
34. **Emlyn D. Q. Witt.** Risk Transfer and Construction Project Delivery Efficiency – Implications for Public Private Partnerships. 2012.
35. **Oxana Kurkina.** Nonlinear Dynamics of Internal Gravity Waves in Shallow Seas. 2012.
36. **Allan Hani.** Investigation of Energy Efficiency in Buildings and HVAC Systems. 2012.

37. **Tiina Hain**. Characteristics of Portland Cements for Sulfate and Weather Resistant Concrete. 2012.
38. **Dmitri Loginov**. Autonomous Design Systems (ADS) in HVAC Field. Synergetics-Based Approach. 2012.
- 8 39. **Kati Kõrbe Kaare**. Performance Measurement for the Road Network: Conceptual Approach and Technologies for Estonia. 2013.
40. **Viktoria Voronova**. Assessment of Environmental Impacts of Landfilling and Alternatives for Management of Municipal Solid Waste. 2013.
41. **Joonas Vaabel**. Hydraulic Power Capacity of Water Supply Systems. 2013.
42. **Inga Zaitseva-Pärnaste**. Wave Climate and its Decadal Changes in the Baltic Sea Derived from Visual Observations. 2013.
43. **Bert Viikmäe**. Optimising Fairways in the Gulf of Finland Using Patterns of Surface Currents. 2014.
44. **Raili Niine**. Population Equivalence Based Discharge Criteria of Wastewater Treatment Plants in Estonia. 2014.
45. **Marika Eik**. Orientation of Short Steel Fibers in Concrete. Measuring and Modelling. 2014.
46. **Maija Viška**. Sediment Transport Patterns Along the Eastern Coasts of the Baltic Sea. 2014.
47. **Jana Põldnurk**. Integrated Economic and Environmental Impact Assessment and Optimisation of the Municipal Waste Management Model in Rural Area by Case of Harju County Municipalities in Estonia. 2014.
48. **Nicole Delpeche-Ellmann**. Circulation Patterns in the Gulf of Finland Applied to Environmental Management of Marine Protected Areas. 2014.
49. **Andrea Giudici**. Quantification of Spontaneous Current-Induced Patch Formation in the Marine Surface Layer. 2015.
50. **Tiina Nuuter**. Comparison of Housing Market Sustainability in European Countries Based on Multiple Criteria Assessment. 2015.
51. **Erkki Seinre**. Quantification of Environmental and Economic Impacts in Building Sustainability Assessment. 2015.
52. **Artem Rodin**. Propagation and Run-up of Nonlinear Solitary Surface Waves in Shallow Seas and Coastal Areas. 2015.
53. **Kaspar Lasn**. Evaluation of Stiffness and Damage of Laminar Composites. 2015.
54. **Margus Koor**. Water Distribution System Modelling and Pumping Optimization Based on Real Network of Tallinn. 2015.

55. **Mikk Maivel.** Heating System Efficiency Aspects in Low-Energy Residential Buildings. 2015.
56. **Kalle Kuusk.** Integrated Cost-Optimal Renovation of Apartment Buildings toward Nearly Zero-Energy Buildings. 2015.
57. **Endrik Arumägi.** Renovation of Historic Wooden Apartment Buildings. 2015.
58. **Tarvo Niine.** New Approach to Logistics Education with Emphasis to Engineering Competences. 2015.
59. **Martin Thalfeldt.** Total Economy of Energy-Efficient Office Building Facades in a Cold Climate. 2016.